8-26-2022

Molecular mechanisms that regulate centrosome movement during tissue morphogenesis

Nikhila Krishnan
Syracuse University, nikrishn@syr.edu

ABSTRACT

Coordination of cell division, cellular epithelialization and ciliogenesis is necessary for tissue development *in vivo*. We argue that the process of epithelialization and ciliogenesis requires positioning the centrosomes to specific cellular locales. We identified that the centrosome can be repositioned to these locales in a Rab11-dependent manner towards the cytokinetic bridge during abscission and to the apical membrane for cilia formation. Rab11 is an essential GTPase that is involved in regulating abscission, cleavage of the cytokinetic bridge and cilia formation. Here we identified the role of Rab11 endosomes in regulating centrosome positioning during these processes *in vivo*. To study the role of Rab11 endosomes during abscission we devised an optogenetic system to acutely inhibit Rab11 mediated membrane trafficking both in human cell culture and in zebrafish embryos (Chapter 2). We found that acute inhibition of Rab11 mediated membrane trafficking results in cells being binucleated due to incomplete abscission. Using this approach, we investigated the role of Rab11 endosomes in centrosome function and movement during pre-abscission. We identified that Rab11 endosomes regulate the organization of the centrosome protein, Pericentrin, during pre-abscission that is required for centrosome placement towards the cytokinetic bridge that we argue is required for abscission completion (Chapter 3). Based on this work we examined whether Rab11 was required for centrosome positioning during Kupffer's Vesicle (KV) development. The KV is a ciliated organ of asymmetry in zebrafish that we used as a model to study tissue formation *in vivo.* During KV formation, KV mesenchymal cells move their centrosome to the site of lumen formation while the cell's centrosome is constructing a cilium intracellularly. We identified that Rab11 endosomes regulate cilia formation and centrosome movement to the site of lumen formation during KV development,

independent of Rab8 (Chapter 4). Taken together, these findings identify that Rab11 endosome mediated centrosome movement is necessary to coordinate abscission and ciliogenesis during tissue morphogenesis *in vivo*.

Molecular mechanisms that regulate centrosome movement during tissue morphogenesis

by

Nikhila Krishnan

B.Tech, Sri Venkateswara College of Engineering, Anna University, 2013

M.Sc., Brandeis University, 2015

Dissertation

Submitted in partial fulfillment of the requirements for the degree of

Doctor of Philosophy in Biology.

Syracuse University

August 2022

Acknowledgements:

I have always liked the saying “it takes an entire village to complete your PhD”. I did not accomplish this giant feat on my own and I would like to take this opportunity to sincerely thank everyone involved.

First and foremost, I would like to thank Dr. Heidi Hehnly for being the most supportive advisor one could ask for. I have had the privilege of learning from one of the most dedicated teachers in the field and I am forever humbled to have had this opportunity. Anyone who met me early in my time at Syracuse would know how nervous and anxious I was during talks, presentations and completing daily tasks in the lab. Within a year of joining Heidi’s lab, I was able to perform at a level where I was exuberating confidence and knowledge. The scientist I am today is because of was the constant encouragement and support from Heidi. With this lab, it has been an honor to be able to travel the world and present our science. I will always cherish the time we went on every ride at the Tivoli gardens in Copenhagen, however, the adrenalin rush is not as satisfying as impressing Heidi with masterful science. The most notable time was when the world shut down for the pandemic, Heidi was with us every day in lab but also helped me find a place to stay during those scary times. I thank you Dr. Hehnly, I am very proud to be a part of the Hehnly lab! I will strive to make you proud wherever my career may lead.

To my committee members, I have had the best time working with each of you and am forever grateful for each of you for sharing your expertise and guidance with me. Dr. Alison Patteson, we have worked together closely, and I greatly appreciate your insights into my work. Dr. Melissa Pepling, I will always remember the day from my first CDBIG talk where you were so excited about my talk and since then been a big part of my PhD journey. Dr. Roy Welch, I thank you for your insightful

conversations on science and life as a scientist. Dr. Jessica MacDonald, I am very glad to have had the opportunity to work with you, you make me think about the bigger picture involved with my work and are very patient with me while I work through my answers. Dr. Carlos Castaneda, thank you for always greeting me with a smile in the hallways and the small talks that were very light and encouraging during the last few years. I thank you all, for your support and thoughtful comments that have made me grow as a scientist and a human being.

The Hehnly lab will always be my family. Judy Freshour, without you I would be lost on the way to the TC room. Your kindness and wisdom have helped me become a better person. I am very glad I have had the privilege to work with you. Abrar Aljiboury, you adopted me into your family after mere weeks of meeting me. If I have managed 4 years in Syracuse it is because I was with you, your kindness, intelligence and work ethic know no bounds. Life in the lab would surely have been harder without you. Michael Bates, I do not know how to thank you. I would not have survived the year of COVID or any year in my PhD for that matter. Everyone in the Hehnly lab has played a part in helping me graduate Favour Ononiwu, Peter Fioramonti, Christopher Taveras, Julie Manikas, Nicole Hall, Eric Ingram, Lindsay Rathbun, Debadrita Pal, Yan Wu, Jonah D'Silva, Yiling Lan, Thomas Cammerino, Denise Magny and Kirsten Rassmusen.

Work life aside, family and friends are a major part of my success during my tenure as a PhD student. I would not be here if not for my parents, thank you Appa (S. Krishnan) and Amma (Rama Krishnan) for being the best people I know. Even when you are halfway across the world you are always with me wherever I am, encouraging and supporting me constantly. Nithin Krishnan, my younger brother, my biggest advocate and constant support through life and work. Your voice of reason

and encouragement mean a lot to me, thank you. Prasanna, Laavanya, Khushali, Malavika, Kalpana, Meena, Sheetal and Akila, Neerja, Shiv, Perima (Uma Kumar), Attai (Lalitha Balakrishnan), Aswath, Sandhya and Sitara, thank you for being there for me and my family when I am so far away and helping out wherever you can. It is humbling to be a part of such a big group of closely knit family who care for each other.

Zeeshan, Shibjyoti, Karan, Gagneet, Amisha, Rachana and Sarah K., 716 family forever for keeping me alive! Amber, Sarah A.B., Ian, Anne, Billy Haws, Niko, Linnea, Leanne, Franki, Alex N, Alex E., Trosporsha, Jess Comstock, Maxx Swoger, Dr. Thuy Dao, Dr. Sam England, Dr. Angelica Kowalchuck and Ginny Grieb for being there for me throughout my time here in Syracuse, life would have been a lot harder without you all.

Table of contents

List of Figures

Chapter One: Molecular mechanisms that regulate centrosome movement during tissue morphogenesis

Chapter Two: Optogenetics, an acute method to inhibit Rab11 mediated membrane trafficking *in vivo*.

Chapter Three: Rab11 endosomes and Pericentrin coordinate centrosome movement during pre-abscission *in vivo*.

Chapter Four: Rab11 dependent mechanisms of centrosome positioning and cilia formation during Kupffer's Vesicle development

Chapter Five: Summary and future directions

CHAPTER ONE: Introduction.

Molecular mechanisms that regulate centrosome movement during tissue morphogenesis

This chapter features a possible review to be published.

Molecular mechanisms that regulate centrosome movement during tissue morphogenesis

Nikhila Krishnan[1] and Heidi Hehnly[1*]

[1] Syracuse University, Department of Biology, 107 College Place, Syracuse, NY 13244, USA

*Lead contact, correspondence: hhehnly@syr.edu, Twitter: @LovelessRadio

1.1 Abstract

Mesenchymal epithelial transition is the process by which non-polarized cells migrate together while establishing apicobasal polarity to create a tissue. During this process, cellular events like migration, polarization, ciliogenesis and cell division are coordinated in space and time. One cellular component, integrated throughout all these processes, is the centrosome. The centrosome is the major microtubule organizing center of the cell that is required for microtubule organization, cilia formation, and formation of the mitotic spindle. However, how the centrosome knows where to position itself during cellular migration, changes from mesenchymal to epithelial cellular states, or during mitotic exit is currently unknown. The following explores what is currently known about the spatio-temporal mechanisms that coordinate centrosome positioning with 1) cell migration, 2) cell division, 3) polarity establishment and 4) cilia formation.

1.2 Introduction

Cells need to proliferate and self-organize to create complex tissues *in vivo*. During development of an organism, non-polarized cells transition into polarized cells (Bryant and Mostov, 2008; Fomicheva et al., 2020; Nejsum and Nelson, 2009; Rodriguez-Boulan and Nelson, 1989). There are several types of polarized cells generated during development (modeled in Figure 1.1). For example, neural progenitor cells become neurons which have a distinct top known as a dendrite and bottom, axon which are essential for its function. Another example is migrating cells which are characterized by their front or leading edge and rear or lagging edge (modeled in Figure 1.1, (Barnes and Polleux, 2009; Seetharaman and Etienne-Manneville, 2020)).

Non-polarized mesenchymal cells need to establish apical (top or front) and basal (bottom or rear) cellular domains to facilitate the cell polarization necessary for tissue creation (Gjorevski and Nelson, 2010; Schelski and Bradke, 2017). Cell polarity is a conserved cellular event which is characterized by the asymmetric localization of physical aspects within the cell, including but not limited to cell surfaces proteins, intracellular organelles and the cytoskeleton (Goldstein and Macara, 2007; Ohno, 2001). To establish this apical and basal axis, the cell orients itself to a signaling cue (usually provided externally, e.g., cell-cell contacts or cell-matrix interaction) initiated at a point on the cell surface (Ivanov et al., 2010). This point of signaling creates a hierarchical pathway for the cell to orient to and begin its polarization. The cell then coordinates the asymmetrical distribution of polarity complexes by directing cytoskeletal reorganization to facilitate vesicle delivery (membrane trafficking) to the appropriate cellular landmarks (Bryant and Mostov, 2008; Fomicheva et al., 2020; Nelson, 2009).

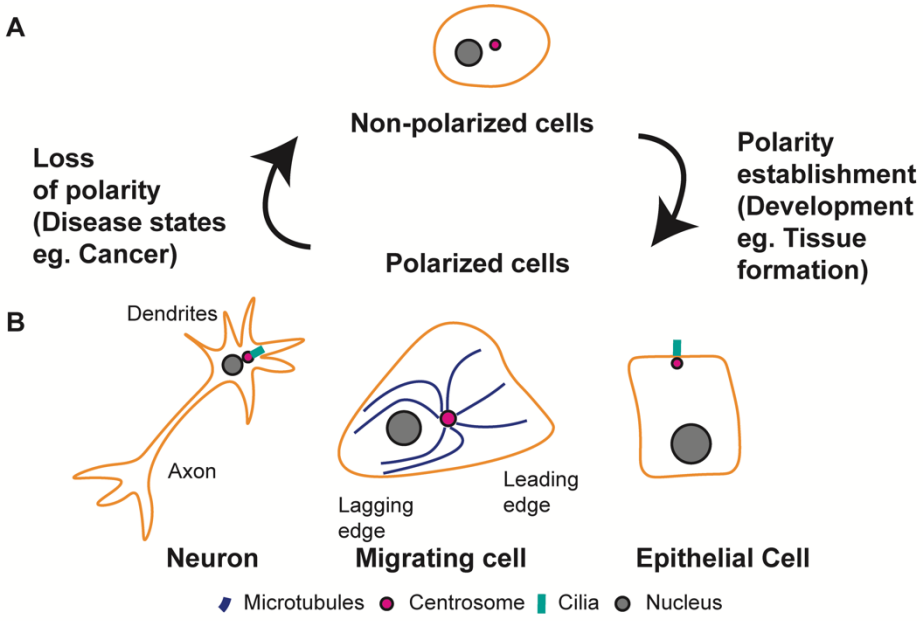

Figure 1.1: Cell polarization is necessary for generating different types of cells during development.
(A) Non polarized cells establish polarity by asymmetric localization of cellular components to create tissues during development. (B) Different types of polarized cells found in organisms during development. Neuron, migrating cell and epithelial cell (from left to right). Mistakes in cell polarization, causing loss of cell polarity lead to disease states like cancer.

The centrosome is one major component of the cell that regulates directed membrane trafficking by facilitating the creation of microtubule networks in a cell (Vertii et al., 2016). This component is comprised of two centrioles, a mother centriole and a daughter centriole, surrounded by pericentriolar material (PCM). In an interphase non-polarized cell, the centrosome is centrally located. This localization is thought to facilitate cellular homeostasis by modulating the organization of other cellular structures relative to the position of the centrosome (Jimenez et al., 2021).

To create a tissue, a group of cells migrates and establishes apical-basal polarity to generate epithelial tissues *in vivo*. We will focus on epithelial formation and then touch upon neuronal differentiation, highlighting that in these situations the cells need to create a “top” and “bottom” of a cell necessary during tissue development and discuss aspects of this process that are conserved (modeled for epithelial cells, Figure 1.2A). We present a model where the centrosome itself is assisting in the coordination of cellular processes necessary in establishing tissues during development (Figure 1.2B-C). We provide supporting studies that attempt to outline the spatial and temporal mechanisms that coordinate centrosome positioning during cell migration, cell division, polarity establishment and cilia formation within a tissue during development (Figure 1.2C).

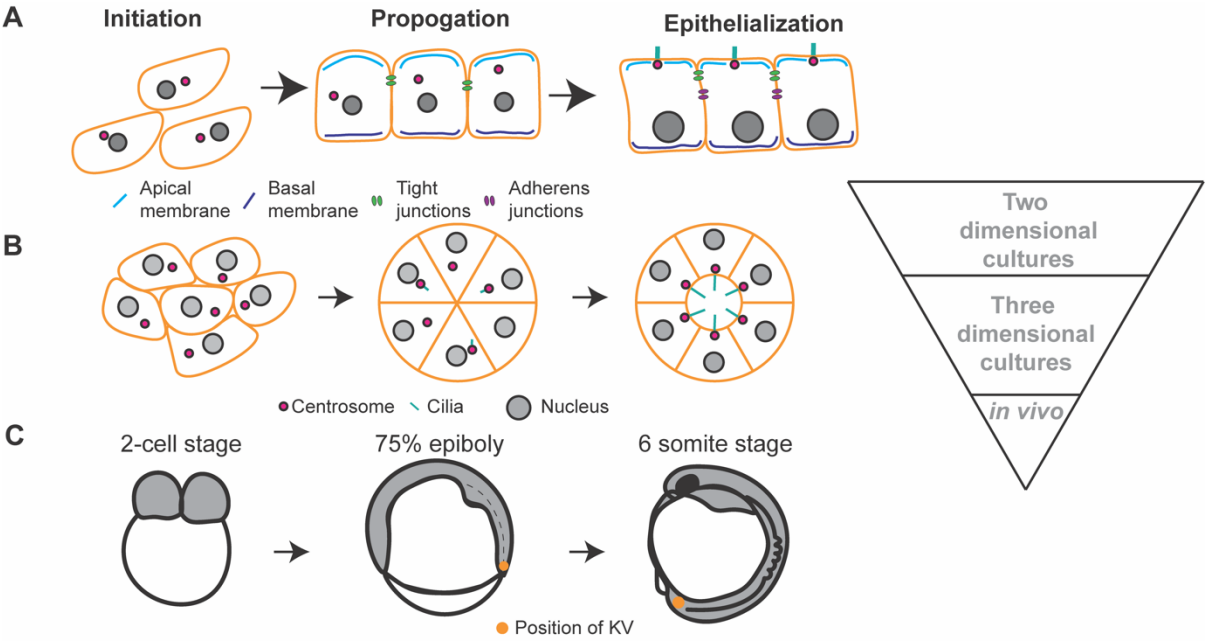

Figure 1.2: Spatio-temporal coordination of cell polarization studied using a range of model systems. (A) Cell polarization in cells that make a linear epithelium. (B) Cell polarization in cells that make a lumenal tissue. (C) Developmental stages of a zebrafish from 2 cell stage to 6 somite stage where in multiple tissues are made in vivo with molecular components coordinated in space and time. The downward triangle is indicating the extent of studies discussing centrosome movement in two-dimensional cell culture compared to three-dimensional cell culture and studies carried out *in vivo*.

1.3 Centrosome positioning during cell migration

Cell migration is the ability of the cell to move from one spot to another. This ability is an essential cellular process necessary for creating tissues during development (Etienne-Manneville, 2013). A wound healing assay is a traditional way to observe how a monolayer of cells migrate *ex vivo*. A wound healing assay is when a scratch is placed across a monolayer of cells and a time series is obtained on how long the cells take to close a wound. Using this technique, it was discovered that cell migration consists of four steps: protrusion, adhesion, contraction, and retraction (reviewed in (SenGupta et al., 2021)). For this movement to happen, the front of the cell needs to protrude which in turn creates new membrane adhesions. Then the rear-end of the cell performs contraction and retraction (Figure 1.3A). This creates asymmetry that defines the front end of the cell known as the leading edge which is characterized by the localization of active Rac and Cdc42. Rac and Cdc42 are small GTPases from the Rho family of GTPases essential in regulating the actin-cytoskeleton (Etienne-Manneville and Hall, 2001; Seetharaman and Etienne-Manneville, 2020). RhoA is found near the cell soma and is necessary to promote maturation of cell adhesion and contraction. Rac, Cdc42, and Rho1 are most commonly known to regulate the actin cytoskeleton during cell migration (Mayor and Etienne-Manneville, 2016; Seetharaman and Etienne-Manneville, 2020; Tapon and Hall, 1997).

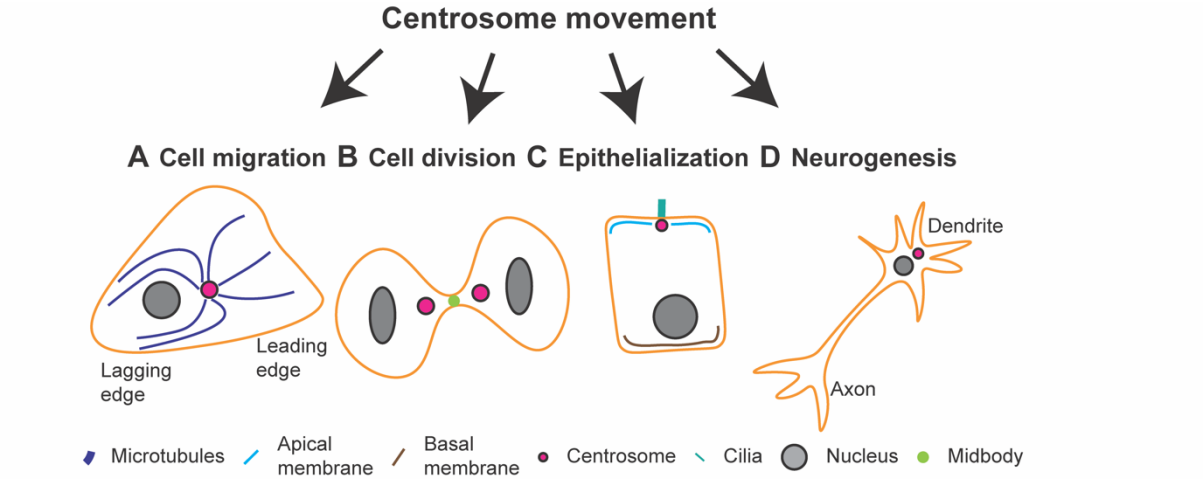

Figure 1.3: Centrosome movement is necessary during cell migration, cell division, cellular epithelialization and neurogenesis.
(A) Centrosomes move to set the leading edge of a migrating cell. (B) Centrosomes move from the polar ends of the cell to the cytokinetic bridge during pre-abscission.
(C) Centrosomes move to the apical membrane during polarity establishment and cilia formation. (D) Neuronal cell centrosome located near the dendrites.

The microtubule network also contributes to cell migration by facilitating membrane protrusion formation at the leading edge of the cell (Etienne-Manneville and Hall, 2001; Nobes and Hall, 1995; Tapon and Hall, 1997; Zegers and Friedl, 2014). The centrosome organizes microtubular networks. In specific contexts, the centrosome is thought to potentially sense the leading or trailing edge of the cell. During fibroblast cell migration *ex vivo*, the centrosome situates itself in between the nucleus and the leading edge of the cell (modeled in Figure 1.3A, (Luxton et al., 2011)). This reorientation of the nuclear centrosome axis, relative to the cellular axis, could aid in stabilizing the microtubule network in the direction of migration (Luxton et al., 2011). The microtubules orient their minus ends toward the centrosome and plus ends toward the cell cortex. At this point the plus ends of the microtubules interact with minus end directed motor proteins such as dynein. Disturbing microtubule dynamics using nocodazole impairs centrosome movement during cell migration (Hung et al., 2016). Inhibition of dynein or the depletion of Lis1 (a protein that interacts with dynein and when mutated causes lissencephaly) present with impaired centrosome reorientation towards the leading edge causing cell migration defects in mammalian neural precursor cells (Tsai et al., 2007). Yet, how the centrosome regulates the direction of cell migration is unclear. Cell polarity is one mechanism that can contribute to centrosome movement towards the leading edge of migrating cells. During polarized cell movement, the PAR complex and Cdc42 are localized at the leading edge. PAR3 is a protein part of the PAR complex, that is known to directly interact with dynein (Schmoranzer et al., 2009). Depletion of PAR3 results in centrosome reorientation defects (Schmoranzer et al., 2009). Together, this suggests a possible role for PAR3, dynein, and microtubule interactions at the

cell cortex, coordinating centrosome reorientation towards the direction of cell migration.

Most of the components, discussed this far, involve molecular machinery at the cell cortex that can reposition the centrosome through microtubules. Rather than relying solely on the molecular machinery of the cell cortex, the centrosome, itself, contains molecular components necessary for regulating its position during cell migration. Cenexin, the mother centriole appendage protein, is necessary for centrosome positioning during directed cell migration (Hung et al., 2016). This mechanism potentially involves the ability of the centrosome through cenexin, to directly interact and anchor stabilized microtubules (Hung et al., 2016; Piel et al., 2000). Stabilized microtubules, which are positive for acetylated tubulin, are the preferred track for microtubule motors to move along or for dynein to potentially bind to at the cell cortex (Reck-Peterson et al., 2018). This provides a linkage between the centrosome, microtubules, and interactions of a potentially specific microtubule population at the cell cortex used to reposition the centrosome. This stabilized microtubule network may also aid in positioning the Golgi apparatus and recycling endosomes at the right place to enable efficient cargo delivery of components essential to establishing polarity during directed migration (Luxton and Gundersen, 2011; Pouthas et al., 2008). Our lab's prior studies identified that Rab11, a GTPase that regulates the recycling endosome, interacts with the centrosome through mother centriole appendages (Hehnly et al., 2012). We propose that the impairment of the ability of the centrosome to interact with the recycling endosome is a factor that leads to failed centrosome movement and abnormal cell migration.

The centrosome has also been reported to reposition towards the rear of migrating cells *in vivo* (Guo and Wang, 2012; Zhang and Wang, 2017). This

phenomenon was observed in cells when they were confined in space that allowed unidirectional movement, or when they were met with a physical barrier that forces cells to reverse direction of movement. When microtubules and/or dynein mediated transport is inhibited, centrosomes are unable to reorient to the rear end of the cell and subsequently block cell migration (Guo and Wang, 2012; Zhang et al., 2014). The migrating cells of the lateral line primordium in *Danio rerio* (zebrafish) are a good example of this centrosome movement to the rear end of the cell. During development of this tissue, cells migrate from the head to the tail of the animal (Pouthas et al., 2008). This study also observed the Golgi apparatus organized with the centrosome at the rear end of the cell (Pouthas et al., 2008). Another example of centrosome moving to the rear end of the cell is the Potoroo Kidney cells (PtK2 cells) grown in culture in a wound healing assay (Yvon et al., 2002). These studies compared PtK2 cells to Chinese hamster ovary (CHO) cells that repositioned the centrosome towards the leading edge. This suggests that different cell types and potentially different contexts use distinct mechanisms for centrosome positioning during cell migration.

An example of a cell type that incorporates centrosome positioning both at the rear of the cell and at the leading edge is with Cytotoxic T-cells (CTLs). CTLs migrate towards their target, pathogenic cells, where they attach creating an immunological synapse that then leads to pathogenic cell destruction. When CTLs migrate towards their target, the centrosome is located at the rear end of the cell (Ritter et al., 2015), but once the CTLs identify their target cells through their T-cell receptors (TCR) they undergo cytoskeletal reorganization to position the centrosome towards the leading edge that associates with the target cell where it docks at the forming immunological synapse between the two cells. At the time the centrosome

reorients towards the immunological synapse the Golgi apparatus and recycling endosomes remain organized at the centrosome (Angus and Griffiths, 2013; Aniento et al., 1993). A potential mechanism could exist to regulate centrosome positioning to the rear end that is then repositioned to the site of the immunological synapse following a signaling event.

We speculate that in most cases movement of the centrosome (front or rear end) begins only after the front (leading) end of the cell is established. However, it is unclear if the centrosome potentially dictates and coordinates the position of the cell during migration. It is necessary to identify the spatial-temporal mechanisms that coordinate when and how centrosomes move and position themselves during cell migration. Next, one must acutely inhibit these events to determine the exact role of the centrosome during these processes. Taken together, these studies suggest that a cell's centrosome positioning can potentially dictate asymmetric localization of cellular components through its ability to organize a stabilized microtubule population. Further, these studies suggest a cell's centrosome positioning affects its potential ability in directing membrane transport that aids in cell movement.

1.4 Centrosome positioning during cell division:

The initiation of DNA replication is not the only master regulator of cell division. The duplication of the centrosome at the same time to make two mitotic centrosomes, is also a regulator. The two mitotic centrosomes display unique movements as the cell transitions from prophase to metaphase to assemble the

mitotic spindle, as well as during metaphase exit as the cell progresses through anaphase and cytokinesis.

To understand some of these movements, we first need to explain the inherent asymmetry that occurs between the two mitotic centrosomes. Due to the nature of centrosome duplication, one mitotic centrosome is inherently older than the other (Azimzadeh and Bornens, 2007). An interphase centrosome is made up of an older (mother) centriole and a younger (daughter) centriole that are structurally distinct from one another. The mother centriole contains appendage like structures, where the daughter is devoid of them (Colicino et al., 2019; Hall and Hehnly, 2021; Hung et al., 2016; Ishikawa et al., 2005). The mother and daughter centriole each create a new daughter centriole (Chang and Stearns, 2000). Due to this, the two newly formed mitotic centrosomes are asymmetric in nature (refer to Figure 1.4). This is important to consider, because in some cell types during G2 after the centrosome has duplicated during S-phase, one mitotic centrosome (the mother) moves around the nucleus while the other centrosome does not move. *Drosophila melanogaster* neuroblast (NB) asymmetric divisions are one example cell type that are known to do this (Rusan and Peifer, 2007). A striking mechanism was proposed to regulate the movement of the oldest (mother) centrosome involved Pericentrin (PCNT)-like-protein (PLP). In this scenario, the youngest (daughter) centrosome remains active and immobile at the apical side of the NB, and the oldest centrosome is transported to the basal end. PLP presence is required for the older centrosome movement so that a bipolar spindle can be assembled and positioned correctly (Lerit and Rusan, 2013). Recently it was discovered that PLP is a Kinesin-1 activator. This has led to an advancement in the molecular mechanism that regulates NB centrosome motility during G2. Kinesin-1 is a microtubule plus-end directed motor

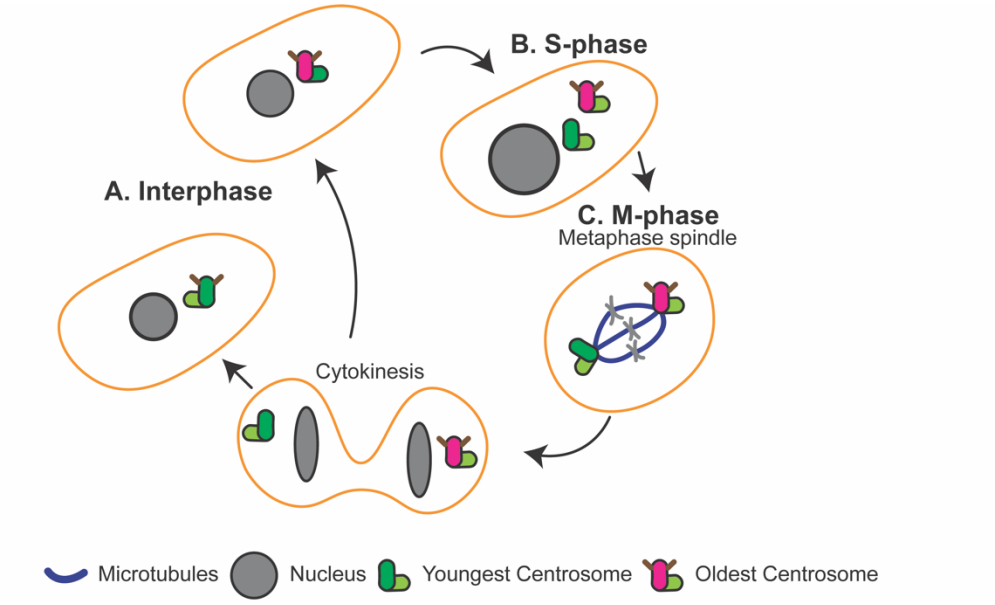

Figure 1.4: Due to the nature of centrosome duplication, the centrosomes inherited by the newly formed daughter cells during mitosis show an age dependent asymmetry.
(A) An interphase cell with oldest centriole (pink, appendage proteins cartooned in brown), younger centriole (dark green) and nucleus (gray). (B) During S-phase the cell duplicates it genetic material (nucleus, gray) and centrosome (new daughter centriole, light green). Two new daughter centrioles are templated on to each of the older centrioles creating an asymmetry in age of the centrosomes formed. The cell undergoes mitosis, centrosomes move to the polar ends of the cell, construct the mitotic spindle (microtubules, teal) and the chromosomes align at the metaphase plate. The cell undergoes cytokinesis with each cell inheriting a centrosome. The cytokinetic bridge is cleaved and two daughter cells are formed with one cell inheriting the centrosome with the oldest centriole (pink) and the other cell with the younger centriole (dark green).

protein that can directly transport the centrosome along microtubules to the opposite end of the cell in a PLP dependent manner (Hannaford et al., 2022).

Some mechanisms of centrosome movement in early mammalian dividing cells occurs mostly during prophase to pro-metaphase after the nuclear envelope has broken down. The positioning of the two mitotic centrosomes during prophase-to-metaphase is less dependent on centrosome age and is thought to ultimately dictate the orientation of the mitotic spindle. In prophase, the two mitotic centrosomes are located adjacent to one another as they start to nucleate microtubules. A plus-end directed microtubule motor protein that binds to anti-parallel microtubules, Eg5, is recruited to areas in between the two mitotic centrosomes where antiparallel microtubules form. Eg5's ability to bind antiparallel microtubules creates a sliding mechanism that moves the two mitotic centrosomes apart (Sawin et al., 1992). This movement facilitates centrosome placement during spindle formation (Tanenbaum et al., 2008). However, opposing forces are also needed to make sure that centrosomes do not separate too early or too much. This mechanism involves the minus-end directed microtubule motors Kif25 and the dynein-dynactin complex (Decarreau et al., 2017; Tanenbaum et al., 2008). Dynein-dynactin complex along with interacting partners Lis1 and CLIP170 coordinately diminish the separation of the centrosome facilitated by Eg5 to ensure correct centrosome positioning at the polar ends of the cell. This mechanism is thought to maintain appropriate spindle size and orientation (Tanenbaum et al., 2008). Centrosome movement during migration also requires the coordination of microtubules, dynein and Lis1 (Tsai et al., 2007). These studies suggest that the temporal coordination of centrosome positioning may be conserved across cellular processes.

Once the centrosomes have separated and start to make the bipolar microtubule-based spindle, the two mitotic centrosomes position themselves to set up the spindle along the longest cell axis (Tanenbaum and Medema, 2010; Tanenbaum et al., 2008). Thus, cell geometry can dictate how the centrosomes find the longest axis. In some cases, this geometry can even occur before the cells start setting up their bipolar spindle (Strauss et al., 2006). In certain contexts, the spindle's positioning defines where the daughter cells will be placed. Astral microtubules that emanate from the centrosomes orient themselves to project and anchor at the cell cortex which interact with a complex of cortical proteins. Dynein is one of these cortical proteins that interacts with the plus-ends of astral microtubules pulling the centrosome towards the cell cortex. This dynein-driven movement orients the centrosome and spindle.

In epithelial cells, the orientation of the centrosome and spindle are dependent on polarity proteins, such as the small GTPase CDC42 to recruit dynein to the cell cortex (Tuncay et al., 2015). A study from the Macara lab showed that localized activation of Cdc42 by its Guanine Exchange Factor, Tuba, is required at the cell cortex to facilitate appropriate spindle orientation in cyst forming canine kidney cells (Hao et al., 2010; Qin et al., 2010; Seldin and Macara, 2017). These findings suggest that spatial and temporal activation of Cdc42 and its regulated dynein's cortical distribution can regulate centrosome positioning and spindle orientation. These studies suggest that the placement of the centrosome during spindle formation relies on the spatial and temporal coordination of motor protein mediated microtubule movement (Eg5, Kif25,dynein), polarity cues and the shape of the cell.

While cortical signals are important in spindle positioning, the centrosome itself can dictate the position of the spindle likely through its regulation of astral microtubules. Pericentrin is a pericentriolar material protein that has been clearly linked to spindle positioning. Pericentrin mutations both in murine embryonic fibroblasts and fibroblasts obtained from patients suffering from Microcephalic osteodysplastic primordial dwarfism type II (MOPDII) present with spindle positioning defects likely due to a loss in astral microtubule formation (Chen et al., 2014). MOPDII is caused by mutations in Pericentrin that lead to severe pre- and postnatal growth retardation. Pericentrin is not the only centrosome protein whose removal results in a loss of astral microtubules. The mother centriole appendage protein, cenexin, is another (Hung et al., 2016). Cenexin regulation of astral microtubules could occur through its ability to bind Polo-Like Kinase (PLK)1. Recent studies identify that cenexin depletion disrupts PLK1 activity at the centrosome that leads to loss in pericentriolar material integrity, specifically the organization of Pericentrin (Aljiboury et al., 2022). These findings suggest a molecular mechanism by which cenexin, through its ability to regulate PLK1 activity and subsequently Pericentrin organization at the centrosome promotes centrosome placement and spindle orientation. These studies suggest that centrosome proteins coordinate kinase activity that influence microtubule network organization so that the centrosome is positioned appropriately during mitotic spindle establishment.

Following anaphase exit when the mitotic spindle starts to disassemble, the two mitotic centrosomes are at the polar ends of the cell. Cytokinesis begins with the cytokinetic furrow constricting at the equatorial axis through the assembly of an actomyosin ring (Reichl et al., 2008). This results in the formation of a cytokinetic midbody from components of the central spindle within the intracellular bridge

connecting the two daughter cells (O' Halloran et al.,2000; Eggert et al.,2006). The centrosomes move from the polar ends of the cell towards the cytokinetic midbody (Figure 1.3B (Krishnan et al., 2022; Piel et al., 2001)). The bridge is then cleaved by a process called abscission. The small GTPase Rab 11 and its associated membrane compartment regulate the resolution and cleavage of the cytokinetic bridge (RE, (Wilson et al., 2005)). In the absence of functional Rab11, centrosomes are unable to track to the cytokinetic bridge during pre-abscission. This results in cells being binucleated due to failed abscission (Krishnan et al., 2022).

Rab11 endosomes that regulate centrosome positioning during pre-abscission are known to cause abscission defects. Therefore, it is unclear whether centrosome movement to the cytokinetic bridge is necessary for abscission. Studies using laser ablation that removed centrosomes from human cells in culture identified that the cells were unable to sever the cytokinetic bridge and became binucleated (Piel et al., 2001). Centrosome free prostate epithelial cells treated with centrinone resulted in forming multinucleated cells indicative of inability to abscise the cytokinetic bridge (Wang et al., 2020). These studies suggest that centrosome bridge directed movement may coordinate appropriate abscission completion.

The centrosome requires optimal Pericentrin organization to function during mitosis, yet Pericentrin's role during cytokinesis and pre-abscission is less known. Depletion of Pericentrin or acute inhibition of Rab11 mediated membrane trafficking in dividing cells in the zebrafish embryo results in cells unable to move their centrosomes to the cytokinetic bridge. These cells were unable to abscise and ultimately become binucleated. Rab11 was found to act upstream of Pericentrin organization at the centrosome, which means Rab11-loss resulted in decreased Pericentrin at the centrosome. These findings suggest a molecular mechanism

wherein Rab11 endosomes coordinate the organization of Pericentrin at the centrosome necessary to facilitate bridge directed centrosome movement and abscission completion (Krishnan et al., 2022).

CEP55 and centriolin are centrosome proteins that localize to the cytokinetic midbody during pre-abscission. CEP55 facilitates the recruitment of ESCRT-I and ESCRT-III proteins, essential for abscission (Christ et al.,2016; Yang et al.,2008; Elia et al.,2011). Centrosome mediated vesicle trafficking towards the cytokinetic midbody could facilitate the recruitment of these proteins to the midbody preceding cytokinetic bridge abscission (Gromley et al., 2005; Luxton and Gundersen, 2011). Therefore, a temporal and spatial organization of these centrosome proteins at the cytokinetic midbody could rely on bridge directed vesicle trafficking facilitated by centrosome movement to cytokinetic bridge promoting appropriate abscission completion.

The centrosome needs to relocate to the apical membrane to construct a cilium during cellular epithelialization (Figure 1.2B). This movement of the centrosome is interesting in the context of a developing tissue *in vivo*. One model tissue we utilize, is the development of Kupffer's vesicle (KV) which is the ciliated organ of asymmetry in zebrafish. The KV uses a rosette-like intermediate where KV cells divide and place their cytokinetic bridges toward the center of the rosette where a lumen will form (Figure 1.2B-C, (Rathbun et al., 2020a)). Additionally, a recent study identified that the midbody remnant is necessary to regulate cilia formation (Bernabé-Rubio et al., 2016). It is therefore likely that the cytokinetic bridge and the midbody act as a symmetry breaking event to direct centrosome movement so that they can facilitate cilia formation at the right place and time during tissue formation.

These studies suggest a functional role for centrosome movement during pre-abscission in the context of tissue formation.

1.5 Centrosome positioning during epithelialization and neurogenesis:

Cellular polarization is an essential cellular process wherein non-polarized cells gradually establish apical basal polarity (reviewed in, (Bryant and Mostov, 2008)). To resolve the spatial and temporal mechanisms of centrosome movement during cell processes, two dimensional cells in culture are largely used (highlighted by the inverted triangle in Figure 1.2). During development *in vivo*, cells establish polarity while assembling into complex tissues at appropriate orientations necessary for their function. However, the molecular and cellular mechanisms that modulate centrosome movement during polarity establishment in tissues *in vivo* is not well known. For example, the Kupffer's Vesicle (KV), the organ of asymmetry in zebrafish, is one such tissue, where a mesenchymal group of cells establish apical basal polarity with the centrosomes being transported to the apical membrane to facilitate cilia construction and extension into the lumen formed (Amack and Yost, 2004). These cilia generate a leftward-fluid flow necessary to enable gene expression that set up the left-right body axis of the animal (Grimes and Burdine, 2017). This model tissue is excellent to study the molecular mechanisms of centrosome placement during polarity establishment *in vivo*. It is relevant to note that studies using two-dimensional cell culture and three-dimensional cell culture have identified molecular insights into centrosome placement and provide a basis for targeting these molecules in relation to tissue formation *in vivo*.

A very consistent phenomenon that is observed during cell polarization is that the centrosome reorients towards the apical membrane (Figure 1.3C). Yet, the

spatio-temporal mechanisms that regulate centrosome movement during cellular epithelialization are still unknown. To understand some of these mechanisms we first need to introduce the molecules that regulate cell polarity. Current mechanisms for epithelialization in cells involve cell migration or cell division to find or create neighboring cells that can establish cell-cell contacts. When cell contacts are made, E-cadherin is recruited to these sites creating spatial cues to form primordial adherens junctions (modeled in Figure 1.2A, (Wang and Margolis, 2007)) and tight junctions (modeled in Figure 1.2A, (Baum and Georgiou, 2011)). Around this same time, it is thought that PAR3-PAR6-aPKC and Cdc42 are recruited potentially through the formation of an Apical Membrane Initiation Site (AMIS, (Bryant et al., 2010)). This site is an intracellular grouping of membranes that then fuses with the plasma membrane. The membrane organelles, Golgi apparatus and recycling endosomes, are juxtaposed with the centrosome in many cell types (Hehnly et al., 2012; Pouthas et al., 2008). The centrosome could coordinate cell polarization during tissue formation *in vivo* due to its proximity to the Golgi apparatus and recycling endosomes, as well as the centrosome's ability to transition from a central cellular locale to docking at the apical membrane during epithelial formation.

Molecular components that regulate polarity formation in epithelial cells like E-Cadherin, PAR3 and CDC42 are necessary in centrosome movement to the apical membrane (Donati et al., 2021; Feldman and Priess, 2012; Hong et al., 2010; Inaba et al., 2010; Jiang et al., 2015; Macara and Seldin, 2017). Therefore, it is unclear whether centrosome movement to the apical membrane is necessary for polarity formation or maintenance. Studies using laser ablation to remove centrosomes in *C. elegans* intestinal cells showed that centrosome movement to the apical membrane is involved in cellular epithelialization (Feldman and Priess, 2012). Intriguingly,

studies have also shown that when the apical positioning of the centrosome is disrupted, cell polarity is reversed leading to epithelial cells transitioning to a mesenchymal cell state (Burute et al., 2017). These findings suggest a role for centrosome movement in coordinating cell polarity. Additionally, the studies suggest that the disruption of centrosome positioning during cell epithelialization may promote cells to trigger epithelial to mesenchymal transition, which is a hallmark of cancer progression (Burute et al., 2017; Roche, 2018).

Another cell type that establishes cell polarity are neurons. The centrosome is positioned at the axonal initiation site during neurogenesis in neuronal cells in culture (Barnes and Polleux, 2009; Dotti et al., 1988; Nakamuta et al., 2011; Yogev and Shen, 2017). This localization of the centrosome is dependent on PAR3 at the axon initiation site and is necessary for axon formation during neurogenesis in neuronal cells in culture (de Anda et al., 2005; Shi et al., 2003). During neuronal migration, the centrosome is placed at the leading edge of the cell in a dynein dependent manner and this orientation is necessary for cell migration (Tsai et al., 2007). Since PAR3 directly interacts with dynein during centrosome movement in migrating cells, a similar molecular mechanism may exist in positioning the centrosome at the site of axon formation during neurogenesis. Axon-dendrite polarity in sensory neurons of *C. elegans* depends on the ability of the PAR complex and dynein to recruit the centrosome to the apical membrane to promote formation of dendrites (Lee et al., 2021). The disruption of a centrosome's positioning at the apical junction leads to severe defects in dendrite and axon formation in these neurons (Lee et al., 2021). These findings suggest a molecular mechanism through which polarity proteins and dynein regulate centrosome placement in neurons facilitate microtubule organization at the dendrite or axon during neurogenesis.

1.6 Centrosome positioning during cilia formation.

Centrosomes need to move to the apical membrane during cellular epithelialization to facilitate the formation of cilia (Figure 1.3C). Cilia are microtubule-based structures that are templated from the older centriole of the cell (Mirvis et al., 2018). These structures extend into the extracellular space to sense extracellular cues and relay those cues to the cell body. Most cells in a developed vertebrate have either primary (non-motile) or in some cases motile cilia (Pazour and Witman, 2003; Satir and Christensen, 2007; Shah et al., 2009). Motile cilia can be used to generate and establish fluid flow that mediate function of the tissue. For example, in the node organ of asymmetry in vertebrate organisms, the cilia extending into the lumen create a leftward fluid flow necessary to facilitate asymmetric gene expression to establish the left-right asymmetry of the organism (Grimes and Burdine, 2017; Nonaka et al., 1998).

Intraflagellar transport (IFT) proteins (e.g., IFT88) and the BBSome (Bardet-Biedl syndrome) complex (e.g., BBS4) that are required for cilia function, may also be involved in centrosome positioning during ciliogenesis. These cilia proteins organize at the centrosome even in the absence of a cilium (Delaval et al., 2011; Kim et al., 2004, 2005; Qin et al., 2007; Wood et al., 2012). It was identified that IFT88 was localized at the centrosome and interacts with cytoplasmic dynein during mitosis to recruit spindle pole components involved in centrosome maturation necessary for centrosome placement, spindle formation and orientation (Delaval et al., 2011). BBSome complex of proteins through BBS4 directly interact with the IFT proteins during cilia formation and function (Uytingco et al., 2019). Therefore, it is possible that BBS4 and IFT88 organization at the centrosome is necessary to

regulate centrosome movement in a dynein dependent manner during cilia formation.

Sub structures of the mother centriole, sub-distal and distal appendages, are implicated in centrosome movement and docking to the plasma membrane during cilia formation. The subdistal appendage protein, cenexin, is implicated in both centrosome positioning and cilia formation, whereas the distal appendage protein, CEP164, was dispensable for centrosome positioning, but required for cilia formation (Hung et al., 2016; Ishikawa et al., 2005). Specifically, loss of the distal appendage proteins, CEP164 and CEP83, caused centrosome docking defects at the plasma membrane, a response necessary in cilia formation (Graser et al., 2007; Schmidt et al., 2012). These findings suggest that potentially the sub-distal appendages that are known to anchor microtubules (Hung et al., 2016) are required for positioning the centrosome at the apical membrane, where distal appendages then dock the centrosome to the apical membrane.

One possible mechanism where the subdistal appendage protein, cenexin, could regulate centrosome positioning during cilia formation is to recruit active Rab11 at the centrosome. Rab11 regulates centrosome movement and cilia formation *in vivo* (Knödler et al., 2010; Krishnan et al., 2022; Westlake et al., 2011). Yet, the spatial and temporal organization of when a cell's centrosome constructs a cilium and is transported to the apical membrane in the context of a developing tissue *in vivo* is not known. Using the KV as a model to study centrosome movement and cilia formation *in vivo*, we identify that mesenchymal KV cell's centrosome constructs a cilium intracellularly while rearranging to form a rosette like structure and moving their centrosomes from random intracellular locations to the site of lumen formation in a Rab11 dependent manner (Chapter 4). It is therefore a

possibility that Rab11 through its interaction with cenexin at the centrosome at the right time and place is necessary for the regulation centrosome positioning during cilia formation in tissue development *in vivo*.

Mechanisms that regulate centrosome positioning and docking at the plasma membrane during ciliogenesis are markedly similar to the cytotoxic T-cell lymphocyte immune response. For example, IFT20 is a ciliary transport protein that is involved in clustering lytic granules at the IS in CTLs necessary during immune cell responses to destroying the antigen presenting cell (Finetti et al., 2009, 2014; Stinchcombe et al., 2006). Studies identify that this directed transport is through the interaction of Rab11 associated membrane trafficking and IFT20 (Finetti et al., 2014). Additionally, docking of the centrosome through CEP83 to the IS plasma membrane is necessary for the immune response to destroy the target cell (Stinchcombe et al., 2015). These findings suggest that a relationship between Rab11 endosomes and IFT20 could regulate centrosome movement towards the IS possibly in a cenexin dependent manner. Following which, mother centriolar appendage proteins can facilitate centrosome docking to the plasma membrane required to promote CTL mediated immune response to destroy the target cell. Therefore, suggesting that mechanisms of centrosome movement and docking at the plasma membrane in cells that make a cilium could be conserved in cytotoxic T-cell lymphocytes (CTLs) when they dictate an immune response.

Overall, we provide mechanistic insight into how centrosome positioning is modulated by the coordination of polarity cues, motor protein mediated transport mechanisms, membrane trafficking and ciliary proteins during cell migration, cell division, cellular epithelialization, and cilia formation (Figure 1.5). We highlight that the centrosome itself could modulate its placement and movement through

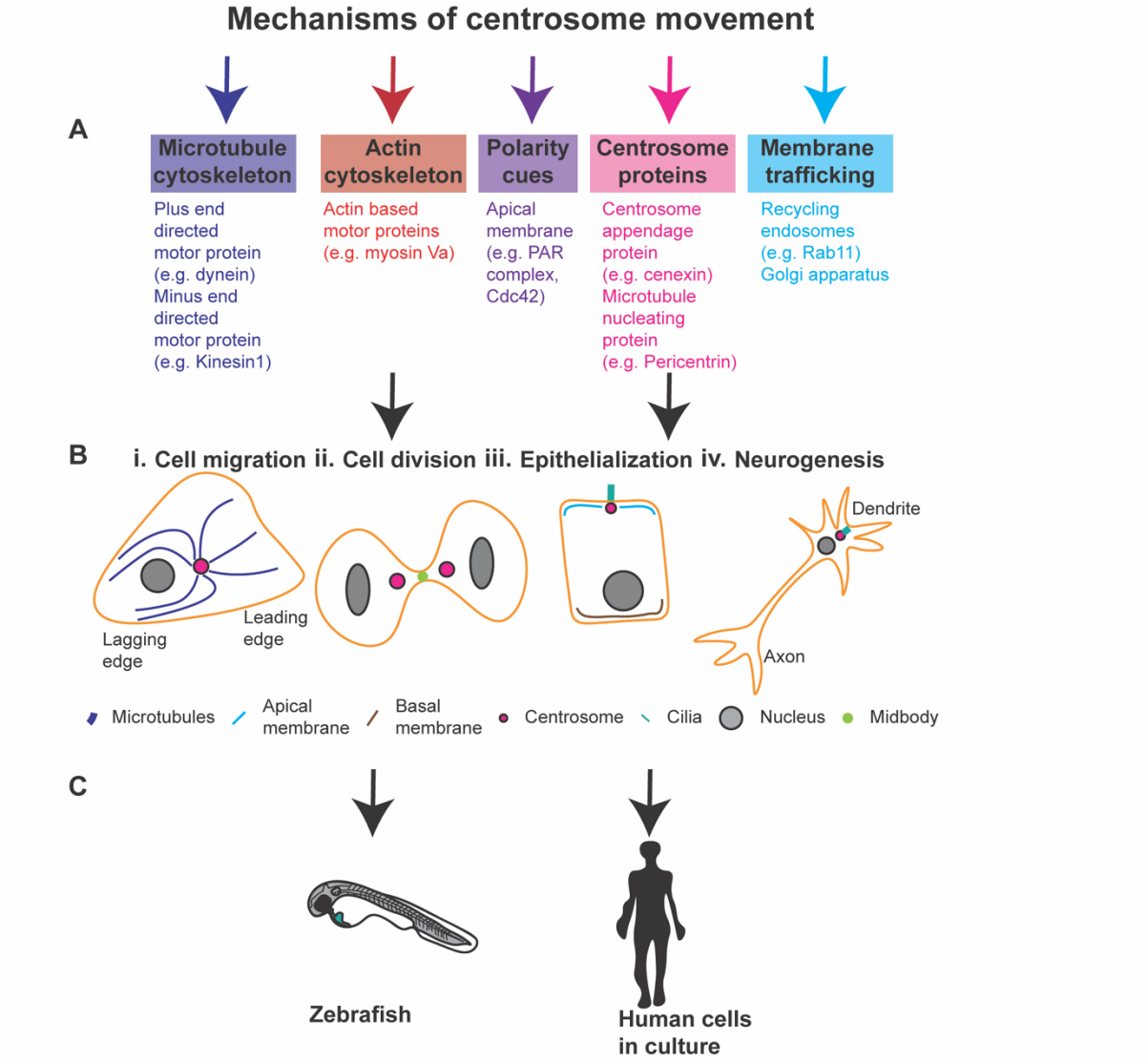

Figure 1.5: Molecular mechanisms that regulate centrosome movement in cells using multimodal approaches.
(A) Molecular mechnaisms that modulate centrosome movement that we have discussed. (B) i. Centrosomes move to set the leading edge of a migrating cell. ii. Centrosomes move from the polar ends of the cell to the cytokinetic bridge during pre-abscission. iii. Centrosomes move to the apical membrane during polarity establishment and cilia formation. iv. Neuronal cell centrosome located near the dendrites. (C) Model organisms zebrafish (*in vivo*) and human cells in culture (Hela cells, *in vitro*) I utilize to study centrosome movement during pre-abscission and cilia formation.

centrosome proteins. For example, contributions of centrosome proteins cenexin, a centriole appendage protein, and Pericentrin, a PCM protein, involved in facilitating centrosome movement and function are discussed. Ascertaining aspects of centrosome movement and function during development will allow us to understand how and when these molecular mechanisms are disrupted in disease states such as MOPDII. Thereby allowing for the identification of molecular targets that could have the potential to be therapeutic interventions.

Spatial organization of the centrosome in cells is dependent on the type of cells used. Studies have largely utilized two dimensional cells in culture to pinpoint the spatio-temporal mechanisms that regulate centrosome movement. There is a growing body of research that is transitioning to the use of three-dimensional cell culture and animal model systems *in vivo* to expand upon the molecular mechanisms identified in cultured cells *in vitro*. Mechanisms from vertebrate animals (e.g. human, mouse, canine and zebrafish) and invertebrates (e.g. fruit flies) demonstrate that centrosome movement is highly regulated (Hannaford et al., 2022; Hehnly et al., 2012; Hung et al., 2016; Lerit and Rusan, 2013; Pouthas et al., 2008; Reck-Peterson et al., 2018; Rusan and Peifer, 2007; Tsai et al., 2007; Zhang et al., 2014). Molecular mechanisms identified in these different cells on how they coordinate centrosome positioning at different cellular processes using different mechanisms create a basis to target specific mechanisms in tissue formation *in vivo*. Our studies, here in, highlight the need for a multimodal approach in identifying the temporal and spatial mechanisms that regulate centrosome movement and placement during tissue formation.

In conclusion, centrosome positioning is necessary in regulating tissue formation *in vivo*. Even though we know centrosomes are organized at particular

locations in the cell during cellular processes, little is known about the molecular mechanisms that regulate centrosome movement to these locales. In this thesis, I aim to identify the spatio-temporal mechanisms that regulate centrosome movement during tissue formation *in vivo*. A potential mechanism that could regulate centrosome movement and placement is the small molecular GTPase, Rab11 and its associated membrane compartment the recycling endosomes. Rab11 endosomes regulate centrosome function during metaphase and organize at the centrosome during interphase (Hehnly and Doxsey, 2014; Hehnly et al., 2012). A cellular event that regulates tissue formation *in vivo* is abscission, cleavage of the cytokinetic bridge (Rathbun et al., 2020a). Studies have identified that cytokinetic bridge directed centrosome movement during pre-abscission is necessary for appropriate abscission completion (Piel et al., 2001). However, the molecular mechanism that regulates centrosome movement to the cytokinetic bridge during pre-abscission was not tested. To study Rab11's involvement in centrosome positioning we generated, characterized, and optimized Rab11 null cells in human cells in culture and an optogenetic approach to acutely inhibit Rab11 endosome mediated membrane trafficking *in vivo* (Chapter 2). We then tested the role of Rab11 endosomes in centrosome bridge directed movement during pre-abscission in human cells in culture and in dividing cells of the zebrafish embryos (Chapter 3). During tissue formation *in vivo,* centrosomes are positioned at the apical membrane with cilia extending into the lumen. Yet the molecular mechanisms that regulate centrosome positioning in this case are not known. Even though Rab11 and Rab8 endosomes are known to regulate ciliogenesis, their role in centrosome and cilia positioning during tissue formation has not been tested. Using the Kupffer's Vesicle ciliated organ of asymmetry in zebrafish as a model to study cell polarization and tissue

formation, we test the role of Rab11 and Rab8 endosomes in centrosome positioning and cilia formation *in vivo* (Chapter 4). We propose a model wherein Rab11 endosomes are necessary for centrosome movement and function during abscission and cilia formation required to create tissues, organs, and organ systems.

CHAPTER TWO:

Optogenetics, an acute method to inhibit Rab11 mediated membrane trafficking *in vivo*.

This chapter features my contributions and select supporting materials to the work published in Nature Communications in 2020.

Cytokinetic bridge triggers *de novo* lumen formation *in vivo*

Rathbun LI[1], Colicino EG[1,2,6], Manikas J[1], O'Connell J[1], **Krishnan N[1]**, Reilly NS[3], Coyne S[2,4], Erdemci-Tandogan G[5], Garrastegui A[1], Freshour J[1], Santra P[2], Manning ML[5], Amack J[2], Hehnly H[*1]

1 Biology Department, Syracuse University, Syracuse, NY, USA

2 Department of Cell and Developmental Biology, SUNY Upstate Medical School, Syracuse, NY, USA

3 Department of Physics and Astronomy, University of Rochester, Rochester, NY, USA

4 Department of Biology, SUNY Geneseo, Geneseo, NY, USA

5 Department of Physics, Syracuse University, Syracuse, NY, USA

6 Current location: Department of Cell and Developmental Biology, University of Michigan Medical School Ann Arbor, MI, USA

Citation: Rathbun, L. I., Colicino, E. G., Manikas, J., O'Connell, J., **Krishnan, N.,** Reilly, N. S., Coyne, S., Erdemci-Tandogan, G., Garrastegui, A., Freshour, J., Santra, P., Manning, M. L., Amack, J. D., & Hehnly, H. (2020). Cytokinetic bridge triggers de novo lumen formation in vivo. *Nature communications*, *11*(1), 1269. https://doi.org/10.1038/s41467-020-15002-8

2.1 Abstract

Cells need to proliferate to increase cell number and facilitate tissue formation. Mitosis consists of four main stages: prophase, metaphase, anaphase, and telophase. These stages ensure that a cell's genome is duplicated and segregated into two daughter cells. After DNA segregation, cytokinesis begins through the formation of an actomyosin based contractile ring that constricts at the equatorial plane of the cell creating a cytokinetic bridge between the two cells. The bridge is cleaved in a process called abscission. When abscission is disrupted, cells become binucleated and can lead to cell death. Rab11, is a small molecular GTPase that regulates pre-abscission mechanisms through its membrane compartment, the recycling endosomes (REs) that transport into the cytokinetic bridge during abscission in mammalian cells in culture. The molecular and cellular mechanisms that regulate abscission *in vivo* is less known. In this chapter we optimize and validate an optogenetic system to acutely inhibit Rab11-mediated membrane trafficking *in vivo*. We find that like Rab11-null cells, acutely inhibiting Rab11-mediated membrane trafficking blocks abscission and leads to cell becoming binucleated *in vitro* and *in vivo*.

2.2 Introduction

The Kupffer's Vesicle (KV) is a ciliated organ of asymmetry in *Danio rerio* (zebrafish). Mechanism of asymmetry establishment is that the organ of asymmetry creates a leftward flow through motile cilia in the extracellular lumen to initiate the asymmetrical expression of three genes, *Nodal*, *Lefty*, and *Pitx2*, across the embryo (Dasgupta and Amack, 2016). In zebrafish, Rab11 depletion is associated with KV morphology defects such as lumen size depletion (Tay et al., 2013; Westlake et al., 2011). Rab11 could potentially modulate lumen size by regulating the ability of polarity components implicated in lumen formation, the Par3/aPKC polarity complex, transport to the apical membrane where the lumen forms (Citations). Interesting, the Par3/aPKC polarity complex also assembles within the cytokinetic bridge along with Rab11 before cytokinetic bridge abscission and their timely positioning in the bridge is required for bridge absicssion (Blasky et al., 2015). Together these findings suggest that the cytokeintic bridge may provide a symmetry breaking event where the apical membrane is marked next to the bridge and once the bridge is cleaved between the two cells (if grown in three-dimensions) a lumen could potentially form between the two. To test whether cytokinetic bridges are used in the construction of a KV lumen, we needed a way to acutely block abscission. An optogenetics system targeting the Rab11 vesicle trafficking pathway was potentially an ideal method (Nguyen et al., 2016).

We created a strategy to acutely disrupt Rab11-membrane trafficking during KV development using optogenetics and compared it control cells and cells that were null for Rab11. While previous studies all relied on siRNAs to deplete Rab11 in mammalian cells (Bryant et al., 2010; Hehnly and Doxsey, 2014; Hehnly et al., 2012; Wilson et al., 2005) based on the rationale that animals null for Rab11 results in

embryonic lethality (Giansanti et al., 2007; Sobajima et al., 2015) . With the onset of CRISPR Cas9 genome editing creating a null-cell line in any cell background has become much easier to obtain. We decided to attempt creating a Rab11-null line in HeLa cells that lack p53 based regulation, a tumor suppressor gene necessary to sense cell cycle errors that then promotes cell death. We rationalized that using HeLa cells may bypass the potential cell-lethality that likely occurs from mitotic errors resulting from Rab11-loss (mitotic errors reported in (Hehnly and Doxsey, 2014; Wilson et al., 2005)).

To determine the temporal role of Rab11-associated vesicles in KV lumen formation and abscission *in vivo*, we acutely inhibited Rab11-associated membrane vesicles through an optogenetic oligomerization approach (modeled from ref., (Nguyen et al., 2016)). Optogenetics, spatial control of protein localization using light, entails the use of proteins that undergo protein-protein heterodimerization in the presence of light. We use CRY2 (Cryptochrome 2) and CIB1 (cryptochrome-interacting basic helix loop helix) proteins native to the *Arabidopsis* plant (Liu et al., 2008). These two proteins undergo hetero dimerization in the presence of blue light (488 nm). We first tested the efficacy of the system in HeLa cells (Figure 2.3) and compared if we obtained the same binucleate phenotype as the Rab11-null cell line. Once confirming that the optogenetic system worked in cell culture, we then acutely inhibit Rab11-associated membrane trafficking *in vivo* and determined whether KV cells also became binucleated (Figure 2.3). Lastly, we examined the role of Rab11 endosomes in lumen formation *in vivo* in the KV (Figure 2.4).

2.3 Results

2.3.1 Rab11-null cells present with abscission defects.

Rab11 endosomes are recruited to the cleavage furrow and regulate abscission completion (Wilson et al., 2005). Western blot analysis was used to confirm Rab11 loss in Rab11-null cells compared to control cells (Figure 2.1A). Control cells exit anaphase and the daughter cells formed are held together by a cytokinetic bridge (white arrow in top panel, Figure 2.1B). These cells contain Rab11 and hence undergo abscission around four hours post cytokinesis (white arrow top panel, Figure 2.1B) . However, Rab11-null cells exit anaphase, and remain attached at the cytokinetic bridge that is unable to sever (yellow arrow, Figure 2.1B) causing the daughter cells to fuse and become binucleated. We quantified the population of binucleated cells in control and Rab11 null cells (Figure 2.1C) and identified a significant increase in the percentage of binucleated cells in Rab11 null cells compared to controls (Figure 2.1D). Taken together, these results suggest that Rab11-null cells demonstrate similar abscission defects to that reported with studies using siRNA to deplete Rab11 in cells (Hehnly et al., 2012; Wilson et al., 2005).

2.3.2 Optogenetic clustering of Rab11-associated vesicles results in failed abscission *in vitro*.

Our goal was to specifically test whether acutely inhibiting Rab11 endosomes during pre-abscission disrupts cleavage of the cytokinetic bridge. To this end we first wanted to test whether our optogenetic system could cluster Rab11 vesicles in the presence of blue light in human HeLa cells. To test this, we first expressed cryptochrome 2-mCherry (CRY2-mCherry) and CIB1-mCerulean-Rab11 in HeLa cells (hetero-interaction between CRY2-fluorescent protein (FP) and CIB1-FP-Rab11

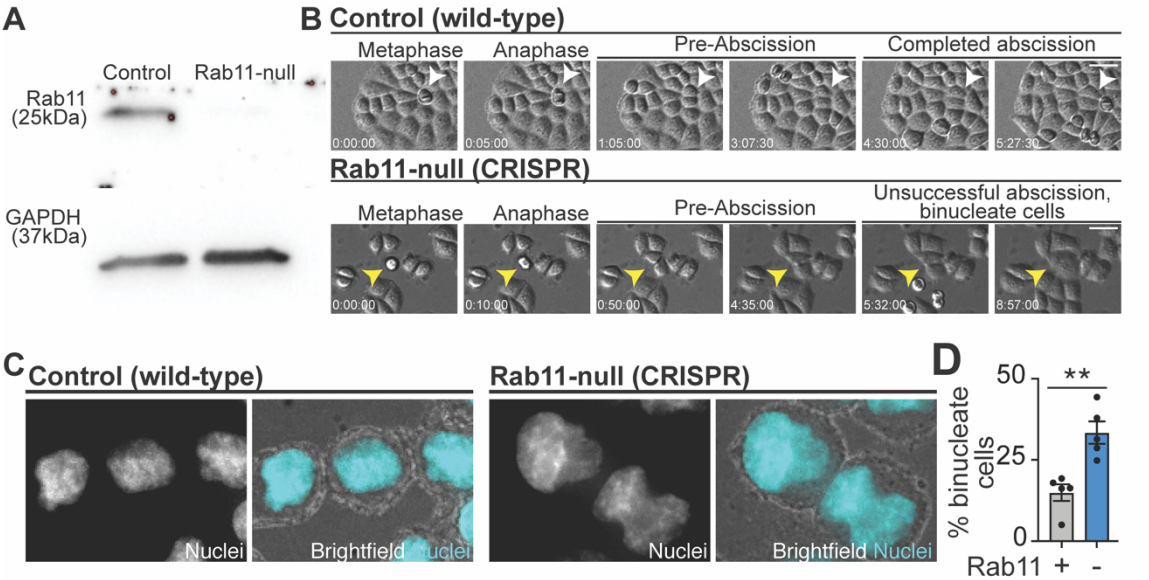

Figure 2.1: Rab11-null cells present with abscission defects.
(A) Western blot depicting Rab11 protein expression in wild-type (left) and Rab11-null CRISPR HeLa cells (right). Rab11 (25kDa) and GAPDH (37kDa) loading control shown. (B) Time lapse images of cell divisions in wild-type (control, top) and Rab11-null CRISPR cells (bottom). Metaphase, anaphase, pre-abscission stages shown with either subsequent completed (white arrowhead) or unsuccessful abscission with binucleate cell resulting (yellow arrowhead). Bar, 50μm. (C) Representative maximum projections of nuclei in wild-type (left) and Rab11-null CRISPR cells (right). Brightfield (grayscale) and nuclei (DAPI, cyan) shown. Bar, 10μm. (D) Bar graph depicting percentage of binucleate cells in wild-type (Rab11-positive, gray) and Rab11-null CRISPR cells (Rab11-negative, cyan). Two-tailed Mann-Whitney p=0.0079 (**), u=0. n=100 cells across n=5 experiments.

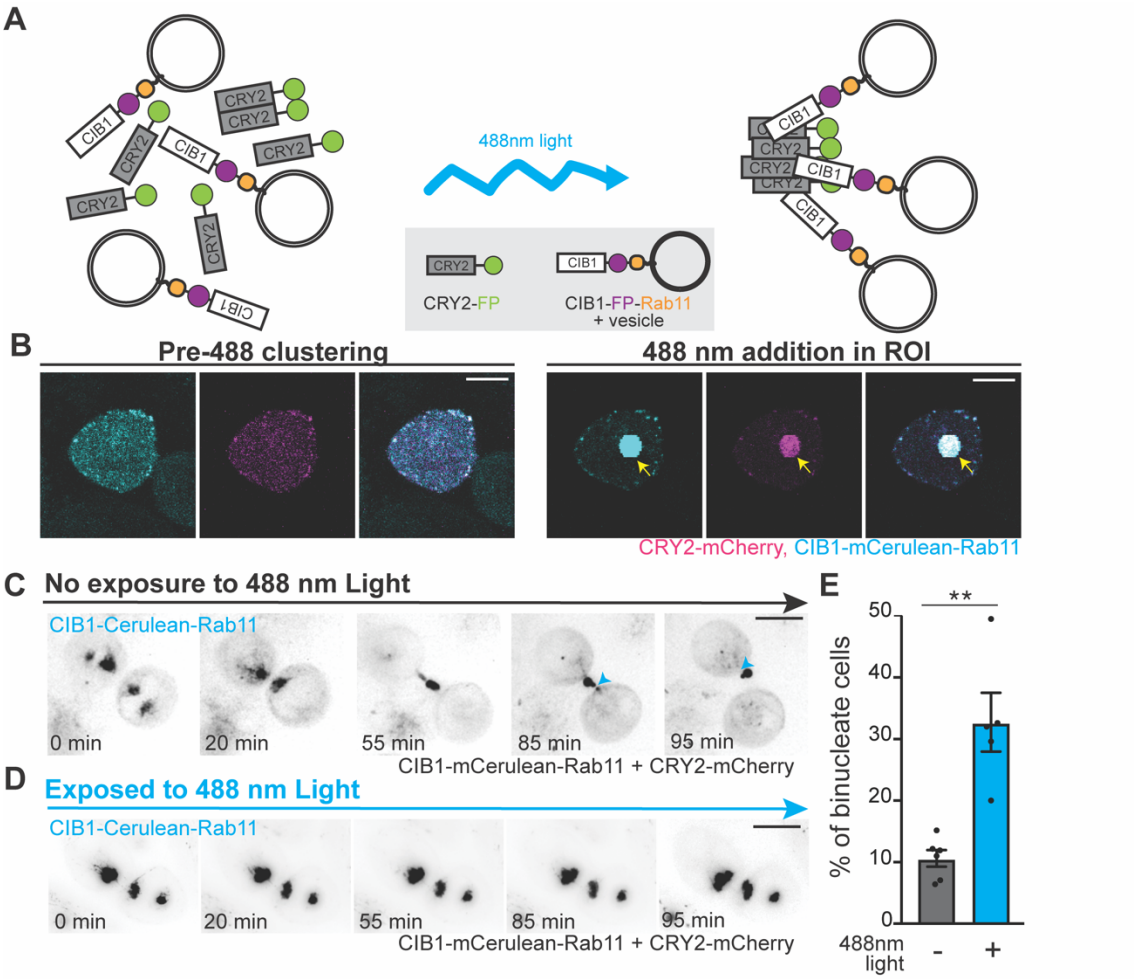

Figure 2.2: Optogenetic clustering of Rab11-associated vesicles results in failed abscission *in vitro*.
(A) Model depicting CRY2/CIB1 optogenetic system utilized in these studies. Since multiple fluorescent molecules are used, FP (fluorescent protein) is used in model for simplicity. CRY2-FP and CIB1-FP-Rab11 shown under conditions of no light (no clustering) or 488nm light (clustering). (B) Example micrograph of HeLa cells before (left) and after (right) exposure to 488nm light within a circular ROI. CRY2-mCherry (magenta) and CIB1-mCerulean-Rab11 (cyan) shown. Bar, 5μm. (C,D) Time-lapse of cytokinetic HeLa cells transfected with CRY2-mCherry and CIB1-mCerulean-Rab11 (black) in the absence (C) or presence of 488 nm light (D). Bar, 10 μm. Note the cleavage events of cytokinetic bridge (blue arrows, A), but not in B. (E) Bar graph depicting the percentage of total HeLa cells displaying a binucleate phenotype after being released from a metaphase synchronization for 2 h in the presence or absence of 488 nm light. Cells were transfected with CRY2-mCherry and CIB1- mCerulean-Rab11 as in A. Unpaired, two-tailed Mann–Whitney test, **p = 0.0043. Mean displayed ± SEM. n = 100 cells per treatment for n > 5 experiments. Dots represent individual values. Statistical results detailed in Methods table 2.1.

modeled in Figure 2.2A). A blue-light (488 nm) was used to induce hetero-interaction between CRY2-mCherry and CIB1-mCerulean-Rab11 within a specific region of interest (ROI), to initiate cellular aggregation of Rab11-associated membranes (Figure 2.2B). To examine whether the cellular aggregation of Rab11-associated membranes disrupts function, HeLa cells expressing the optogenetic constructs in pre-abscission were treated with normal light conditions or 488 nm blue light (Figure 2.2 C-E). Under control conditions, where cells were imaged in the absence of blue light, cells can progress through cytokinesis to abscission within ~90 min (Figure 2.2C). It is noteworthy that CIB1-mCerulean-Rab11 transports into the cytokinetic bridge, where a cleavage event occurs at one side of the midbody (blue arrow; Figure 2.2C) and another event occurs on the other side of the midbody 10 min later (blue arrow, Figure 2.2C). When cells are exposed to 488 nm light throughout the 90-minute time course, Rab11-associated vesicles are unable to move into the cytokinetic bridge and remain clustered within the cell body, inhibiting the ability of this cell to abscise (Figure 2.2D). Under conditions of CRY2-mCherry and CIB1-mCerulean-Rab11 expression with 488 nm blue-light exposure, a significant increase in the percentage of binucleated cells occurred when compared with cells not exposed to the blue light (Figure 2.2E) similar to what we found in the Rab11-null cells (Figure 2.1 C-D).

2.3.3. Optogenetic clustering of Rab11-associated vesicles results in failed abscission *in vivo*.

We next wanted to determine whether this optogenetic approach of acutely clustering Rab11-associated vesicles *in vivo*, using zebrafish could recapitulate the binucleate phenotype seen in HeLa cells (Figure 2.3). To do this we used transgenic zebrafish lines that express fluorescent markers to label KV cells. The transgenic

lines used were Sox17:GFP-CAAX (KV cell membranes) and CFTR-GFP (Cystic Fibrosis Transmembrane conductance Regulator) to label KV cells. We injected mRNA into zebrafish embryos to express CRY2-FP (FP, mCherry, or no FP) and CIB1-FP-Rab11 (FP, either mCerulean or mCherry; Figure 2.3A). Uninjected embryos (control), embryos injected with CRY2-FP mRNA only (control), CIB1-FP-Rab11 mRNA only (control) or injected with both CRY2-FP and CIB1-FP-Rab11 mRNA (experimental) were exposed to normal light or 488 nm blue-light conditions starting at 50–60% epiboly until a late lumen expansion stage (14 hpf, experimental protocol diagram in Figure 2.3A). Embryonic lethality during optogenetic experiments was similar in all injection groups (Figure 2.3B), suggesting that acute clustering of Rab11 membranes during KV development did not result in embryo mortality. Embryos were fixed and the number of binucleate cells were evaluated in KV cells (Figure 2.3 C-D). Strikingly we found a significant increase in the number of binucleated cells in KV under experimental conditions (Figure 2.3E), suggesting that clustering Rab11 vesicles *in vivo* blocks abscission.

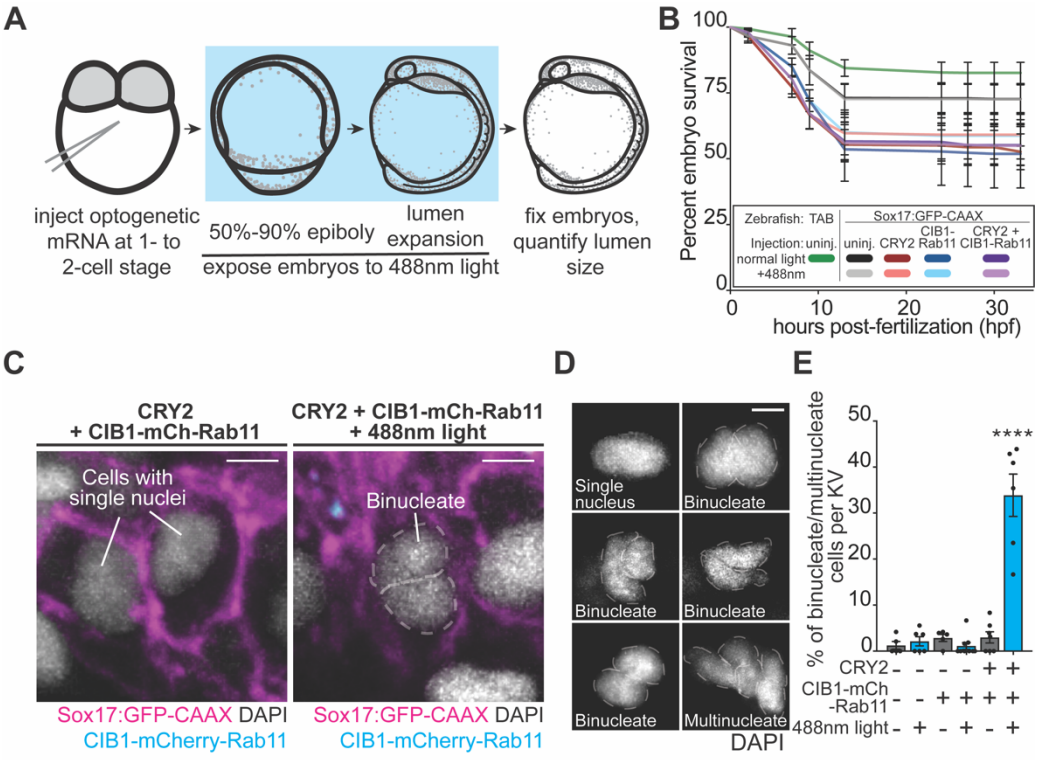

Figure 2.3: Optogenetic clustering of Rab11-associated vesicles results in failed abscission *in vivo*.

(A) Model depicting optogenetic experiment protocol in zebrafish during KV development. (B) Line graph depicting embryo survival during the first 33hpf. Wild-type (TAB) embryos (green, n=655 embryos from 3 clutches), uninjected transgenic embryos +/- 488nm light exposure (grayscale, n=831 embryos from 4 clutches), CRY2-FP-injected transgenic embryos +/- 488nm light exposure (red), CIB1-FP-Rab11-injected transgenic embryos +/- 488nm light exposure (blue), and CRY2-FP + CIB1-FP-Rab11-injected transgenic embryos +/- 488nm light exposure (purple, n=555 embryos from 4 clutches) shown. Mean ± SEM shown. Statistical results detailed in Methods table 2.1. (C) A 3D rendering of embryos expressing CRY2 and CIB1-mCherry-Rab11 in the absence (left) and presence (right) of 488 nm light. Sox17:GFP-CAAX (magenta), CIB1-mCherry-Rab11 (cyan), and nuclei (DAPI —white) shown. Bar, 5 μm. (D) Representative images of single nuclei, binucleate, or multinucleate cells. Nuclei shown in grayscale (DAPI). Bar, 5 μm. (E) Bar graph depicting percentage of binucleate and/or multinucleate cells per KV in uninjected embryos and embryos expressing CIB1-mCherry-Rab11 or CRY2 and CIB1-mCherry-Rab11 plus or minus 488 nm light. One-way ANOVA with Dunnett's multiple comparison test used, compared with uninjected embryos in the absence of 488 nm light exposure. Analyses performed in n > 5 embryos over three experiments. Mean displayed ± SEM. Dots represent individual values. Statistical results detailed in Methods table 2.1.

2.3.4. Optogenetic clustering of Rab11 during KV development results in abnormal lumen formation.

Rab11 mediated membrane trafficking towards apical membrane is necessary to regulate lumen formation in some cell types grown ex-vivo (Bryant et al., 2010). We tested whether acutely clustering Rab11 membranes resulted in KV lumen formation defects. Due to the mosaic nature of mRNA expression in zebrafish, embryos were categorized into five groups: uninjected (control), CRY2-FP mRNA only (control), CIB1-FP-Rab11 mRNA only (control), CRY2-FP plus CIB1-FP-Rab11 mRNA without KV expression (control), and CRY2-FP plus CIB1-FP-Rab11 mRNA with KV expression (experimental). Injected embryos were exposed to 488 nm light at either 50–60% epiboly or 75–90% epiboly (Figure 2.3A). Zebrafish developmental speed can vary due to variations in ambient room temperature (Schnurr et al., 2014). To control for this, lumen area was normalized to the mean of uninjected control embryos within each clutch. This minimized the variation in lumen area due to differences in clutch developmental speed, as control groups demonstrated a range in basal lumen area dependent on the clutch. In double-injected embryos where KV cells have clustered Rab11-associated membranes (488 nm exposure beginning at 50–60% or 75–90% epiboly), significant defects in KV lumen formation occurred such as decreased lumen area or an inability to form a lumen at all (Figure 2.4 A-C) compared with control conditions (Figure 2.4C, left). When clustered Rab11 membranes only occurred in a proportion of KV cells, lumen formation in the non-clustered areas occurred (Figure 2.4A, left; 2.4C, right). In embryos with clustered Rab11 in cells surrounding KV, but not KV cells, KV lumen size was comparable to unclustered-Rab11 control conditions (Figure 2.4 B-C). Overall, these findings

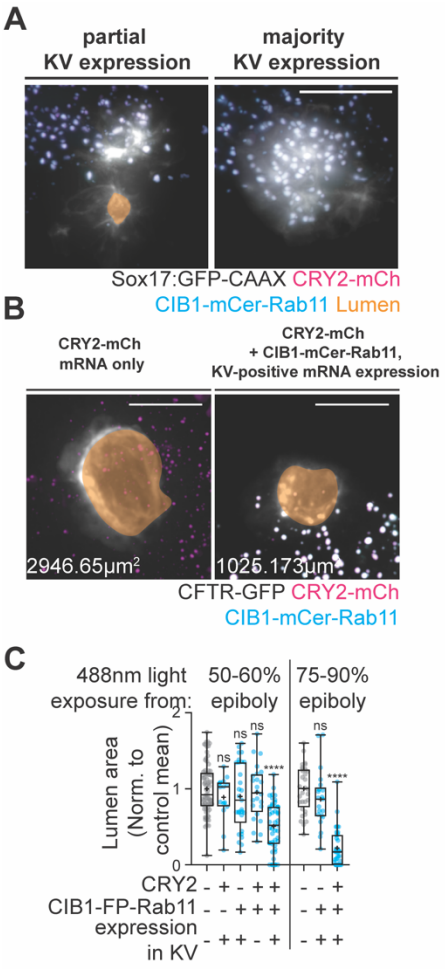

Figure 2.4: Optogenetic clustering of Rab11 during KV development results in abnormal lumen formation.

(A) Representative 3D rendering of KV under conditions of CRY2-mCherry/CIB1-mCerulean-Rab11 plus 488 nm light with partial (top) or majority KV mRNA expression (bottom). 3D rendering with lumen trace (orange), cell membrane (GFP-CAAX, white), CRY2-mCherry (magenta), and CIB1-mCerulean-Rab11 (cyan) shown. Bar, 50 μm.

(B) Representative 3D renderings of KV under conditions of CRY2-mCherry mRNA only, or CRY2-mCherry + CIB1-mCerulean-Rab11 with KV-positive mRNA expression. KV cells (CFTR-GFP, white), CRY2-mCherry (magenta), and CIB1-mCerulean-Rab11 (cyan) shown. Bars, 50 μm.

(C) Box and whisker plot depicting two-dimensional lumen area normalized to uninjected control values plus or minus 488 nm light beginning at 50–60% epiboly (left, n > 15 embryos) or 75–90% epiboly (right, n > 21 embryos). Dots represent individual KV values. Whiskers denote minimum and maximum values,25th and 75th percentiles denoted by box boundaries. Median denoted by line within box and mean denoted by plus sign. One-way ANOVA with Dunnett's multiple comparison test, compared with uninjected embryos.

Statistical results detailed in Methods table 2.1.

suggest that acute inhibition of Rab11-associated vesicles within KV-destined cells disrupts lumen formation.

2.4 Discussion

Abscission has been difficult to study in vivo due to many of the regulators, such as Rab11, being essential for embryo viability (Sobajima et al., 2015). Thus, the ability to acutely block components that regulate this process at different times in development or at specific times in the cell cycle could be transformative to the field. Rathbun et al., optimized and validated an optogenetic approach to acutely inhibit Rab11-associated membrane trafficking *in vivo*. The study identified that inhibiting the Rab11-associated membrane compartment specifically during KV development results in cells being binucleated, due to failed abscission and subsequently unable to make lumens. Additionally, we created a Rab11-null cell line that demonstrated abscission defects as seen when Rab11 vesicles are optogenetically clustered in cells. Based on these findings we conclude that spatial and temporal coordination of Rab11-associated membrane trafficking is necessary for regulating abscission and lumen formation *in vivo*. Optogenetic control of Rab11 endosomes *in vivo* is therefore an invaluable tool for establishing the role of Rab11 endosomes in regulating cell division and tissue morphogenesis *in vivo* (Rathbun et al., 2020a) that is employed in the subsequent chapters of my thesis.

2.5 Materials and methods

2.5.1 Rab11 optogenetic clustering in HeLa cells: HeLa cells were transfected with CIB1-mCerulean-Rab11 and CRY2-mCherry using Mirus TransIT-LT1 and then synched at prometaphase in nocodazole (100 nM) and released after 6 h in the presence or absence of 488 nm light. Cells were imaged on a spinning disk confocal microscope. Images of dividing cells were acquired for a time-lapse series or cells were imaged 2 h post release to quantify binucleate cells.

2.5.2 Rab11a CRISPR: HeLa cells expressing FIP3-GFP stably were used throughout the study, maintained at 37 °C with 5% CO_2. Rab11A CRISPR vector (Santa Cruz SC-400617) and Rab11A HDR vector (Santa Cruz SC-400617-HD) were transfected into cells using the Mirus TransIT-LT1 transfection reagents (catalog number MIR2305) using the manufacturer's specifications. Cells were grown in puromycin selection medium (5 µg/ml). Three single clones were isolated and tested for Rab11 levels using western blotting. HeLa cells are maintained at 37 °C with 5% CO_2.

2.5.3 Zebrafish optogenetics experiments: Optogenetic experiments were performed by injecting CRY2-mCherry and/or CIB1-mCerulean-Rab11 (or CRY2 and/or CIB1-mCherry-Rab11) mRNA into zebrafish embryos at the one-cell stage. Embryos were exposed to 488 nm light using the NIGHTSEA fluorescence system from 60% or 75–90% epiboly (late exposure experiments) until six- to eight-somite stage. Embryos were either fixed with 4% paraformaldehyde (PFA) + 0.5% Triton X-100 in phosphate buffered saline (PBS) or incubated overnight in the absence of 488 nm light to evaluate death rates. Fixed embryos were then imaged on a confocal microscope as described above.

2.5.4. Immunofluorescence of zebrafish embryos: Zebrafish embryos were fixed using 4% PFA containing 0.5% Triton X-100 overnight at 4 °C. Zebrafish were then dechorionated and incubated in PBST (PBS + 0.1% Tween) for 30 min. Embryos were blocked using a Fish Wash Buffer (PBS + 1% bovine serum albumin (BSA) + 1% DMSO + 0.1% Triton X-100) for 30 min followed by primary antibodies incubation (antibodies diluted in Fish Wash Buffer in concentrations stated in method table 2) either overnight at 4 °C or 3 h at room temperature. Embryos are then washed five times in Fish Wash Buffer before incubating with secondary antibodies for 3 h at room temperature. After five more washes, embryos were incubated with 4′,6-diamidino-2-phenylindole (DAPI; NucBlue® Fixed Cell ReadyProbes® Reagent) for 30 min. For imaging, embryos were either halved and mounted on slides using Prolong Diamond (Thermo Fisher Scientific catalog number P36971) or whole-mounted in 2% agarose (Thermo Fisher catalog number 16520100).

2.5.5 Western blot: Cell lysates were acquired by suspending cells in lysis buffer (HSEG buffer pH 7.4: 40mM HEPES, 40mM NaCl, 5mM EDTA, 4% Glycerol, 20mM NaF; 1% TritonX-100; 1X protease inhibitor; 0.1mM PMSF). After collecting post-nuclear supernatant from lysates, protein concentration was calculated using Bio-Rad Protein Assay Kit II (see method table 2). Standard Western blot procedures were performed. Nitrocellulose membranes were probed with primary antibody and/or primary antibody conjugated to horseradish peroxidase diluted in TBS-Tween20 and incubated overnight at 4^{o}C. The membranes were probed using appropriate secondary antibody for an hour at room temperature. The protein levels were visualized using Clarity^{TM} Western ECL substrate (see supplementary key resource table) and imaged using Bio-Rad ChemiDoc^{TM} imager.

2.5.6 Image and data analysis: Images were processed using both FIJI/ImageJ software, IMARIS (Bitplane), and/or Adobe Photoshop. Angles were calculated using FIJI/ImageJ software and Microsoft Excel. All graphs were generated and statistical analysis performed using GraphPad Prism software. The 3D images, movies, and surface rendering were performed using Bitplane IMARIS (Surface, Smoothing, Masking, and Thresholding functions).

2.5.7 Statistics and reproducibility: Unpaired, two-tailed Student's *t*-tests, Mann–Whitney, and one-way analysis of variance analyses were performed using GraphPad Prism software; ****p-value < 0.0001, ***p-value < 0.001, **p-value < 0.01, *p-value < 0.05. See method table 1 for detailed information regarding statistics.

All graphs, micrographs, images, and blots in this study are representative of at least three independent experiments.

2.5.8 METHODS TABLE 1: Statistical analysis reported.

Figure	Category	n	Statistical test	Parameters	Result	p-value
2.1	Control vs Rab11 CRISPR	5	Mann-Whitney test (two-tailed)	U = 0	**	0.0079
2.2	CRY2 + CIB1-mCherry -Rab11	6	Mann-Whitney test (two-tailed)	U = 0	**	0.0043
	CRY2 + CIB1-mCherry -Rab11 + 488nm light	5				
2.4C early	uninjected	73	One-way ANOVA with Dunnett's multiple comparison	df=183 F(4,183)=15.43	control	n/a
	CRY2 only	15			ns	0.8467
	CIB1 only	29			ns	0.7293
	CRY2+CIB1, no KV	24			ns	0.9946
	CRY2+CIB1, +KV	47			****	<0.0001
late	uninjected	11	One-way ANOVA with Dunnett's multiple comparison	df=83 F(2,83)=58.28	control	n/a
	CIB1 only	8			ns	0.6908
	CRY2+CIB1, +KV	18			****	<0.0001

2.5.9 METHODS TABLE 2: Key resource table

Reagent or RESOURCE	Source	Identifier
Antibodies		
Rab11	Cell Signaling Technologies	3539S; RRID: AB_2253210
GAPDH-HRP	Proteintech	HRP-60004; RRID: AB_2737588
Donkey Anti-Rabbit-HRP	Jackson Immuno Research	711-035-152; RRID: AB_10015282
Anti-GFP	GeneTex	GTX13970; AB_371416
Chemicals, Peptides, and Recombinant Proteins		
DAPI	SigmaAldrich	D9542-10mg
NucBlue™ Fixed Cell stained Ready Probes	ThermoFischer	R37606
NucBlue™ Live Ready Probes	ThermoFischer	R37605
Agarose	ThermoFischer	16520100

BSA	Fisher Scientific	BP1600-100
BIO BASIC Maxi Prep Kit	BIO BASIC	9K-0060023
Dimethylsulphoxide	Fisher Scientific	BP231-100
Paraformaldehyde	Fisher Scientific	O4042-500
Phosphate Buffered Saline	Fisher Scientific	10010023
Life Technologies Prolong Diamond Antifade Moutant with DAPI	Fisher Scientific	P36971
35 mm Dish| No.1.5. coverslip| 20 mm Glass Diameter	MatTek Corporation	P35G-1.5-20-C
Molecular Probes Prolong Gold Antifade Moutant	Fisher Scientific	P36934
Triton X-100	Fisher Scientific	BP151500
Tween 20	ThermoFischer	BP337500
Tris-HCl	Fisher Scientific	BP153
APS	Fisher Scientific	BP179-100

40% Acrylamide	Sigma-Aldrich	A4058-100ML
97% Sodium acrylate	Sigma-Aldrich	408220-25G
40% Bisacrylamide	EMD Millipore	1300-500ML
TEMED	Fisher Scientific	BP150-100
Ethylenediaminetetraacetic acid (EDTA)	Fisher Scientific	BP120
Sodium Chloride	Fisher Scientific	BP358
NEBuilder HiFi DNA assembly Cloning Kit	New England BioLabs	E5520S
mMESSAGE mMACHINE^{TM}SP6	Invitrogen	AM1340
Mirus TransIT-LT1 transfection	Mirus	MIR2305
Rab11A CRISPR Vector	Santa Cruz Biotechnology	SC-400617
Rab11A HDR Vector	Santa Cruz Biotechnology	SC-400617-HD
BioRad Protein Assay Kit II	BioRad Laboratories	5000002
Ponceau Stain	Boston BioProducts	ST-180-500

Clarity™ Western ECL substrate	BioRad Laboratories	170560
Experimental models: Cell lines		
HeLa Cells with stable GFP-FIP3	Hehnly and Doxsey 2014; Hehnly et al., 2012; Wilson et al., 2005	N/A
Rab11KO HeLa Cells with stable GFP-FIP3	Rathbun et al., 2020	N/A

2.5.10 METHODS TABLE 3: Plasmid constructs

Construct	**Backbone**	**Tag**	**Injection Type**	**Concentration [pg]**
CRY2	pCS2	mCherry/untagged	mRNA	100
CIB1-Rab11	pCS2	mCerulean/mCherry	mRNA	100

2.5.11 METHODS TABLE 4: Zebrafish Transgenic Lines

Type	**Name**	**Source**
Wild-Type	TAB	Zebrafish International Resource Center (ZIRC)
Transgenic	*Tg(sox17:GFP-CAAX)^{sny101}*	Dasgupta et al., 2018
Transgenic	*Tg(sox17:GFP)*	Sakaguchi et al., 2006
Transgenic	*Tg(sox17:dsRED)*	Chung et al., 2008
Transgenic	*TgBAC(cftr-GFP)*	Navis et al., 2013

CHAPTER THREE:

Rab11 endosomes and Pericentrin coordinate centrosome movement during pre-abscission *in vivo*.

This chapter features work from my first author paper published in Life Science Alliance in 2022.

Rab11 endosomes and Pericentrin coordinate centrosome movement during pre-abscission *in vivo*.

Nikhila Krishnan[1], Maxx Swoger[2], Lindsay I. Rathbun[1,3], Peter J. Fioramonti[1], Judy Freshour[1], Michael Bates[1], Alison E. Patteson[2], and Heidi Hehnly[1]

[1] Syracuse University, Department of Biology, 107 College Place, Syracuse, NY 13244, USA

[2] Syracuse University, Department of Physics, Syracuse, Physics Building, Syracuse, NY 13244, USA

[3]Current location: University of Rochester, Rochester, NY

*Lead contact, correspondence: hhehnly@syr.edu, Twitter: @LovelessRadio

This work is a duplicated version of the published manuscript.

Citation: Krishnan, N., Swoger, M., Rathbun, L. I., Fioramonti, P. J., Freshour, J., Bates, M., Patteson, A. E., & Hehnly, H. (2022). Rab11 endosomes and Pericentrin coordinate centrosome movement during pre-abscission in vivo. *Life science alliance*, *5*(7), e202201362. https://doi.org/10.26508/lsa.202201362

3.1 Summary

Cell division completes when the two daughter cells move their oldest centrosome towards the cytokinetic bridge, which is then cleaved during abscission. The GTPase, Rab11, and the centrosome protein, Pericentrin, work together to coordinate this movement.

3.2 Abstract

The last stage of cell division involves two daughter cells remaining interconnected by a cytokinetic bridge that is cleaved during abscission. Conserved between the zebrafish embryo and human cells, we found that the oldest centrosome moves in a Rab11-dependent manner towards the cytokinetic bridge sometimes followed by the youngest. Rab11-endosomes are organized in a Rab11-GTP dependent manner at the mother centriole during pre-abscission, with Rab11 endosomes at the oldest centrosome being more mobile compared to the youngest. The GTPase activity of Rab11 is necessary for the centrosome protein, Pericentrin, to be enriched at the centrosome. Reduction in Pericentrin expression or optogenetic disruption of Rab11-endosome function inhibited both centrosome movement towards the cytokinetic bridge and abscission, resulting in daughter cells prone to being binucleated and/or having supernumerary centrosomes. These studies suggest that Rab11-endosomes contribute to centrosome function during pre-abscission by regulating Pericentrin organization resulting in appropriate centrosome movement towards the cytokinetic bridge and subsequent abscission.

3.3 Introduction

During the onset of cell division, the centrosome duplicates to build a bipolar mitotic spindle, which is a macromolecular machine that ensures each daughter cell receives an equal complement of chromosomes. Following chromosome separation, cytokinetic furrow formation, and the dismantling of the bipolar spindle, the daughter cell centrosomes migrate from one end of the cell towards the cytokinetic bridge in HeLa cells and were suggested to be required for cytokinetic bridge cleavage, referred to as abscission (Piel et al., 2001). Supporting this idea, human cells lacking centrioles, following centrinone treatment can present with increased multinucleation, indicative of abscission defects (Wang et al., 2020). Bringing into possible question the role of the centrosome movement towards the bridge during pre-abscission was a study that demonstrated in different mammalian cell lines a range of centriole motions during pre-abscission, with some directed towards the bridge and other motions being highly irregular (Jonsdottir et al., 2010). We propose that directed movement of the centrosome towards the cytokinetic bridge may be used during tissue morphogenesis (Hall and Hehnly, 2021), where the cytokinetic bridge and associated midbody can act as a symmetry breaking event to direct events at the apical membrane such as cilia formation (Bernabé-Rubio et al., 2016). This would require the centrosome to migrate towards this site and then subsequently dock with the apical membrane to form a cilium. A model tissue that can be used to examine this is the ciliated organ of asymmetry known as Kupffer's vesicle (KV) in *Danio rerio* (zebrafish). KV morphogenesis first requires a group of migratory cells to divide and then self-assemble into a rosette-like structure. KV cells then position their cytokinetic bridges towards the rosette center before the rosette transitions into a cyst-like structure with a hollow fluid-filled lumen (Rathbun et al.,

2020a). Our studies expand upon these ideas, where we find that centrosomes reorient towards the cytokinetic bridge at the center of the rosette. In addition, we identify a potential mechanism involving the small GTPase Rab11 in centrosome motility both in human cell culture and in zebrafish embryonic cells.

Rab11 and its associated membrane compartment, recycling endosomes (REs), localize to a specific sub-structure of the interphase centrosome, mother centriole appendages (Hehnly et al., 2012). This association was shown to help modulate cargo transport through the RE (Hehnly et al., 2012; Naslavsky and Caplan, 2020). REs are an endocytic compartment that accepts endocytosed cargo from the early endosomes and recycles it back to the plasma membrane (Welz et al., 2014). Owing to the nature of centriole duplication, the two daughter cell centrosomes are inherently asymmetric from one another with the oldest centrosome being enriched with centriole appendage proteins (Colicino et al., 2019; Hung et al., 2016) and more competent for cilia formation (Anderson and Stearns, 2009). When RE function is disrupted by depleting Rab11 in human cells in culture, centrosome function is potentially disrupted resulting in a loss of cilia formation during G_0 (Knödler et al., 2010; Westlake et al., 2011; Xie et al., 2019). Based on this relationship between Rab11-REs and the oldest of the centriole pair (the mother centriole) during interphase, we hypothesize that the centrosome requires an association with Rab11-REs during pre-abscission for its directed movement towards the cytokinetic bridge.

Many modes of centrosome movement have been documented (Vaughan and Dawe, 2011), of note is centrosome migration during *Drosophila melanogaster* neuroblast divisions (Hannaford et al., 2022; Lerit and Rusan, 2013; Rebollo et al., 2007; Rusan and Peifer, 2007). In this context, the centrosome duplicates during S-

phase where one centrosome migrates to the distal side of the cell to mature. This migratory process involves Pericentrin-like protein (PLP) along with Polo Kinase (Lerit and Rusan, 2013). Our studies have expanded upon these findings where we identify that directed centrosome movement towards the cytokinetic bridge uses mechanisms involving both Pericentrin and Rab11-endosomes.

The recycling endosome compartment is involved in numerous cellular processes including, but not limited to, cilia formation, lumenogenesis, apical polarity formation, and abscission (Bryant et al., 2010; Knödler et al., 2010; Rathbun et al., 2020a; Westlake et al., 2011; Wilson et al., 2005). Rab11-associated recycling endosomes transport with their associated cargo into the cytokinetic bridge (Montagnac et al., 2008) where they fuse at the cleavage furrow (Goss and Toomre, 2008). Following furrow ingression, animal cells stay interconnected for some time by a narrow intercellular bridge that contains a proteinaceous structure known as the midbody (reviewed in (Chen et al., 2012)). These endosomes can fuse and potentially prime the membranes next to the midbody for an abscission event (Schiel et al., 2012). When depleting Rab11 using siRNAs (Wilson et al., 2005) or inhibiting the ability of Rab11-associated vesicles to transport into the bridge using optogenetics (Rathbun et al., 2020a), abscission failure occurs both in cell culture and in the zebrafish embryo. However, the relationship between Rab11-associated recycling endosomes and the centrosome during this process has not been investigated. Here we investigate whether Rab11 can influence centrosome function and movement during pre-abscission.

3.4 Results

3.4.1. Differences in mitotic centrosome movement towards the cytokinetic bridge during pre-abscission between zebrafish embryos and human cells.

We tested whether centrosome reorientation towards the cytokinetic bridge is a conserved process by comparing zebrafish embryo cells at 50% epiboly (3-5 hours post fertilization, Figure 3.1A, 3.1E, S3.1A), zebrafish KV cells (Figure 3.1B-3.1E), and human HeLa cells (Figure 3.1E, S3.1B). Dividing zebrafish cells expressing two different centrosome markers, centrin-GFP (Rathbun et al., 2020b; Zolessi et al., 2006) or PLK1-mCherry (PLK1-mCh) (Rathbun et al., 2020a), were imaged (Figure 3.1A-3.1D, S3.1A, Video S3.1) and compared to human (HeLa) cells expressing the centrosome markers DsRed-PACT (a C-terminal centrosome targeting domain taken from Pericentrin, Figure S3.1B) or centrin-GFP (Figure 3.1E, (Kuo et al., 2011; Piel et al., 2001)). Dividing cells are marked by expression of PLK1-mCh during epiboly and KV development, which can mark the centrosome and cytokinetic midbody (Figure 3.1a', 3.1C-D). Live cell Imaging was performed on both dividing epiboly cells and KV cells where we note at least one centrosome reorienting towards the cytokinetic bridge (Figure 3.1A, 3.1a', 3.1C-3.1D). Specifically, with KV dividing cells we find that the dividing cell within a rosette pinches its cytokinetic bridge towards the rosette center, and then begins to reorient at least one of the two centrosomes towards that site (Figure 3.1B-3.1D).

Centrosome movement was quantified by monitoring live-cell acquisitions from embryos and human cells. We calculated whether both daughter cell centrosomes, only one daughter cell centrosome, or neither centrosome moved from the polar ends of the daughter cells across the cell centroid position (modeled in Figure S3.1D) towards the cytokinetic bridge (Figure S3.1C-S3.1E). We also

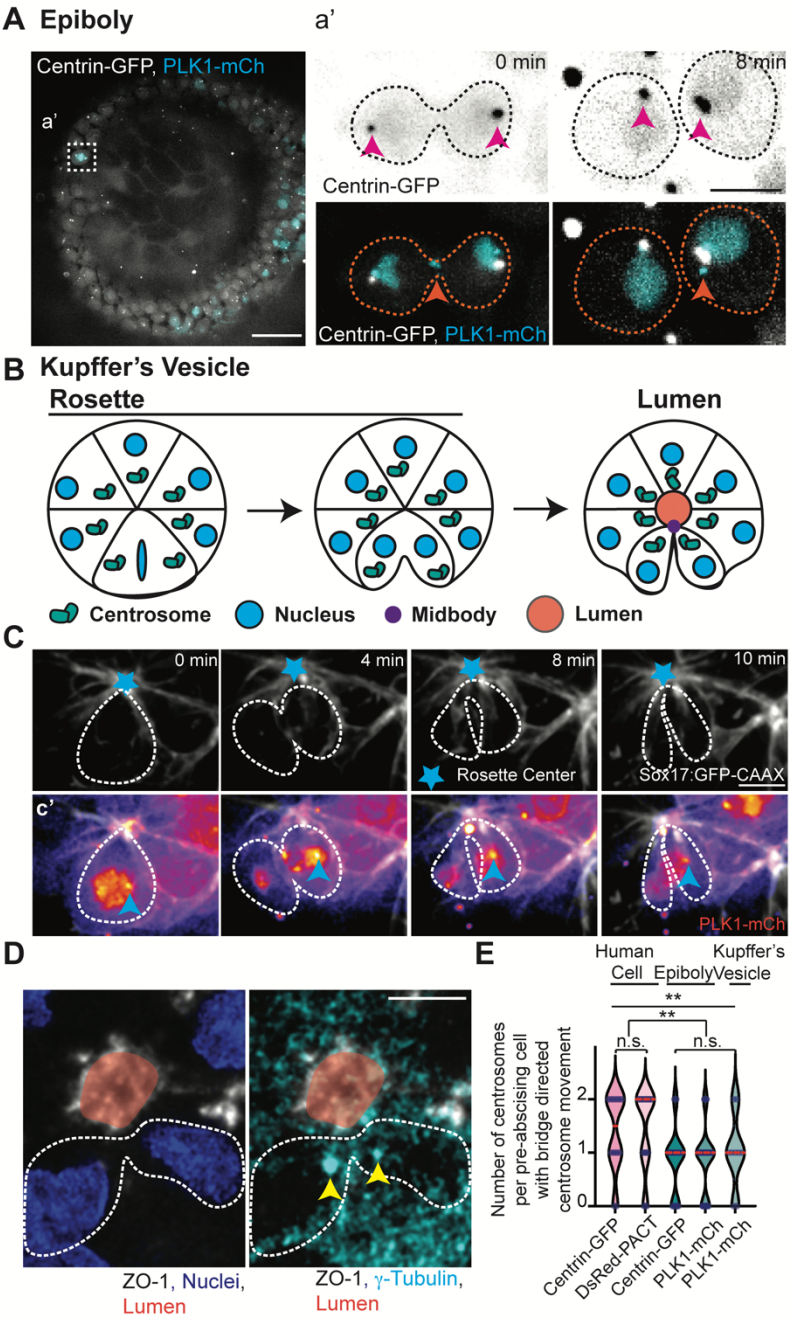

Figure 3.1: Differences in mitotic centrosome movement towards t he cytokinetic bridge during pre-abscission between zebrafish embryos and human cells.
(A) Zebrafish embryo (5 hours post fertilization) with centrin-GFP (gray) and PLK1-mCh (cyan). Scale bar, 50 μm. (a') Inset of dividing cell in A. Time-lapse of centrin-GFP (inverted grays, top panel; grays, bottom panel) and PLK1-mCh (cyan). Video S1. Pink arrow, centrosome. Orange arrow, midbody. Dashed lines, cell boundaries. Scale bar, 10 μm. (B) Model depicting centrosome (green) movement towards the cytokinetic bridge in dividing cells within the Kupffer's Vesicle (KV) during its development. Cyan, Nucleus. Purple, Midbody. Orange, Lumen. Dark lines, KV membranes. (C) Time-lapse of a dividing cell within the KV. KV cell membranes marked with Sox17:GFP-CAAX (gray). Cyan star, rosette center. Cyan arrow, centrosome. Dashed lines, cell boundaries. Scale Bar, 10 μm. (c') Dividing cell depicted with PLK1-mCh (fire LUT). Cyan arrow, centrosome. (D) A KV pre-abscising cell fixed and immunostained for ZO-1 (gray), γ-tubulin (cyan) and DNA (DAPI, blue). Yellow arrow, centrosome. Dashed lines, cell boundaries. Scale bar, 10 μm. (E) Number of centrosomes per pre-abscising cell with bridge directed centrosome movement calculated as both centrosomes (2 centrosomes), only one centrosome (1 centrosome) and neither centrosome (0 centrosomes) moved shown as a violin plot with median (orange) and quartiles (dark dotted lines). Two-tailed student's t-test between Centrin-GFP and DsRed-PACT in Human (HeLa) cells (pink background). n>10 cells across n>3 experiments n.s. not significant. One-Way ANOVA across zebrafish epiboly cells and KV cells (green background), n.s. not significant. n>10 cells across n>2 embryos. One-Way ANOVA, across all columns, **p<0.01. Two-tailed student's t-test between Human (HeLa) cells and zebrafish (Epiboly, KV) cells, **p<0.01. n-values, detailed statistical results in Table S1.

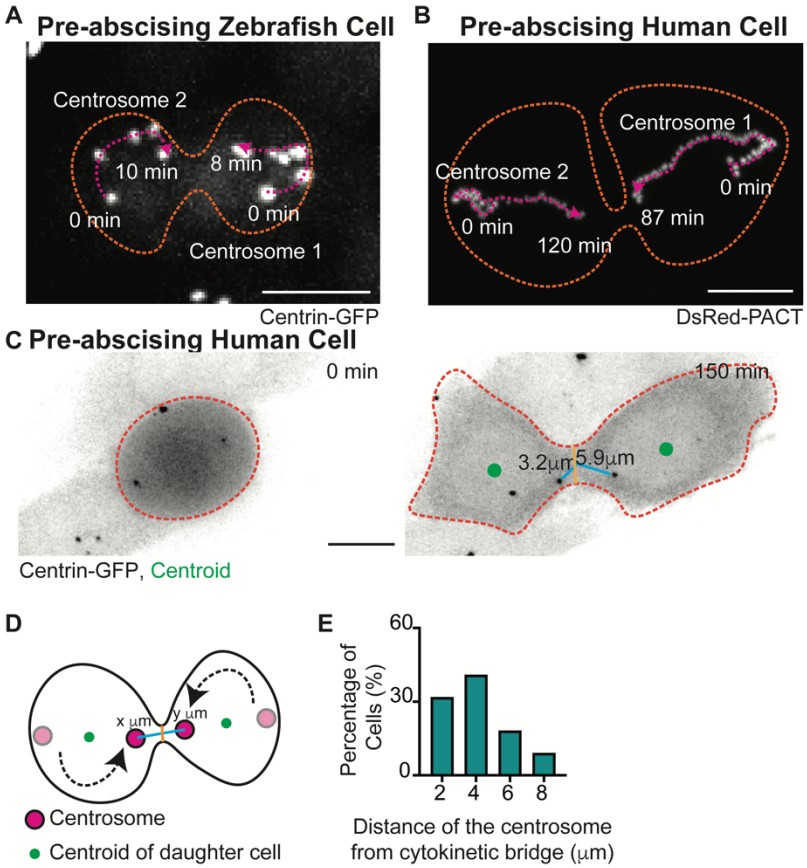

Figure S3.1: Differences in mitotic centrosome movement towards the cytokinetic bridge during pre-abscission between zebrafish embryos and human cells. (A-B) Overlay of centrosome movement within pre-abscising zebrafish embryo cell (A) and human (HeLa) cell (B) over time. The centrosome is labeled with centrin-GFP (zebrafish embryo cell, gray) and DsRed-PACT (human HeLa cell, gray). Pink dashed line with arrow, centrosome track. Orange dashed lines, cell boundaries. Scale bar, 10 μm. (C) Time-lapse of a pre-abscising human (HeLa) cell expressing centrin-GFP (inverted grays). Green dot, centroid of cell. Orange dashed lines, cell boundaries. Brown line, width of the cytokinetic bridge. Cyan line, distance of the centrosome from the midpoint of the cytokinetic bridge (μm). Scale bar, 10 μm. (D) Model depicting quantification related to centrosome movement towards the cytokinetic bridge. Magenta circle, centrosomes. Black line, cell boundaries. Brown line, width of the cytokinetic bridge. Cyan line, distance of the centrosome from the midpoint of cytokinetic bridge (μm). (E) Percentage of pre-abscising cells (%) that moves the centrosome to at least 2, 4, 6, and 8 μm from the midway point of the cytokinetic bridge.

determined the distance of the centrosome from the cytokinetic bridge in human cells by drawing a line from the centrosome to the midpoint of the cytokinetic bridge (modeled in Figure S3.1D). We identified in human cells that most cells moved both their daughter cell centrosomes towards the cytokinetic bridge (Figure 3.1E), and a majority of the centrosomes moved within a 4 μm distance from the bridge center (Figure S3.1E) with very few entering into the cytokinetic bridge itself (example of movements in Figure S3.1A, S3.1C). In zebrafish epiboly cells, KV cells, and human cells we find that in most cases at least one centrosome moves towards the cytokinetic bridge (Figure 3.1E). However, we do find a significant difference between human cells and zebrafish cells in which both centrosomes (human) or one centrosome (zebrafish) preferentially moves towards the bridge (Figure 3.1E). Unlike human cells where one centrosome moves in before the other (Figure S3.1B), we find that a significant majority of zebrafish pre-abscising cells during epiboly and KV development had only one centrosome move consistently towards the cytokinetic bridge before bridge abscission (Figure 3.1E). One possibility with KV cells is that the other centrosome moves up to the apical site following abscission. Since one centrosome moves towards the cytokinetic bridge before the other in human cells, and invariably only one centrosome moves towards the bridge in zebrafish pre-abscising cells, this suggests a potential asymmetry between the two centrosomes, such as centrosome age, contributing to this behavior.

3.4.2. Mitotic centrosomes associate with Rab11 endosomes as they reorient towards the cytokinetic bridge.

Rab11 could be a modulator of centrosome movement since its known to associate with mother centriole appendage proteins during interphase (Hehnly et al., 2012). However, its dynamic organization in relation to the centrosome during mitotic exit hasn't been specifically investigated. We examined Rab11 localization between human (HeLa) cells and dividing cells in the zebrafish embryo.

We monitored spatial and temporal association of Rab11, and its effector protein, family of Rab11-interacting protein (FIP3), with the centrosome during pre-abscission in HeLa cells. The Rab11-effector protein FIP3 was tagged with GFP (Wilson et al., 2005) and expressed in HeLa cells with a centrosome marker, DsRed-PACT (Figure 3.2A). We found a population of REs at the centrosomes during anaphase and this population significantly increased as the cell progressed through cytokinesis and pre-abscission (Figure 3.2A, S3.2A-B, Video S3.2). A second population of REs then forms adjacent to the cytokinetic bridge following the formation of the centrosome population, the centrosome then reorients with a population of REs to this second RE population (Figure 3.2A, 3.2E, S3.2A, Video S3.2). Another membrane organelle, the Golgi apparatus (labeled with MannII-mRuby2), is dispersed in small puncta during cytokinesis and starts to form two separate fragmented compartments next to the centrosome and the bridge (Figure S3.2C). This localization pattern is different from the REs that remain tightly organized at the centrosome and adjacent to the bridge (Figure S3.2A). To test if the second population of REs originated from the REs organized at the centrosome, a photo-convertible Dendra-Rab11 was used. The centrosome population of Dendra-Rab11a endosomes were photoconverted from a 507 nm emission to a 573 nm

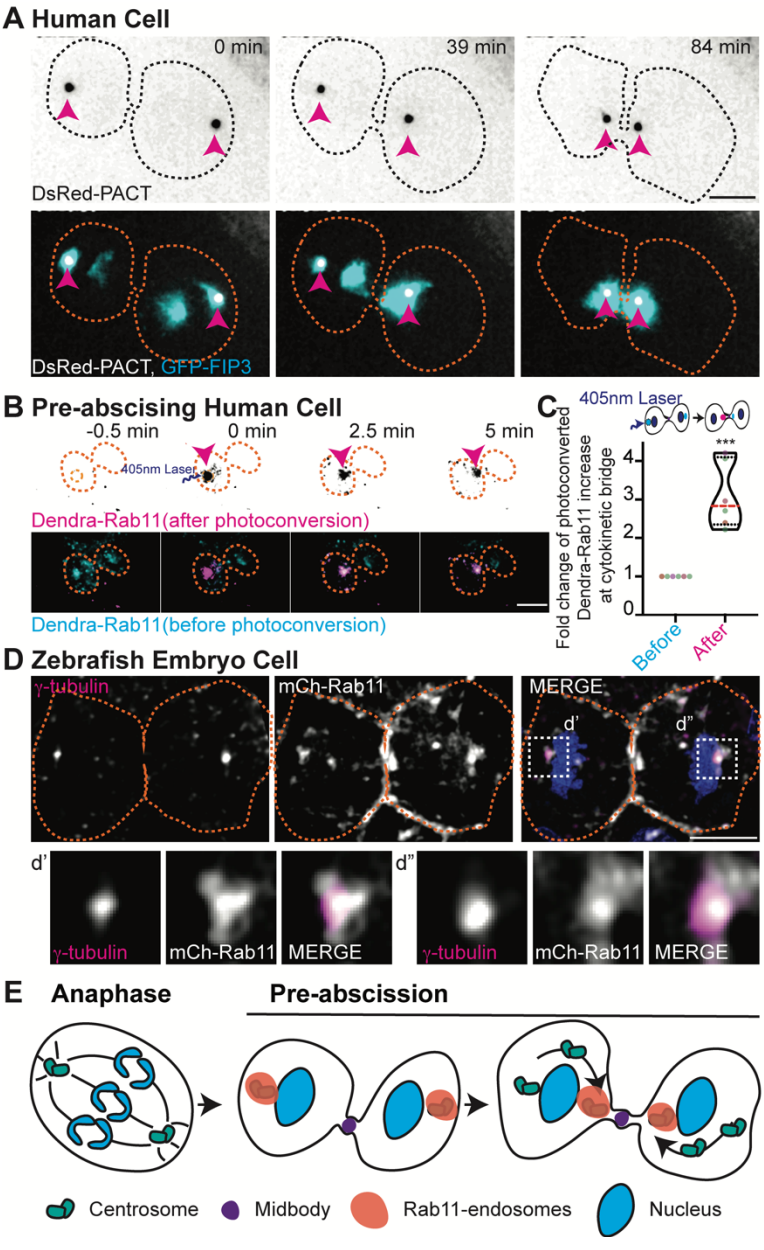

Figure 3.2: Mitotic centrosomes associate with Rab11- endosomes as they reorient towards the cytokinetic bridge.
(A) Time-lapse of pre-abscising human (HeLa) cell expressing DsRed-PACT (inverted grays, top panel; gray in merge, bottom panel) and GFP-FIP3 (cyan in merge, bottom panel). Video S2. Pink arrow, centrosome. Dashed lines, cell boundaries. Scale bar, 10 μm. (B) Time-lapse of a pre-abscising human (Hela) cell expressing Dendra-Rab11. Dendra-Rab11 is photoconverted from 507 nm emission (cyan in merge, bottom panel) to 573 nm emission (inverted grays, top panel; magenta in merge, bottom panel) using 405nm light within an ROI over the centrosome (pink arrow) at 0 min. Dashed lines, cell boundaries. Scale bar, 10 μm. (C) Violin plot with median (orange dashed line) and quartiles (black lines) depicting fold change of photoconverted Dendra-Rab11 (573 nm emission) increase at the cytokinetic bridge. Each dot in the plot represents a cell and the different colors depict separate experiments. n=6 cells and n=4 experiments. Two-tailed student's t-test, ***p<0.001. n-values and statistical results detailed in Table S1. (D) A zebrafish embryo pre-abscising cell expressing mCh-Rab11 (gray) fixed and immunolabeled for γ-tubulin (magenta) and DNA (DAPI, blue). Dashed lines, cell boundaries. Scale bar, 10 μm. Insets (d' and d''), 2X magnification. (E) Model depicting centrosomes (green) containing Rab11-endosomes (orange) reorienting towards the cytokinetic bridge with associated midbody (purple) during pre-abscission.

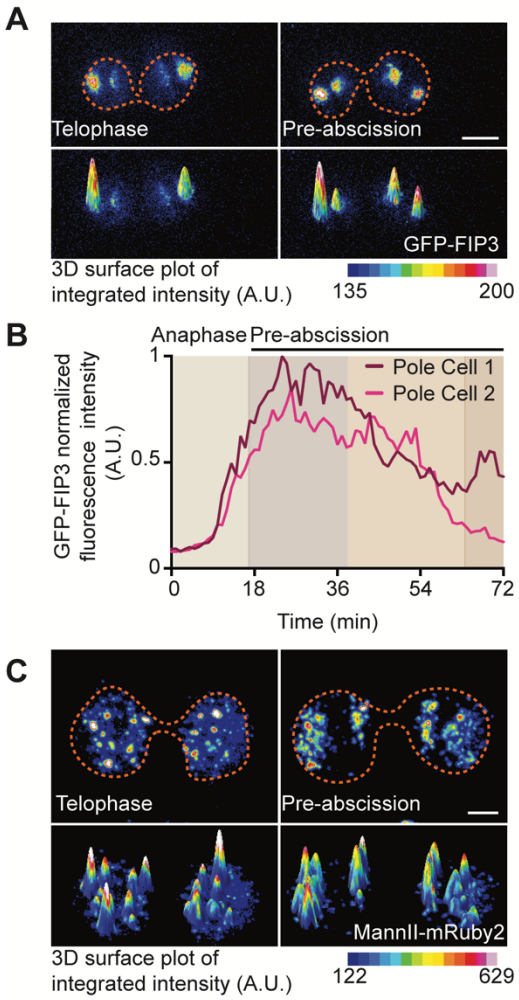

Figure S3.2: Mitotic centrosomes associate with Rab11 endosomes as they reorient towards the cytokinetic bridge.
(A) Time-lapse of a pre-abscising human (HeLa) cell expressing GFP-FIP3 (16-color LUT). Bottom panels depict three-dimensional surface plot of the intensities portrayed in top panels. Dashed lines, cell boundaries. Scale bar, 5 μm. (B) Line graph depicting GFP-FIP3 normalized fluorescence intensity from anaphase exit to late abscission at the polar compartments from (A). Intensities of the brighter pole (pole 1), dark magenta and the less bright pole (pole 2), light pink.
(C) Time-lapse of a pre-abscising human (HeLa) cell expressing MannII-mRuby2 (16-color LUT). Bottom panels depict three-dimensional surface plot of the intensities portrayed in top panels. Dashed lines, cell boundaries. Scale bar, 5 μm.

emission by placing a region of interest (ROI) over the centrosome where 405 nm light was applied. A significant population of 573 nm REs formed the second population of REs adjacent to the bridge (Figure 3.2B-C), suggesting that the second population of REs originated from the centrosome population of REs. Zebrafish pre-abscising cells showed a similar localization of Rab11-REs at the centrosome (Figure 3.2D) and this organization was similar to what was reported for another RE associated GTPase, Rab25 (Willoughby et al., 2021). These findings suggest REs organization at the centrosome is a conserved process during pre-abscission.

3.4.3. The oldest mitotic centrosome in pre-abscission moves towards the cytokinetic bridge first and has a more dynamic population of Rab11.

One centrosome is inherently older than the other between the two daughter cells due to the nature of centriole duplication. We tested whether the oldest centrosome was more likely to be the predominantly motile centrosome between the two daughter cells. The oldest centrosome can be identified by having elevated centrin-GFP levels (Colicino et al., 2019; Hung et al., 2016; Kuo et al., 2011), (Figure 3.3A, 3.3B). Once the oldest centrosome was noted, live cell imaging was used to test whether the oldest moved towards the bridge before the youngest. Both human and zebrafish pre-abscising cells preferred the oldest centrosome to move towards the cytokinetic bridge over the youngest (Figure 3.3A-3.3C, 61.5% in zebrafish compared to 80% in HeLa cells).

We next determined if an asymmetry in Rab11 dynamics and organization between the oldest and youngest centrosomes occurred in a pre-abscising cell. Using Fluorescence Recovery After Photobleaching (FRAP), the oldest and youngest centrosomes were identified using centrin-GFP and a ROI was placed over

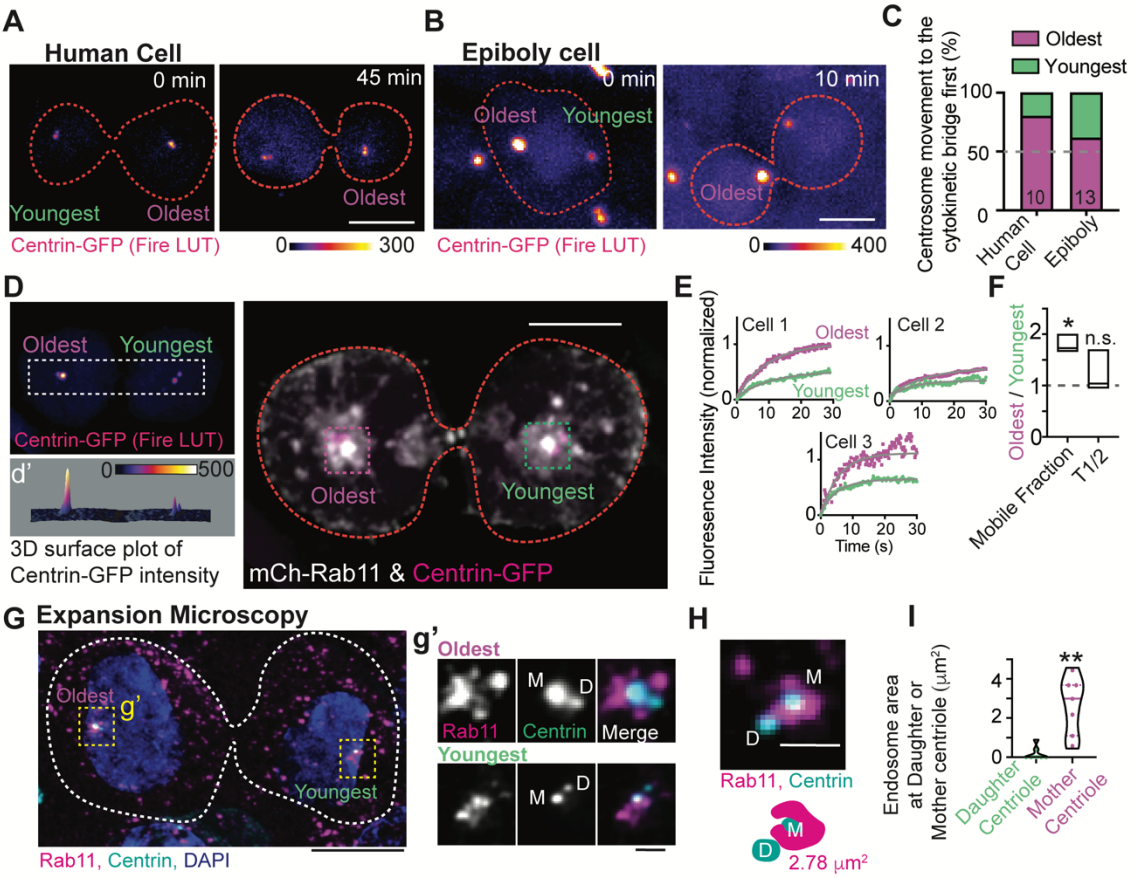

Figure 3.3: The oldest mitotic centrosome in pre-abscission moves towards the cytokinetic bridge first and has a more dynamic population of Rab11.

(A-B) Time lapse of a pre-abscising human (HeLa) cell (A) and zebrafish embryo cell at epiboly (B), expressing centrin-GFP (fire LUT). Orange dashed lines, cell boundaries. Scale bar, 10 μm. (C) Percentage of daughter cells with centrosome movement towards the cytokinetic bridge in zebrafish embryos and human (HeLa) cells. n-values on graph, Table S1. (D) Pre-abscising human (HeLa) cell expressing centrin-GFP (fire LUT, magenta in merge) and mCh-Rab11 (gray). (d') Three-dimensional surface plot of centrin-GFP to note oldest and youngest centrosome. Orange dashed lines, cell boundaries. Scale bar 10 μm. (E) FRAP traces of mCh-Rab11 at the oldest mitotic centrosome (magenta) and youngest mitotic centrosome (green) from 3 cells depicted. (F) mCh-Rab11 mobile fraction and half-life (T1/2) were calculated as a ratio of oldest centrosome/youngest centrosome and presented as a box and whisker plot with mean (dark line). n=3. Minimum and maximum values noted by the boxed boundaries. n-values and statistical results detailed in Table S1. (G-H) Expanded pre-abscising human (HeLa) cell expressing centrin-GFP (cyan) and immunostained with Rab11 (magenta) and DNA (DAPI, blue). Dashed lines, cell boundaries. Scale bar, 25 μm. (g') Magnified insets from (G) depicting Rab11 (gray, magenta in merged) and centrin-GFP (gray, cyan in merged). (H) Example pre-abscising expanded cell centrosome with a model below demonstrating Rab11-endosome area at the mother centriole. (g', H) M, denotes mother centriole and D, denotes daughter centriole. Scale bar, 2.5 μm. (I) Endosome area at daughter or mother centriole from pre-abscising cells quantified and presented as a violin plot with median (thick line) and quartiles (dotted lines), n=7 centrosomes, across n=4 cells. Two-tailed student's t-test, **p<0.01. n-values and statistical results detailed in Table S1.

them. mCherry-Rab11a (mCh-Rab11) was photobleached within these regions and recovery was recorded over a 40 second time frame (Figure 3.3D, 3.3E). Mobility of mCh-Rab11 was calculated and depicted as fitted FRAP curves at the oldest centrosome compared to the youngest from three individual pre-abscising cells (Figure 3.3E). While there is variation between curves across individual cells (Figure 3.3E), we find that the oldest centrosome always has an elevated mobile fraction when compared to the younger centrosome in all three pre-abscising cells (Figure 3.3E). To highlight the difference in mCh-Rab11 dynamics between the oldest and youngest centrosomes between the two daughter cells we took a ratio of the mobile fraction and T1/2 of the oldest/youngest centrosome from the 3 cells shown in Figure 3.3E. If there is no difference in the mobile fraction or T1/2, then the ratio should be at 1. For the mobile fraction we find a mean of 1.8±0.2 that significantly deviates from 1, and for the T1/2 we find a mean ratio of 1.2±0.2 that does not significantly deviate from 1 (Figure 3.3F). These studies suggest that mCh-Rab11 has elevated mobility at the oldest centrosome compared to the youngest centrosome.

To examine Rab11 organization between the two mitotic centrosomes during pre-abscission, expansion microscopy was employed. Expansion microscopy is a method that improves the final image resolution up to 4-fold by physically enlarging structures using a polymer system (Asano et al., 2018; Sahabandu et al., 2019). We expanded our centrin-GFP cells and immunostained them for endogenous Rab11 and GFP (Figure 3.3G). The oldest and youngest centrosomes were identified by centrin signal enrichment. Strikingly, at the oldest centrosome Rab11 accumulated around the mother centriole (Figure 3.3g'). The mother centriole is noted by having elevated centrin levels between the two centrioles. This was somewhat the case for the youngest mother centriole, however not to the same extent as the oldest. In both

centrosomes, the daughter centrioles significantly lacked Rab11 signal compared to the mother centriole. We quantified the area of Rab11 endosomes that overlapped/touched the mother centriole compared to the daughter centriole (shown in example Figure 3.3H). We observed that there is significantly higher Rab11 endosome area at the mother centriole ($2.66 \pm 0.56 \mu m^2$) compared to the daughter centriole ($0.18 \pm 0.13\ \mu m^2$, Figure 3.3I). These studies suggest an asymmetry in Rab11 organization and dynamics between the oldest and youngest centrosome that may contribute to the movement of the centrosome towards the cytokinetic bridge.

3.4.4. Rab11 GTPase function is associated with centrosome bridge-directed movement.

To specifically test the role of Rab11 in centrosome movement, we used a strategy to measure centrosome reorientation during pre-abscission by normalizing distance traveled by the centrosome in relation to the cell (Figure S3.3A). This involved recording the movement of the centrosome and the cell body as vectors and using vector subtraction to calculate centrosome movement within the reference frame of the cell in both cell culture (Figure S3.3B) and in zebrafish embryo cells (Figure S3.3C). We employed this strategy with control and Rab11-null, centrin-GFP or GFP-FIP3 HeLa cell lines (Figure S3.3D). The Rab11-null cell lines were created using Rab11a CRISPR vector and Rab11a HDR Vector (see supplementary key resource table) and characterization done in (Rathbun et al., 2020a). Western blot analysis to confirm Rab11a loss used an antibody that detects both Rab11a and Rab11b (Figure S3.3D, supplementary key resource table), where a loss of Rab11 signal in our Rab11-null cells compared to control suggests that both Rab11a and Rab11b are not present or that Rab11b is present at low and undetectable amounts.

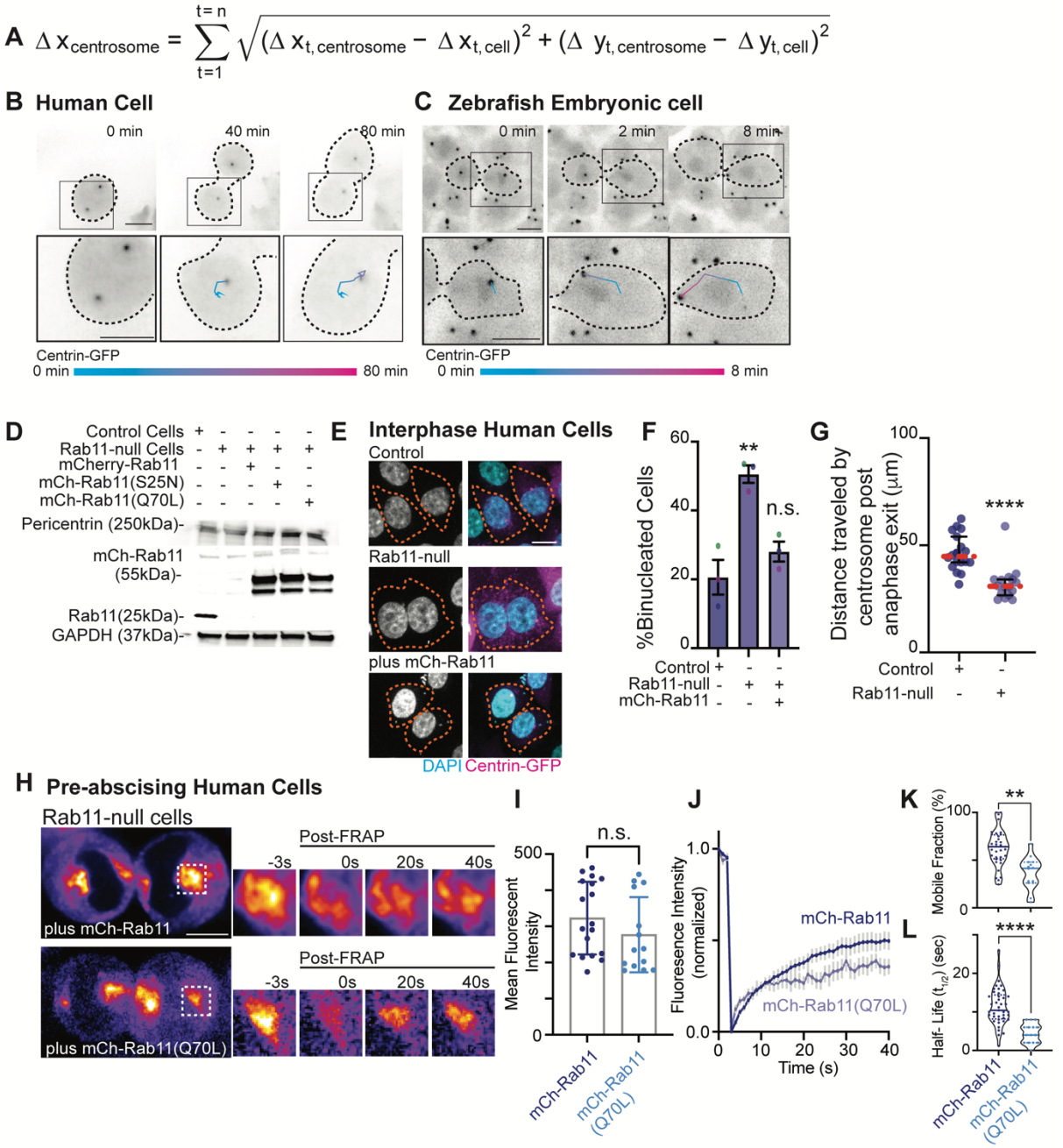

Figure S3.3: Rab11 GTPase function is associated with centrosome bridge-directed movement.

Figure S3.3: Rab11 GTPase function is associated with centrosome bridge-directed movement. (A) Equation to calculate distance traveled by centrosome in relation to the cell. This involves recording movement of the centrosome and the cell body as vectors and using vector s ubtraction to calculate centrosome movement within the reference frame of the cell to accurately calculate distance traveled by the centrosome. (B-C) Time lapse of a pre-abscising human (HeLa) cell (B) and zebrafish embryo cell (C). Inset with associated track (color gradient represents time) of distance traveled by centrosome (cell body centered for each time point) using equation in (A). Scale bar, 10 μm. Black dashed lines, cell boundaries. Color gradient line, time. (D) Western blot immunolabeled for Rab11 and Pericentrin with GAPDH loading control in control cells, Rab11-null cells and Rab11-null cells ectopically expressing mCh-Rab11, -Rab11(S25N) and -Rab11(Q70L). (E-F) Representative images of fixed interphase human (HeLa) cells with a single nucleus or bi-nuclei labeled using DAPI (gray, left; cyan, merge) and Centrin-GFP (magenta) shown (E). Orange dashed lines, cell boundaries. Scale bar, 10 μm. Percentage of binucleate cells calculated for n>100 cells counted per experiment across n=3 experiments (F). One-way ANOVA with Dunnett's multiple comparison to control cells shown, n.s. not significant and **p<0.01. (G) Total distance traveled by centrosome during pre-abscission measured and depicted as a scatter plot with the median (orange dashed line) and quartiles (dark lines) shown. n>8 cells per condition across n>3 experiments. Two-tailed student's t-test, ****p<0.0001. (H-L) Rab11-null cells ectopically expressing mCh-Rab11 and -Rab11(Q70L) shown (fire, LUT). ROI photobleached highlighted in inset (right), pre- and post-FRAP. Scale bar 10 μm (H). mCh-Rab11 (blue dots, lines) and -Rab11(Q70L) (cyan dots, lines) mean fluorescent intensity calculated and presented as a bar graph with mean, SEM, n>15 cells per condition. Two-tailed student's t-test, n.s. not significant (I). FRAP trace of mCh-Rab11 and -Rab11(Q70L) shown for n>15 cells per condition (J). (K-L) mCh-Rab11 and -Rab11(Q70L) mobile fraction (K) and half-life (t1/2, L) calculated and presented as violin plot with median (dark blue line, mCh-Rab11; cyan line, mCh-Rab11(Q70L)) and quartiles (dark blue dotted lines, mCh-Rab11; cyan dotted lines, mCh-Rab11(Q70L)) for n>15 cells per condition. Two-tailed student's t-test, **p<0.01 and ****p<0.0001. n-values and statistical results detailed in Table S1.

Similar to previous reports, cells null for Rab11a resulted in increased binucleated cells indicative of an abscission failure (Rathbun et al., 2020a; Wilson et al., 2005) that was rescued with ectopic expression of mCh-Rab11a (Figure S3.3E, S3.3F). In control cells expressing GFP-FIP3, endogenous Rab11 colocalizes with its effector protein, FIP3, during pre-abscission. In Rab11-null cells, no Rab11 is detected by immunohistochemistry and GFP-FIP3 is no longer organized in a tight centrosome localized compartment (Figure 3.4A). Rab11-null cells were impaired in centrosome movement towards the cytokinetic bridge compared to control cells (Figure 3.4B-3.4C, Video S3.3). When measuring the overall centrosome mobility during pre-abscission, centrosomes moved a significantly shorter distance in Rab11-null cells (32.19 ± 2.025 μm) compared to control (46.50 ± 2.011 μm, Figure S3.3G). While there was centrosome movement in the Rab11-null cells, the centrosome movement was random in its directionality. Thus, we then took distance traveled measurements for cytokinetic bridge directed centrosome movement and identified that the centrosome had significant defects in centrosome-directed distance traveled in Rab11-null cells (2.00 ± 0.86 μm) compared to controls (8.64 ± 1.63 μm, Figure 3.4F), suggesting that Rab11 is needed for directed centrosome movement towards the cytokinetic bridge.

To test the requirement for Rab11 GTPase function, fluorescently tagged versions of Rab11a (referred to as Rab11 from here on) were expressed in Rab11-null cells. These included Rab11 (mCh-Rab11), a mutant that mimic's the GDP-bound state of Rab11 (mCh-Rab11(S25N)), or a mutant that mimics the GTP-bound state of Rab11 (mCh-Rab11(Q70L), Figure 3.4D). Comparable expression levels of ectopically expressed Rab11 demonstrated by Western blot in Figure S3D. mCh-Rab11 and -Rab11(Q70L) had similar centrosome localization patterns whereas -

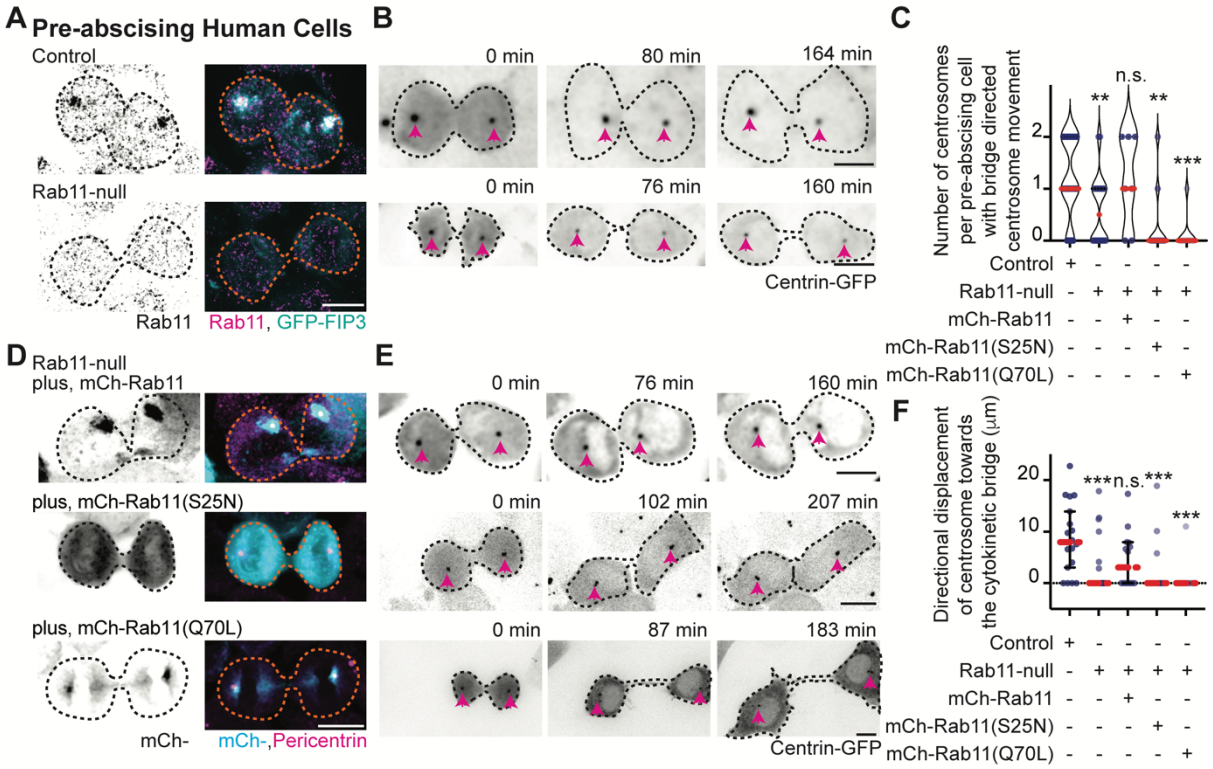

Figure 3.4: Rab11 GTPase function is associated with centrosome bridge-directed movement. (A) Control and Rab11-null expressing GFP-FIP3 (cyan, merge) human (HeLa) cells fixed and immunostained for Rab11 (inverted grays, left; magenta, merge). (B) Time-lapse of control and Rab11-null centrin-GFP (inverted grays) pre-abscising human (HeLa) cells. Pink arrows, centrosome. Dashed lines, cell boundaries (A-B). Scale bar, 10 μm. Video S3. (C-F) Rab11-null cells expressing mCh-Rab11, -Rab11 (S25N) or -Rab11(Q70L). (C) Number of centrosomes per pre-abscising cell with bridge directed centrosome movement calculated as both centrosomes (2 centrosomes), only one centrosome (1 centrosome) and neither centrosome (0 centrosomes) moved shown as a violin plot with median (orange dashed line) and quartiles (dark dotted lines). One-Way ANOVA, with Dunnett's multiple comparison to control, ***p<0.001, **p<0.01 and n.s. not significant. (D) GFP-FIP3 Rab11-null cells expressing mCh-Rab11, -Rab11(S25N) or -Rab11(Q70L) (inverted grays, left; cyan, merge) fixed and immunostained for Pericentrin (magenta, merge). (E) Centrin-GFP (inverted grays) Rab11-null pre-abscising human (HeLa) cells expressing mCh-Rab11, -Rab11(S25N) or -Rab11(Q70L). Pink arrows, centrosome. Dashed lines, cell boundaries (D-E). Scale bar, 10 μm. Video S4. (F) Directional displacement of centrosome towards cytokinetic bridge (scatter plot). Median (orange dashed line) and quartiles (dark lines) shown. One-way ANOVA with Dunnett's multiple comparison to control, ***p<.001 and n.s. not significant. (C, F) n values, statistical results detailed in Table S1.

Rab11(S25N) remained more cytosolic (Figure 3.4D). Expressing mCh-Rab11 in Rab11-null cells rescued bridge directed centrosome movement with a bridge directed distance traveled of 4.57 ± 1.46 μm, compared to -Rab11(S25N) (1.93 ± 1.17 μm) or -Rab11(Q70L) (0.92 ± 0.92 μm) (Figure 3.4C, 3.4E, 3.4F, Video S3.4). These findings suggest that the ability of Rab11 to cycle between a GTP and GDP bound state is important for its contribution to centrosome movement towards the cytokinetic bridge.

We were surprised that mCh-Rab11(Q70L) did not partially rescue centrosome movement towards the cytokinetic bridge since it can mimic the active state of Rab11 and localizes to centrosomes (Figure 3.4D). One possibility is that GTP to GDP cycling is required for Rab11 to regulate centrosome bridge-directed movement and affects the temporal and spatial organization of Rab11 at the mother centriole during pre-abscission. To test this, we examined whether a difference in mCh-Rab11 and -Rab11(Q70L) dynamics occurred using FRAP by photobleaching the population of mCh-Rab11 or -Rab11(Q70L) at the centrosome and comparing the fluorescent recovery over time. We selected cells with a similar range of fluorescent intensities of mCh-Rab11 and -Rab11(Q70L) (Figure S3.3I) for these studies and found significant differences in dynamics between mCh-Rab11 and -Rab11(Q70L) (Figure S3.3H-L). Rab11(Q70L) cells had a decreased mobile fraction of 36.57 ± 4.48%, compared to Rab11 at 59.02 ± 5.08% and Rab11(Q70L) presented with a decreased half-life (2.27 ± 0.33s) compared to Rab11 (9.00 ± 1.31s, Figure S3.3I-S3.3L). One potential interpretation is that Rab11(Q70L) is more stably associated with the mother centriole (as seen in Figure 3.3g'). Collectively, these findings suggest that mCh-Rab11 dynamics at centrosomes is

partly regulated by its ability to cycle GTP to GDP contributing to centrosome movement towards the cytokinetic bridge.

3.4.5. Rab11 GTP-cycling mediates centrosome protein, Pericentrin, centrosome localization during pre-abscission.

We find that γ-tubulin and Pericentrin partially localize to REs during pre-abscission in both human (HeLa) and zebrafish embryo cells (Figure S3.4A-S3.4B), which is consistent with previous studies that identified Pericentrin and γ-tubulin at REs during metaphase in human cells (Hehnly and Doxsey, 2014). We specifically find that REs associate with Pericentrin and γ-tubulin at and outside of the centrosome (Figure S3.4A-B, inset demonstrating acentrosomal localization). In human (HeLa) cells expressing the RE marker, GFP-FIP3 and the centrosome targeting domain from Pericentrin, DsRed-PACT, GFP-FIP3 colocalized with acentrosomal DsRed-PACT. These GFP-FIP3/DsRed-PACT puncta move towards and combine with the main centrosome (Figure S3.4C) suggesting that REs may help contribute to overall centrosome organization and function.

Since Rab11-null pre-abscising cells are unable to orient their centrosome towards the cytokinetic bridge, we analyzed whether localization of centrosome components and RE components at the centrosome were altered in Rab11-null cells compared to control cells (Figure 3.5A-3.5D, S3.4D-E). Fluorescence intensity was measured in fixed early-abscission cells where the centrosomes are still on the polar ends of the daughter cells before they move to the bridge. An ROI was placed over the centrosome and compared between control and Rab11-null cells. The fluorescence intensity values were plotted as a ratio of Rab11-null over control cells (Figure 3.5B). A ratio of 1 implies no difference between Rab11-null cells and

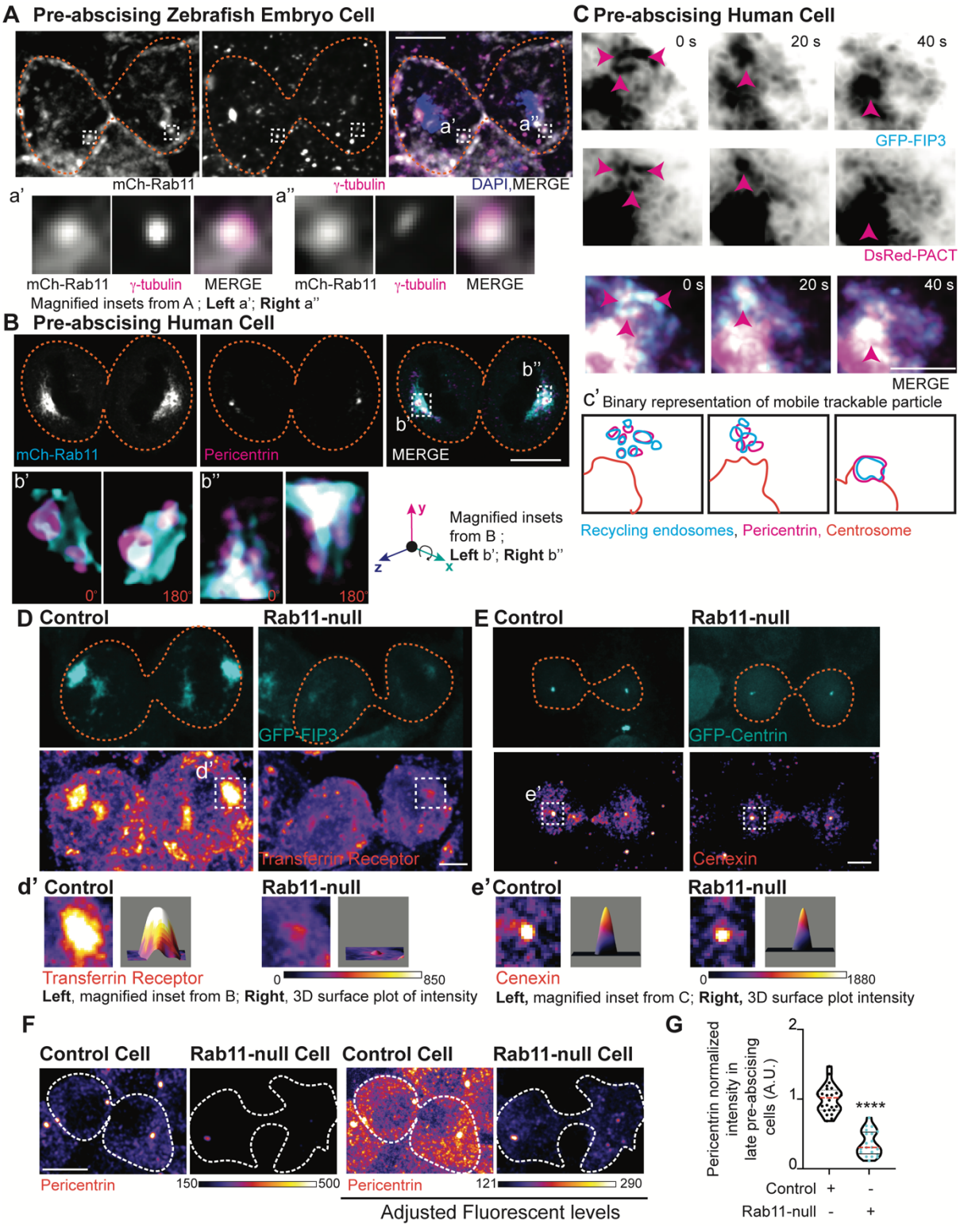
A Pre-abscising Zebrafish Embryo Cell
mCh-Rab11
γ-tubulin
DAPI,MERGE
a'
a''
mCh-Rab11
γ-tubulin
MERGE
Magnified insets from A ; Left a'; Right a''
B Pre-abscising Human Cell
mCh-Rab11
Pericentrin
MERGE
b'
b''
0°
180°
Magnified insets from B ; Left b'; Right b''
C Pre-abscising Human Cell
0 s
20 s
40 s
GFP-FIP3
DsRed-PACT
MERGE
C' Binary representation of mobile trackable particle
Recycling endosomes, Pericentrin, Centrosome
D Control
Rab11-null
GFP-FIP3
d'
Transferrin Receptor
E Control
Rab11-null
GFP-Centrin
e'
Cenexin
d' Control
Rab11-null
Transferrin Receptor
0
850
Left, magnified inset from B; Right, 3D surface plot of intensity
e' Control
Rab11-null
Cenexin
0
1880
Left, magnified inset from C; Right, 3D surface plot intensity
F
Control Cell
Rab11-null Cell
Control Cell
Rab11-null Cell
Pericentrin
150
500
Pericentrin
121
290
Adjusted Fluorescent levels
G
Pericentrin normalized intensity in late pre-abscising cells (A.U.)
2
1
0
****
Control + -
Rab11-null - +

Figure S3.4: Rab11 GTP-cycling mediates centrosome protein, Pericentrin, centrosome localization during pre-abscission.
(A-B) Pre-abscising zebrafish embryonic cell (A) or a Rab11-null human (HeLa) cell expressing mCh-Rab11 (gray, A and B top panel; cyan in merge, B) fixed and immunostained for γ-tubulin (magenta, A), Pericentrin (magenta, B), and DNA (DAPI, blue, A). Scale bar, 10 μm. Magnified insets of acentrosomal site (a', a", b") and centrosome (b'). (C) Time-lapse of GFP-FIP3/Rab11 (inverted grays, left; cyan, merge) centrosome region in a pre-abscising human (HeLa) cell expressing DsRed-PACT (inverted grays, left; magenta, merge). Pink arrows, acentrosomal fragments positive for GFP-FIP3/Rab11/DsRed-PACT. Scale bar, 10 μm. (c') Outline of tracked particles noted by pink arrow. Orange line, centrosome. (D-E) Human (HeLa) pre-abscising cells expressing GFP-FIP3 (cyan, D) or centrin-GFP (cyan, E) were fixed and immunostained for transferrin receptor (fire LUT, D), and cenexin (fire LUT, E). Magnified insets (3x) shown on right (d', e') with associated three-dimensional surface plot of intensity. Scale bar, 5 μm.
(F) Human GFP-FIP3 (HeLa) cells late in pre-abscission were fixed and immunostained for Pericentrin (fire LUT). The same examples are shown with levels adjusted on right showing that there is some Pericentrin at one of the daughter centrosomes, but it is s ignificantly decreased. (G) Violin plot with median (orange dashed line) and quartiles (dark lines) depicting normalized Pericentrin intensities at centrosomes for n>20 centrosomes from a representative experiment. Two-tailed student's t-test, ****p<0.0001. n-values and statistical results detailed in Table S1.

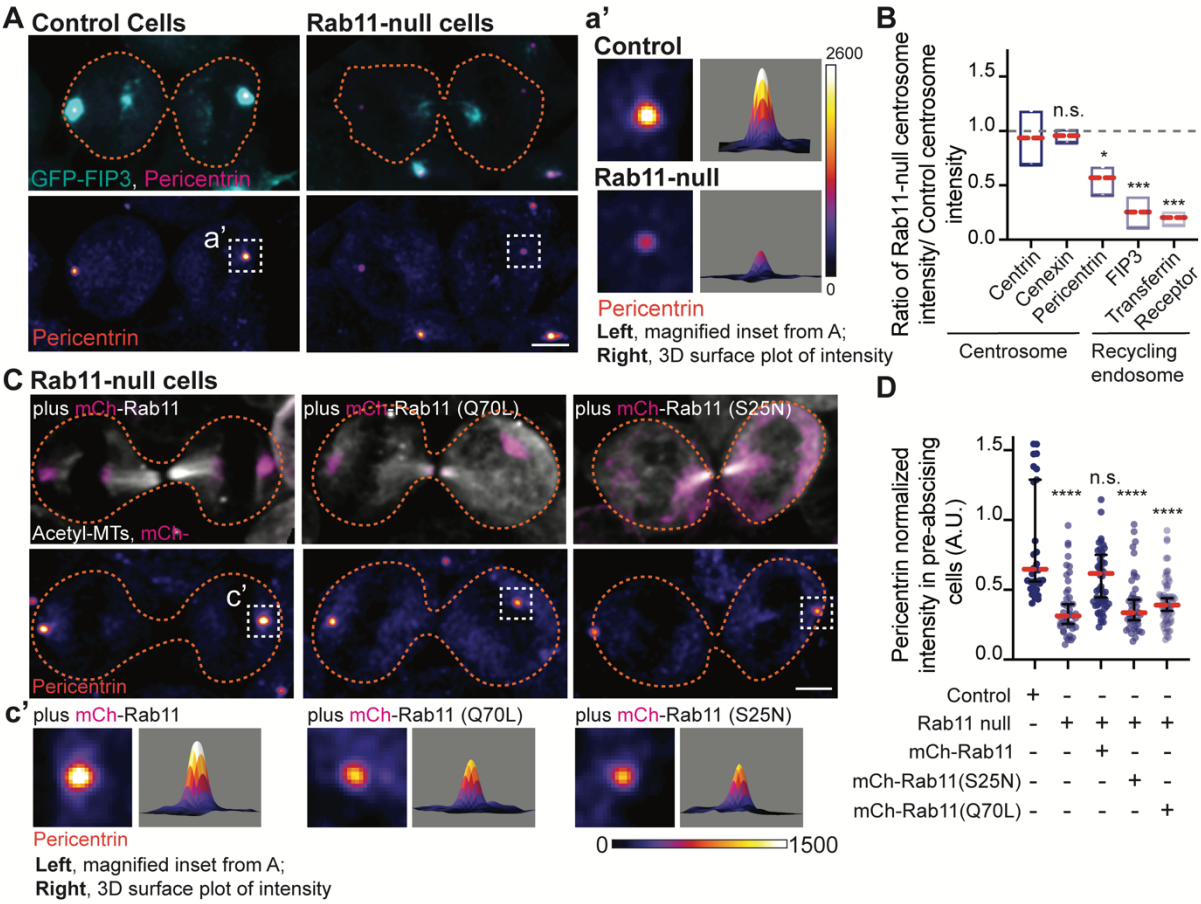

Figure 3.5: Rab11 GTP-cycling mediates centrosome protein, Pericentrin, centrosome localization during pre-abscission.

(A) Human (HeLa) pre-abscising cells expressing GFP-FIP3 (cyan) were fixed and immunostained for Pericentrin (magenta, top panel; fire LUT, bottom panel). Magnified insets (3x) shown on right (a') with associated three-dimensional surface plot of intensity. Scale bar, 5 μm. (B) Box and whisker plot with mean (orange dashed line) depicting ratio of Rab11-null centrosome intensity over control centrosome intensity of cenexin, centrin, Pericentrin, FIP3, and transferrin receptor. Minimum and maximum values noted by boxed boundaries. n>30 centrosomes per experiment across n=3 experiments. One-way ANOVA with Dunnett's multiple comparison to centrin, n.s. not significant, *p<0.05 and ***p<0.001. (C) GFP-FIP3 Rab11-null pre-abscising human (HeLa) cells ectopically expressing mCh-Rab11, -Rab11(S25N) or -Rab11(Q70L) (magenta, top panel) were fixed and immunolabelled for acetylated-tubulin (gray, top panel) and Pericentrin (fire LUT, bottom panel). Scale bar, 5 μm. (c') 3x magnified centrosome inset (left), 3D fluorescent intensity surface plot of inset (right). (D) Scatter plot with median (orange dashed line) and quartiles (dark lines) depicting normalized Pericentrin intensities at centrosomes from pre-abscising human (HeLa) cells. One-way ANOVA with Dunnett's multiple comparison to control, n.s. not significant and ****p<0.0001. n>38 centrosomes across n>3 experiments. (B, D) n values and statistical results detailed in Table S1.

control, and a ratio significantly less than 1 suggests decreased centrosome localization in Rab11-null cells. Rab11-null cells had significantly decreased centrosome localized GFP-FIP3 (Figure 3.5A-3.5B, S3.4D), transferrin receptor (RE cargo, Figure 3.5B, S3.4D), and Pericentrin (Figure 3.5A-3.5B). However, the centriole appendage protein, cenexin, and centriole protein, centrin, were not affected by Rab11 loss (Figure 3.5B, S3.4E). This is interesting because we note Rab11 endosomes at the mother centriole (Figure 3.3G-I) suggesting that Rab11 may interact with mother centriole appendages (as shown for interphase cells, (Hehnly et al., 2012)), but does not seem to affect their structure during pre-abscission (Figure 3.5B, S3.4E). However, Rab11-REs do seem to be implicated in Pericentrin organization both in early stages of pre-abscission (Figure 3.5A, 3.5B) and later stages (Figure S3.4F-G). Pericentrin intensity at the centrosome was rescued in Rab11-null cells by expression of mCh-Rab11, but not mCh-Rab11(S25N) or -Rab11(Q70L) (Figure 3.5C-3.5D). Pericentrin expression levels were unaltered in Rab11-null cells, or cells rescued with mCh-Rab11, -Rab11(S25N), or -Rab11(Q70L) (Figure S3.3D), suggesting that the targeted localization of Pericentrin is disrupted with loss of Rab11 function. Taken together, Rab11 GTPase function is necessary for centrosome movement towards the bridge during pre-abscission (Figure 3.4) by potentially facilitating Pericentrin organization at the centrosome (Figure 3.5).

3.4.6. Pericentrin and Rab11 endosomes coordinate centrosome movement and number during mitotic exit.

Since loss of Rab11 caused a decrease in Pericentrin levels at the centrosome in human cells (Figure 3.5), we tested the role of Pericentrin and Rab11-

endosomes in regulating centrosome movement during pre-abscission *in vivo*. To do this, we used heterozygous Pericentrin (*pcnt*$^{+/-}$) zebrafish embryos (Sepulveda et al., 2018) positive for the centrosome marker centrin-GFP (embryo generation modeled in Figure S5A) or by acutely inhibiting Rab11-associated vesicles through an optogenetic oligomerization approach that relies on a hetero-interaction between CRY2 and CIB1 that is induced by the application of blue light (modeled in Figure S3.5B, (Rathbun et al., 2020a)). *Pcnt*$^{+/-}$ embryos were used due to our inability to obtain reliable *pcnt* null embryos. When comparing *pcnt*$^{+/-}$ and Rab11 optogenetically clustered embryos to control embryos (non-injected or CRY2 injected) at 3.3-5 hours post fertilization, *pcnt*$^{+/-}$ embryo cells and Rab11 clustered embryo cells were significantly impaired at reorienting their centrosomes towards the cytokinetic bridge compared to control conditions (Figure 3.6A-3.6C, confirmation of genotype in Figure S3.5C, CRY2 control in Figure S3.5D). *Pcnt*$^{+/-}$ and Rab11 clustered embryos also demonstrated significant defects in centrosome movement during pre-abscission, where the calculated distance traveled was significantly decreased for *pcnt*$^{+/-}$ and Rab11 clustered embryos compared to control conditions (Figure 3.6D). These studies suggest that both Pericentrin and Rab11 coordinate centrosome bridge directed motility.

We next examined whether decreasing Pericentrin (*pcnt*$^{+/-}$) and acutely clustering Rab11-vesicles resulted in abscission defects. When cells are unable to complete abscission, cells become binucleated (Carter, 1967) or present with supernumerary centrosomes (Pihan et al., 2003). Most cells contain either one or two centrosomes, depending on their cell cycle stage. A G1 cell contains a single centrosome composed of two centrioles. During S phase, two new (daughter) centrioles assemble near the pre-existing (mother) centriole creating two

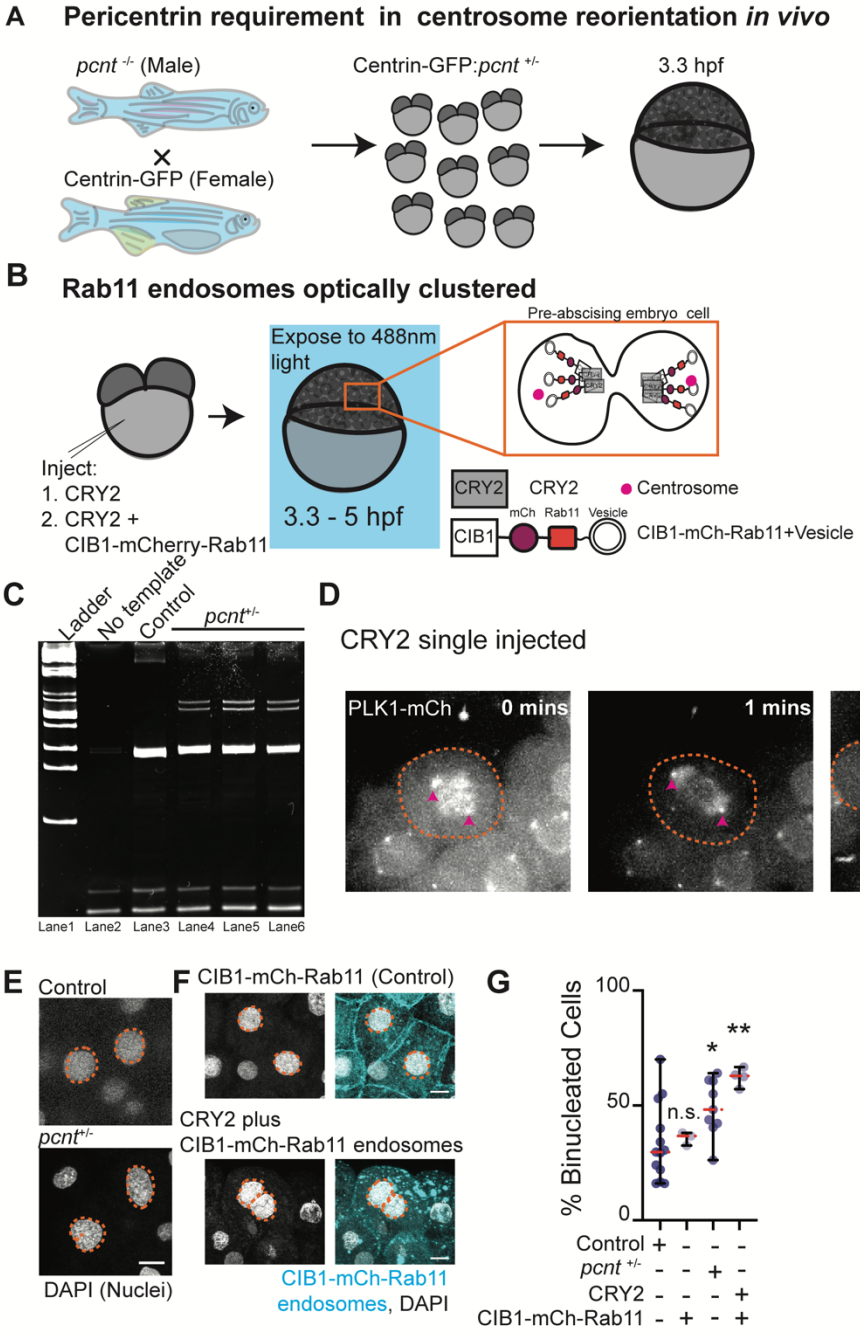

Figure S3.5: Pericentrin and Rab11 endosomes coordinate centrosome movement and number during mitotic exit.

Figure S3.5: Pericentrin and Rab11 endosomes coordinate centrosome movement and number during mitotic exit.
(A) Model depicting generation of pcnt+/- embryos with labeled centrosomes (centrin-GFP) to test the role of Pericentrin in centrosome reorientation and centrosome number in vivo. (B) Model depicting optogenetic clustering protocol for Rab11 endosomes. In short, embryos are injected with CRY2 and/or CIB1-mCh-Rab11 mRNAs, exposed to blue light 3.3-5 hpf causing a heterointeraction between CRY2 and CIB1, and imaged. Orange inset depicts cells imaged within the embryo. Pink circle, centrosome. (C) Ethidium bromide-stained acrylamide gel electrophoresis showing pcnt+/+ and pcnt+/- genotypes with ladder (lane 1), no template (lane 2), DNA extracted from control zebrafish (pcnt+/+, lane 3) and pcnt+/- embryos used in experimental analysis in Fig 6 (lane 4, 5, 6). (D) Time-lapse projections depicting a control dividing cell injected with CRY2 and PLK1-mCh (gray). Pink arrow, centrosome. Dashed lines, cell boundaries. Scale bar, 10 μm. (E-F) Representative images of fixed interphase zebrafish embryonic cells with a single nucleus or bi-nuclei labeled using DAPI in control, pcnt+/-, CIB1-mCh-Rab11 injected, and CRY2 plus CIB1-mCh-Rab11 injected embryos (gray, nuclei outlined with dashed orange line; E-F). Scale bar, 5 μm. Percentage of embryos with cells containing binucleated cells was calculated for n>30 cells per embryo across n>3 embryos (G). One-way ANOVA with Dunnett's multiple comparison to control, n.s. not significant, *$p<0.05$ and **$p<0.01$. n-values and statistical results detailed in Table S1.

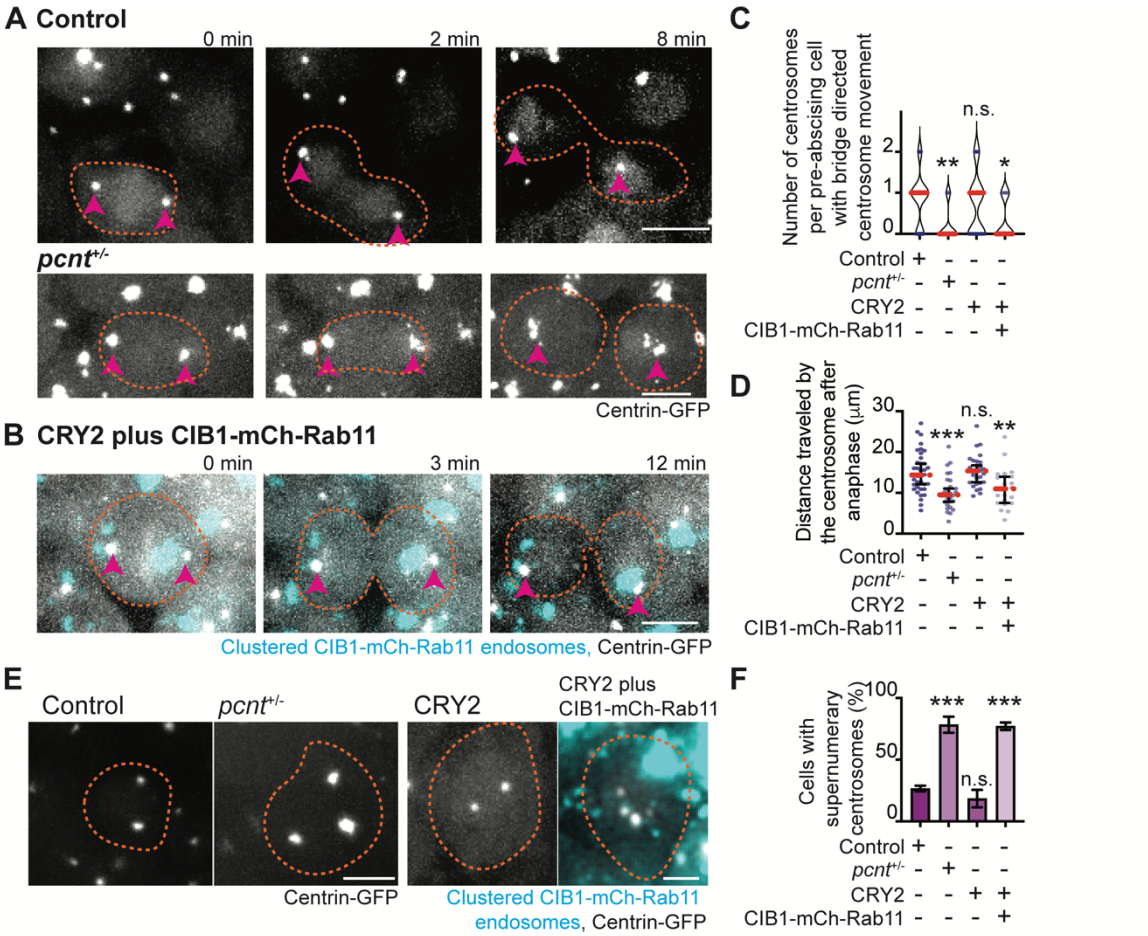

Figure 3.6: Pericentrin and Rab11 endosomes coordinate centrosome movement and number during mitotic exit.

(A-B) Time-lapse imaging of control cells (A), pcnt+/- cells (A), and cells with clustered Rab11 endosomes (B, cyan) from a -5actb2:cent4-GFP(centrin-GFP, gray) embryo. Pink arrows, centrosome. Dashed orange line, cell boundaries. Scale bar, 10 μm. (C-D) Number of centrosomes per pre-abscising cell with bridge directed centrosome movement calculated as both centrosomes (2 centrosomes), only one centrosome (1 centrosome) and neither centrosome (0 centrosomes) moved depicted as a violin plot with median (orange dashed line) and quartiles (dark dotted lines, C), and distance traveled by the centrosome after anaphase (scatter plot with median, orange dashed line, and quartiles, dark lines, D) in control, pcnt+/-, CRY2 injected, or CRY2 plus CIB1-mCh-Rab11 injected embryos is shown. n>16 cells across n>3 embryos. One-way ANOVA with Dunnett's multiple comparison to control, n.s. not significant, *p<0.05, **p<0.01 and ***p<0.001. (E-F) Interphase centrin-GFP (gray) zebrafish embryos with n=2 centrosomes or supernumerary (n>2 centrosomes) in control, pcnt+/-, CRY2 injected, CRY2 plus CIB1-Rab11 injected embryos (cyan, CIB1-mCh-Rab11 plus CRY2). (E) Orange dashed lines, cell boundaries. Scale bar, 5μm. (F) Percentage of cells with supernumerary centrosomes (n>2 centrosomes). n>30 cells per embryo across n>3 embryos. One-way ANOVA with Dunnett's multiple comparison to control, n.s. not significant and ***p<0.001. (C, D, F) n values and statistical results detailed in Table S1.

centrosomes that will move apart to create a bipolar mitotic spindle. When cells fail abscission, the two daughter cells combine gaining an extra centrosome and can present as binucleated. Having too many centrosomes can result in multipolar divisions, chromosome segregation defects, defects in asymmetric cell division, loss in cell polarity, induction of invasive protrusions, and inappropriate activation of signaling pathways (Godinho and Pellman, 2014). In our studies, we counted embryonic cells that had an abnormal number of centrosomes (3 or more) or were binucleated. With *pcnt*$^{+/-}$ embryos, we find a significant increase in embryos with binucleated cells (Figure S3.5E, S3.5G) and supernumerary centrosomes (78.33% ± 6.509 of cells) compared to control (26.57%± 2.293, Figure 3.6E-3.6F). With optogenetic clustering of Rab11-REs we find a similar dramatic increase in both the percentage of cells containing supernumerary centrosomes (77.18%± 3.029) compared to CRY2 injected controls (18.41% ± 7.079, Figure 6E-F) and binucleated cells (Figure S3.5F-G), suggesting that Rab11-endosomes and Pericentrin may work together to coordinate successful abscission.

3.5 Discussion

We propose a model where the cytokinetic bridge and associated midbody may act as a symmetry breaking event marking a position for where the centrosome needs to reorient towards (Figure 3.1). This reorientation is particularly interesting in the context of KV development, where we find in these studies (Figure 3.1B-3.1D) and in our previous studies (Rathbun et al., 2020a) that during pre-abscission, the two daughter cells position themselves so that the cytokinetic bridge is placed where a lumen will form. Herein we found that centrosomes reorient toward the cytokinetic bridge before bridge cleavage. While this isn't specific to just KV cells that are destined to assemble a primary cilium at this locale, providing a biologically useful role for centrosome reorientation to this cite, it also occurs in cells dividing during epiboly. This suggests that centrosome reorientation during pre-abscission may have two underlying functions: 1) centrosome reorientation needs to occur to make sure the cilia forms in the correct place when destined ciliated cells need to self-assemble into a rosette structure that transitions to form a lumen *de novo*, 2) that centrosome reorientation towards the bridge may play a role in successful abscission completion. Our studies that support this with pre-abscising zebrafish epiboly cells containing optogenetically clustered Rab11 membranes or *pcnt*$^{+/-}$ cells that present with significant defects in reorienting their centrosomes towards the cytokinetic bridge. Associated with these defects is a significantly greater propensity for these cells to be binucleated and contain supernumerary centrosomes suggestive of an abscission defect. These studies suggest that centrosome function, Rab11-endosome function, and centrosome reorientation may be needed for abscission completion.

Rab11 has previously been identified to interact with sub-distal appendages in non-ciliated interphase cells (Hehnly et al., 2012). An additional report demonstrated that Rab8, and potentially the Rab11-Rab8 cascade, has an association with distal appendages during ciliogenesis (Schmidt et al., 2012) suggesting that at different cell cycle stages different flavors of Rab11 or RE interactions may occur with the centrosome. It has yet to be reported if there is a relationship between Rab11-endosomes and the mother centriole during mitotic stages. Our findings demonstrate using expansion microscopy that Rab11 continues to organize at the mother centriole during pre-abscission (Figure 3.3G-I) and it will be exciting to investigate whether this organization is dependent on sub-distal or distal appendages. There are ample reports that Rab11 is involved in abscission (Schiel et al., 2012; Wilson et al., 2005), but the relationship of Rab11 with the centrosome during this time had yet to be investigated. Thus, our study is confirming and expanding on the initial foundational studies where we suggest an importance for Rab11-endosome interaction with the centrosome during multiple cell cycle stages. Specifically, we find that Rab11 is needed for centrosome-directed movement towards the cytokinetic bridge.

Connections between the centrosome and cleavage of the cytokinetic bridge exist. For instance, the centrosome protein, Cep55, localizes both to the centrosome and cytokinetic midbody where it contributes to abscission (Little and Dwyer, 2021). Piel et al.'s work was foundational in identifying the centrosome as a possible regulator of abscission where they performed centrosome-removal experiments (Piel et al., 2001). Centrosome-free prostate epithelial cells (Wang et al., 2020), human embryonic stem cells (Renzova et al., 2018), or BSC1 cells (Piel et al., 2001) obtained by either centrinone treatment or by physically severing a portion of the cell

containing the centrosome from the cellular nucleus (Piel et al., 2001) present with abscission defects such as multi-nucleation. Severing the centrosome from the cell could potentially remove Rab11-associated REs affiliated with the centrosome (Figure 2). Rab11-REs are needed for abscission (Figure S3.3E-F, 3.6E-F, S3.5F-G) (Wilson et al., 2005). Here we identified a connection with Rab11 and centrosome function, such that when Rab11 is removed centrosome levels of Pericentrin significantly decrease (Figure 3.5A-3.5B). A loss in Pericentrin levels then leads to centrosome reorientation defects and abscission failure (Figure 3.6A, 3.6C, 3.6D, 3.6F). This suggests a potential molecular mechanism where Rab11 modulates Pericentrin centrosome organization that is needed in centrosome reorientation to the cytokinetic bridge and likely in its subsequent abscission. Taken together, these previous studies and our studies herein suggest that the centrosome has a role in the process of abscission.

3.6 RESOURCE AVAILABILITY

3.6.1 Lead contact: For further information or to request resources/reagents, contact the Lead Contact, Heidi Hehnly (hhehnly@syr.edu)

3.6.2 Materials availability: New materials generated for this study are available for distribution.

3.6.3 Data and Code Availability: All data sets analyzed for this study are displayed.

3.6.4 Experimental Model and Subject Details

3.6.4.1 Fish Lines: Zebrafish lines were maintained using standard procedures approved by Syracuse IACUC (Institutional Animal Care Committee) (Protocol #18-006). Embryos were raised at 28.5^{o}C and staged (as described in ref. (Kimmel et al., 1995)). Control and/or transgenic zebrafish lines used for live imaging and immunohistochemistry are listed in supplementary key resource table.

3.7 Method details

3.7.1 Antibodies: Antibody catalog information used in HeLa cells and zebrafish embryos are detailed in supplementary key resource table.

3.7.2 Plasmids and mRNA: Plasmids were generated using Gibson Cloning methods (NEBuilder HiFi DNA assembly Cloning Kit) and maxi-prepped before injection and/or transfection. mRNA was made using mMESSAGE mMACHINE^{TM}SP6 transcription kit. See supplementary key resource table for a list of plasmid constructs and mRNA used.

3.7.3 Cell Culture: HeLa cells stably expressing GFP-FIP3 or centrin-GFP (from (Hehnly and Doxsey, 2014; Hehnly et al., 2012; Kuo et al., 2011; Piel et al., 2001; Wilson et al., 2005)) were maintained at 37^{o}C with 5% CO_2. Rab11a CRISPR vector and Rab11a HDR vector were transfected into cells using Mirus TransIT-LT1 transfection reagent (supplementary key resource table). Cells were selected in puromycin (5 μg/ml). Rab11a-null cells were transfected with mCh-Rab11a (pCS2-mCh-Rab11a), dominant negative Rab11a (pCS2-mCh-Rab11(S25N)) and constituently active Rab11 (pCS2-mCh-Rab11(Q70L)) using Mirus TransIT-LT1. Cells were tested for Rab11 levels using a Western blot with an antibody that detects both Rab11a and Rab11b.

3.7.4 Western blot: Cell lysates were acquired by suspending cells in lysis buffer (HSEG buffer pH 7.4: 40mM HEPES, 40mM NaCl, 5mM EDTA, 4% Glycerol, 20mM NaF; 1% TritonX-100; 1X protease inhibitor; 0.1mM PMSF). After collecting post-nuclear supernatant from lysates, protein concentration was calculated using Bio-

Rad Protein Assay Kit II (see supplementary key resource table). Standard Western blot procedures were performed. Nitrocellulose membranes were probed with primary antibody and/or primary antibody conjugated to horseradish peroxidase diluted in TBS-Tween20 and incubated overnight at 4^{o}C. The membranes were probed using appropriate secondary antibody for an hour at room temperature. The protein levels were visualized using Clarity^{TM} Western ECL substrate (see supplementary key resource table) and imaged using Bio-Rad ChemiDoc^{TM} imager.

3.7.5 Immunofluorescence: Cells were plated on #1.5 coverslips until they reach 90% confluence fixed in 4% PFA at room temperature (30 min) or 100% ice cold methanol (10 mins). Standard immunofluorescent procedures were performed for PFA fixation (Hehnly et al., 2006) and for methanol (Colicino et al., 2018). Cover slips were rinsed with dH_2O and mounted on glass slides using either Prolong Diamond with DAPI mounting media or Prolong Gold (see supplementary key resource table). For zebrafish embryo immunofluorescent protocols see (Aljiboury et al., 2021).

3.7.6 Expansion microscopy: Cells were plated on #1.5 coverslips until they reach 90% confluence and fixed with 4% PFA at room temperature. Standard immunofluorescent procedures were performed for PFA fixation (Hehnly et al., 2006). Expansion microscopy was modified from (Asano et al., 2018; Sahabandu et al., 2019). Specifically, 20% acrylamide gels (Gelation solution 20% acryl amide, 7% sodium acrylate, 0.04% bis acrylamide, 0.5% APS and 0.5%TEMED in 1X PBS) were poured on coverslips and allowed to solidify on ice. The solidified gels were then carefully sectioned into 4mm gel punches using a disposable biopsy punch on

ice. These gel punches were then digested with digestion buffer overnight (0.5% Triton-X, 0.03% EDTA, 1M TrisHCl pH 8, 11.7% Sodium Chloride). We did not use proteinase K in the digestion step to avoid disruption of centrosome proteins. The gel punches were then subjected to a second round of immunofluorescence procedures with antibody concentration titrated down to half the initial concentration. They were then expanded in water at room temperature for two hours with water exchanged every twenty minutes. The expanded punches were then mounted on to MatTek plates and imaged on the Leica SP8 confocal microscope with Lightning and using a long-range objective (HC PL APO 40x/1.10 W CORR CS2 0.65 water objective) to be able to view the sample effectively through the thickness of the agar.

Rab11-endosome area was quantified at the oldest and youngest centriole (differentiated by elevated levels of centrin-GFP signal at the oldest centriole, (Kuo et al., 2011)). The area around the centriole was quantified by drawing a ROI around Rab11-endosomes that overlapped/ touched the centrioles. The Rab11-endosome areas were then compared between the oldest and youngest centriole using a violin plot, graphed using the PRISM 9 software.

3.7.7 Genotyping pcnt$^{+/-}$ zebrafish: Tail fins of adult zebrafish were clipped, whole embryos or fixed and stained embryos were used to extract genomic DNA and genotyped according to (Sepulveda et al., 2018).

3.7.8 Imaging: Zebrafish and tissue culture cells were imaged using Leica DMi8 (Leica, Bannockburn, IL) equipped with a X-light V2 Confocal unit spinning disk equipped with a Visitron VisiFRAP-DC photokinetics unit, a Leica SP8 (Leica, Bannockburn, IL) laser scanning confocal microscope (LSCM) and/or a Zeiss LSM

980 (Carl Zeiss, Germany) with Airyscan 2 confocal microscope. The Leica DMi8 is equipped with a Lumencore SPECTRA X (Lumencore, Beaverton, OR), Photometrics Prime-95B sCMOS Camera, and 89 North-LDI laser launch. VisiView software was used to acquire images. Optics used with this unit are HC PL APO x40/1.10W CORR CS2 0.65 water immersion objective, HC PL APO x40/0.95 NA CORR dry and an HCX PL APO x63/1.40-0.06 NA oil objective. The SP8 laser scanning confocal microscope is equipped with HC PL APO 20x/0.75 IMM CORR CS2 objective, HC PL APO 40x/1.10 W CORR CS2 0.65 water objective and HC PL APO x63/1.3 Glyc CORR CS2 glycerol objective. LAS-X software. was used to acquire images. The Zeiss LSM 980 is equipped with a T-PMT, GaAsP detector, MA-PMT, Airyscan 2 multiplex with 4Y and 8Y. Optics used with this unit are PL APO 63X/1.4 NA oil DIC. Zeiss Zen 3.2 was used to acquire the images. A Leica M165 FC stereomicroscope equipped with DFC 9000 GT sCMOS camera was used for staging and phenotypic analysis of zebrafish embryos.

For live human cell imaging, cells were plated on #1.5 glass bottom Ibidi slides or MatTek plates (see supplementary key resource table). Cells were imaged using spinning disk confocal, LSCM, or wide-field fluorescent microscopy followed by deconvolution (AutoQuant X3). Cells were imaged in a temperature and CO_2 controlled chamber for 1-10 hours at 0.5 - 4-minute time intervals.

For zebrafish embryo imaging, fluorescent transgenic or mRNA injected embryos (refer to strains and mRNAs in supplementary key resource table, and for injection protocols refer to (Aljiboury et al., 2021)) were embedded in 2% agarose at 3.3-5 hours post fertilization (hpf) and imaged using the spinning disk or LSCM.

3.7.9 Fluorescence Recovery after photobleaching (FRAP) and photoconversion: FRAP experiments to compare mobility of mCh-Rab11 and -Rab11 (Q70L) at the centrosome were conducted 24 hours post transfection of mCh-Rab11 or -Rab11(Q70L) in centrin-GFP cells using the Leica DMi8 with spinning disk and photokinetics unit (Visitron VisiFRAP-DC). A ROI was marked at the centrosome in a cytokinetic cell and a 405nm laser was used to photobleach mCherry within that region. Following photobleaching the cell was imaged live to identify recovery of fluorescent signal at the centrosome at 3 second intervals for 3 minutes.

FRAP experiments to compare whether mobility of mCh-Rab11 at the centrosome was dependent on the age of the centrosome were conducted 24 hours post transfection of mCh-Rab11 in centrin-GFP cells using the Leica DMi8 with spinning disk and photokinetics unit (Visitron VisiFRAP-DC). The age of the centrosome was determined by using elevated centrin-GFP levels at the centrosome to identify the oldest centrosome (Kuo et al., 2011). A ROI was marked at the centrosomes in a cytokinetic cells, and a 405 nm laser was used to photobleach mCh within that region. Following photobleaching the cell was imaged live to identify recovery of fluorescent signal at the centrosome for 40 seconds. The ImageJ FRAP calculator macro plug-in was used to generate FRAP curves and calculate half-life and immobile fraction values. Graphs were generated using PRISM9 software.

For photoconversion experiments Dendra-Rab11 was expressed in HeLa cells. A ROI was placed over centrosome localized Dendra-Rab11 in a single daughter cell during pre-abscission. A 405 nm laser was applied within the ROI to photoconvert Dendra-Rab11 from green emission (507 nm) to a red emission (573 nm).

3.7.10 Rab11 optogenetics experiments in zebrafish: Tg (-5actb2:cent4-GFP), Tg (sox17:GFP-CAAX), Tg *BAC*(cftr-GFP) zebrafish embryos were injected with 50-100pg of CIB1-mCh-Rab11, CIB1-mCerulean-Rab11, CRY2-mCherry and/or CRY2 mRNA at the one cell to 4 cell stage (Rathbun et al., 2020a). Embryos were allowed to develop to a minimum of 3.5 hpf and exposed to 488nm light while being imaged using the spinning disk confocal microscope.

3.7.11 Number of centrosomes per pre-abscising cell with bridge directed centrosome movement: Human (HeLa) cells expressing centrin-GFP or DsRed-PACT and zebrafish embryos expressing centrin-GFP and/or PLK1-mCh were imaged using widefield or confocal based imaging. Cells were monitored for centrosome movement using FIJI/ ImageJ. The number of centrosomes that moved towards the cytokinetic bridge was quantified as both daughter cell centrosomes (2 centrosomes), only 1 daughter cell centrosome (1 centrosome) and neither centrosome (0 centrosomes). Centrosome movement was defined as movement from the polar end of the daughter cell across the centroid of the cell towards the cytokinetic bridge (green circle, modeled in Figure S1D). Findings were plotted as a violin plot using PRISM 9.

3.7.12 Distance of the centrosome from cytokinetic bridge: Cells stably expressing centrin-GFP were live imaged following anaphase exit and were monitored for centrosome movement. Centrosome movement towards the cytokinetic bridge was quantified based on centrosome movement across the centroid of the cell towards the cytokinetic bridge (green circle, Figure S3C modeled

in Figure S1D). Distance of the centrosome from the cytokinetic bridge was quantified at the time point the centrosome was nearest to the bridge by utilizing the line tool on FIJI to trace a line to the midpoint of the cytokinetic bridge (modeled in Figure S1D). Frequency distribution of the distance of the centrosome from the cytokinetic bridge was calculated and graphed as a histogram denoting relative frequency (percentage of pre-abscising cells) that moves the centrosome to at least 2, 4, 6, and 8 μm from the midway point of the cytokinetic bridge using PRISM 9.

3.7.13 Tracking centrosome movement: Human (HeLa) cells and zebrafish embryos expressing centrin-GFP were imaged using widefield or confocal based imaging. Cells were projected and the manual tracking plug-in (FIJI/Image J) was used to track the movement of the centrosome (centrin-GFP) from metaphase exit until 3 hours post anaphase in HeLa cells and up to 12 mins post anaphase or abscission completion in zebrafish embryos. The X and Y coordinates of the centrosome and cell body were recorded at each time-point. The change in position of X and Y of the cell body, marked as the center of the cell at each time point), ($\Delta X_{Cellbody} = X_{cellbody\text{-}t2}\text{-}X_{Cellbody\text{-}t1}$; $\Delta Y_{Cellbody} = Y_{Cellbody\text{-}t2}\text{-}Y_{Cellbody\text{-}t1}$)) was subtracted from the change in position of X and Y of the centrosome ($\Delta X_{Centrosome} = X_{Centrosome\text{-}t2}\text{-}X_{Centrosome\text{-}t1}$; $\Delta Y_{Centrosome} = Y_{Centrosome\text{-}t2}\text{-}Y_{Centrosome\text{-}t1}$) between each time-point to control for the movement of the centrosome resulting from the motion of the cell body ($\Delta X = \Delta X_{Cellbody}\text{-}\Delta X_{Centrosome}$; $\Delta Y = \Delta Y_{Cellbody}\text{-}\Delta Y_{Centrosome}$). Using Pythagorean theorem, net distance was calculated between time-points $d_t = \sqrt{\Delta X^2 + \Delta Y^2}$, which were then added together to calculate the total distance travelled by the centrosome $D = \sum_{t=1}^{n} d_t$; where n=final time point. For directional distance towards the cytokinetic bridge, centrin-GFP positive centrosomes were tracked from when they reach the polar

ends of the daughter cells to when they reach the cytokinetic bridge using the method mentioned above. If the centrosome does not move towards the cytokinetic bridge, then the distance traveled by that centrosome is recorded as 0 μm.

3.7.14 Centrosome Intensity profiles: Z stacks shown are maximum projected representative cells (FIJI/ImageJ). For intensity calculations, z-stacks were sum projected, a ROI was marked around the centrosome, and mean fluorescence intensities were measured. Fluorescent intensities were calculated as mean intensity – minimum intensity. Intensities calculated were then normalized to average intensity of the parent cell population within the experiment. Three-dimensional intensity profiles were created using FIJI/ImageJ. Outliers were identified using an iterative Grubb's test with alpha = 0.05 using PRISM9 software.

3.7.15 Phenotypic analysis of cells exhibiting cytokinetic defects: Human (HeLa) cells and zebrafish embryo cells (described above) were assessed for the presence of binucleated cells, represented as a percentage.

3.7.16 Tracking centrosome number: Zebrafish embryo cells (described above) were assessed for abnormalities in the number of centrosomes at interphase. The number of centrosomes within each cell was counted and the percentage of cells with greater than two centrosomes were graphed using PRISM9 software.

3.7.17 Statistical Analysis: Unpaired, two-tailed t-tests and one way ANOVA were performed using PRISM9 software. **** denotes a p-value< 0.0001, *** p-

value<0.001, ** p-value<0.01, * p-value<0.05. For further information on detailed statistical analysis see Table S1.

3.7.18. METHODS TABLE 1: TABLE S1. Detailed statistical analysis results reported.

Figures	Y-Axis	Category	n (cell)	n (embryo)	n (expt)	Statistical Test	Parameters	Result	p-value
3.1E	Number of centrosomes with bridge directed centrosome movement in pre-abscising cells	Zebrafish embryo cell (Centrin-GFP)	n=26	n=4	N/A	One Way ANOVA	F (4,102) = 0.82	**	0.0082
		Zebrafish embryo cell (PLK1-mCh)	n=40	n=4	N/A				
		Zebrafish embryo cell in the Kupffer's Vesicle	n=10	n=2	N/A				
		Human cell (HeLa) Centrin-GFP	n=15	N/A	n=3				
		Human cell (HeLa) Ds-Red-PACT	n=21		n=4				
3.1E	Number of centrosomes per pre-abscising cell with bridge directed centrosome movement	Zebrafish embryo cell (Centrin-GFP)	n=26	n=4	N/A	One Way ANOVA	F (2,71) = 0.03110		
		Zebrafish embryo cell (PLK1-mCh)	n=40	n=4	N/A			n.s.	0.9973
		Zebrafish embryo cell in the Kupffer's Vesicle	n=10	n=2	N/A			n.s.	0.7506
		Human cell (HeLa) Centrin-GFP	n=15	N/A	N/A	Two-tailed Student's t-test	t = 0.2392, df = 31	n.s.	0.8126
		Human cell (HeLa) Ds-Red-PACT	n=21		N/A				
3.1E	Number of centrosomes per pre-abscising cell with bridge directed centrosome movement	Zebrafish embryo cell (Centrin-GFP)	n=26	n=4	N/A	Two-tailed Student's t-test	t = 3.365, df=80	**	0.0012
		Zebrafish embryo cell (PLK1-mCh)	n=40	n=4	N/A				
		Zebrafish embryo cell in the Kupffer's Vesicle	n=10	n=2	N/A				
		Human cell (HeLa) Centrin-GFP	n=15	N/A	N/A				

		Human cell (HeLa) Ds-Red-PACT	n=21		N/A				
3.2C	Fold change of photoconverted Dendra-Rab11 increase at the cytokinetic bridge	Before Photobleaching	n=6	N/A	n=4	Two-tailed Student's t-test	t = 6.029, dF = 10	***	0.0001
		After Photobleaching							
3.3C	% Centrosome movement towards the cytokinetic bridge first	Human (HeLa) Cells	n=10	N/A	N/A	N/A	N/A	N/A	N/A
		Zebrafish embryo cell at epiboly	n=13	n=4	N/A				
3.3E	Fluorescent Intensity (Normalized)	Oldest centrosome	n=3	N/A	N/A	N/A	N/A	N/A	N/A
		Youngest Centrosome							
3.3F	Oldest centrosome/ Youngest centrosome	Mobile Fraction (%)	n=3	N/A	N/A	One-Way ANOVA	F (2,6) = 7.515	*	0.016
		Half Life (T1/2)						n.s.	0.49
3.3J	Endosome Area at Daughter or Mother Centriole	Oldest Centrosome	n=7 Centrosomes		N/A	Two-tailed Student's t-test	t=4.268, df=12	**	0.0011
		Youngest Centrosome							
3.4C	Number of centrosomes per pre-abscising cell with bridge directed centrosome movement	Control	n=25	N/A	N/A	One Way ANOVA	F (4,79) = 3.148		
		Rab11-null cells	n=35		N/A			**	0.0049
		Rab11-null cells, plus mCh-Rab11	n=7		N/A			n.s.	0.9991
		Rab11-null cells, plus mCh-Rab11(S25N)	n=9		N/A			**	0.0073
		Rab11-null cells, plus mCh-Rab11(Q70L)	n=6		N/A			***	0.0005
3.4F	Directional displacement of	Control	n=9	N/A	N/A	One Way ANOVA	F (4, 87) = 6.21		
		Rab11-null cells	n=15		N/A			***	0.0002
		Rab11-null cells, plus	n=7		N/A			n.s.	0.1019

	centrosome towards the cytokinetic bridge (μm)	mCh-Rab11							
		Rab11-null cells, plus mCh-Rab11(S25N)	n=9		N/A			***	0.0009
		Rab11-null cells, plus mCh-Rab11(Q70L)	n=6		N/A			***	0.0006
S3.3F	% Binucleated cells	Control	n>100	N/A	n=3	One Way ANOVA	F (2,6) = 18.07		
		Rab11-null cells	n>100		n=3			**	0.0021
		Rab11-null cells, plus mCh-Rab11	n>100		n=3			n.s.	0.3245
S3.3G	Total distance traveled by centrosome post anaphase exit (μm)	Control	n=9	N/A	n=4	Two-tailed Student's t-test	t=5.000, df=32	****	<0.0001
		Rab11-null cells	n=8		n=4				
S3.3I	Mean Fluorescent Intensity (A.U.)	Rab11-null cells, plus mCh-Rab11	n=18	N/A	N/A	Two-tailed Student's t-test	t=3.208, df=30	n.s.	0.2183
		Rab11-null cells, plus mCh-Rab11(Q70L)	n=15						
S3.3J	Fluorescent Intensity Normalized (A.U.)	Rab11-null cells, plus mCh-Rab11	n=18	N/A	N/A	N/A	N/A	N/A	N/A
		Rab11-null cells, plus mCh-Rab11(Q70L)	n=15						
S3.3K	Mobile Fraction (%)	Rab11-null cells, plus mCh-Rab11	n=18	N/A	N/A	Two-tailed Student's t-test	t=3.208, df=30	**	0.0032
		Rab11-null cells, plus mCh-Rab11(Q70L)	n=15		N/A				
S3.3L	Half-life (t1/2, sec)	Rab11-null cells, plus mCh-Rab11	n=18	N/A	N/A	Two-tailed Student's t-test	t=4.594, df=31	****	<0.0001
		Rab11-null cells, plus mCh-Rab11(Q70L)	n=14		N/A				
3.5B	Ratio of Rab11-null centro	Centrin	n>30 Centrosomes/ experiment		n=3	One Way ANOVA	F (4, 10) = 16.55	n.s.	0.9991
		Cenexin			n=3				
		Pericentrin			n=3			*	0.0352
		GFP-FIP3			n=3			***	0.0008

	some intensity / Control intensity (A.U.)	Transferrin Receptor			n=3			***	0.0004
3.5D	Pericentrin normalized intensity pre-abscising cells (A.U.)	Control	n=38 Centrosomes		n=5	One Way ANOVA	F (4, 242) = 18.19		
		Rab11-null cells	n=43 Centrosomes		n=5			****	<0.0001
		Rab11-null cells, plus mCh-Rab11	n=62 Centrosomes		n=4			n.s.	0.6632
		Rab11-null cells, plus mCh-Rab11(S25N)	n=61 Centrosomes		n=4			****	<0.0001
		Rab11-null cells, plus mCh-Rab11(Q70L)	n=43 Centrosomes		n=3			****	<0.0001
S3.4G	Pericentrin normalized intensity in late pre-abscising cells (A.U.)	Control	n=22 Centrosomes/ experiment		n=5; 1 representative shown	Two-tailed Student's t-test	t=11.00, df=42	****	<0.0001
		Rab11-null Cells	n=20 Centrosomes/ experiment						
3.6C	Number of centrosomes per pre-abscising with bridge directed centrosome movement	Control	n=26	n=4	N/A	One Way ANOVA	F (3,77) = 2.733		
		PCNT+/-	n=16	n=4				**	0.0025
		Centrin-GFP, plus CRY2	n=21	n=4				n.s.	0.6449
		Centrin-GFP, plus CRY2 and CIB1-mCh-Rab11	n=19	n=4				*	0.0126
3.6D	Distance traveled by centrosome after anaphase (μm)	Control	n=19	n=4	N/A	One Way ANOVA	F (3,110) = 9.907		
		PCNT+/-	n=14	n=4				***	0.0001
		Centrin-GFP, plus CRY2	n=14	n=4				n.s.	0.8335
		Centrin-GFP, plus CRY2 and CIB1-mCh-Rab11	n=11	n=4				**	0.0067
3.6F	Daughter cells with supernumerary centrosomes	Control	n>30/ embryo	n=3	N/A	One Way ANOVA	F (3,8) = 38.51		
		PCNT+/-	n>30/ embryo	n=3				***	0.0003
		Centrin-GFP, plus CRY2	n>25/ embryo	n=3				n.s.	0.5719

		Centrin-GFP, plus CRY2 and CIB1-mCh-Rab11	n>35/embryo	n=3				***	0.0003
S3.5G	% Binucleated cells	Control	n>42/embryo	n=13	N/A	One Way ANOVA	F (3,25) = 5.644		
		PCNT+/-	n>42/embryo	n=9				*	0.0417
		plus CIB1-mCh-Rab11	n>30/embryo	n=3				n.s.	0.9916
		plus CRY2 and CIB1-mCh-Rab11	n>30/embryo	n=4				**	0.0031

3.7.19. METHODS TABLE 2: SUPPLEMENTARY KEY RESOURCE TABLE

Reagent or RESOURCE	Source	Identifier
Antibodies		
Rab11	Cell Signaling Technologies	3539S; RRID: AB_2253210
Gamma-tubulin	SigmaAldrich	T5192; RRID: AB_261690
GAPDH-HRP	Proteintech	HRP-60004; RRID: AB_2737588
Donkey Anti-Rabbit-HRP	Jackson Immuno Research	711-035-152; RRID: AB_10015282
Transferrin Receptor	Abcam	ab1086; RRID: 297535
Pericentrin	Abcam	ab4448; RRID: AB_304461
Cenexin	ProteinTech	12058-1-AP; RRID: AB_2156630
Anti-GFP	GeneTex	GTX13970; AB_371416
ZO-1 Monoclonal Antibody (ZO-1, 1A12) Alexa Fluor 488	Life Technologies	339188; RRID: AB_2532187
Alexa Fluor Anti-Rabbit 488	Life Technologies	A21206; RRID: AB_2535792
Alexa Fluor Anti-Rabbit 568	Life Technologies	A10042; RRID: AB_2534017
Alexa Fluor Anti-Rabbit 647	Life Technologies	A31573; RRID: AB_2536183
Alexa Fluor Anti-Mouse 488	Life Technologies	A21202; RRID: AB_141607
Alexa Fluor Anti-Mouse 568	Life Technologies	A10037; RRID: AB_2534013
Alexa Fluor Anti-Mouse 647	Life Technologies	A31571; RRID: AB_162542
Anti-aTubulin antibody Alexa Fluor 555conjugated	EMD millipore	05-829-AF555
Chemicals, Peptides, and Recombinant Proteins		
DAPI	SigmaAldrich	D9542-10mg
NucBlue™ Fixed Cell stained Ready Probes	ThermoFischer	R37606

NucBlue™ Live Ready Probes	ThermoFischer	R37605
Agarose	ThermoFischer	16520100
BSA	Fisher Scientific	BP1600-100
BIO BASIC Maxi Prep Kit	BIO BASIC	9K-0060023
Dimethylsulphoxide	Fisher Scientific	BP231-100
Paraformaldehyde	Fisher Scientific	O4042-500
Phosphate Buffered Saline	Fisher Scientific	10010023
Life Technologies Prolong Diamond Antifade Moutant with DAPI	Fisher Scientific	P36971
35 mm Dish| No.1.5. coverslip| 20 mm Glass Diameter	MatTek Corporation	P35G-1.5-20-C
μ-Slide 8 Well Glass Bottom: No. 1.5H (170 μm +/- 5 μm) D263 M Schott glass, sterilized	IBIDI	80827
Molecular Probes Prolong Gold Antifade Moutant	Fisher Scientific	P36934
Triton X-100	Fisher Scientific	BP151500
Tween 20	ThermoFischer	BP337500

Tris-HCl	Fisher Scientific	BP153
APS	Fisher Scientific	BP179-100
40% Acrylamide	Sigma-Aldrich	A4058-100ML
97% Sodium acrylate	Sigma-Aldrich	408220-25G
40% Bisacrylamide	EMD Millipore	1300-500ML
TEMED	Fisher Scientific	BP150-100
Disposable Biopsy Punch	Integra Miltex	33-34
Ethylenediaminetetraacetic acid (EDTA)	Fisher Scientific	BP120
Sodium Chloride	Fisher Scientific	BP358
NEBuilder HiFi DNA assembly Cloning Kit	New England BioLabs	E5520S
mMESSAGE mMACHINE^{TM}SP6	Invitrogen	AM1340
Mirus TransIT-LT1 transfection	Mirus	MIR2305
Rab11A CRISPR Vector	Santa Cruz Biotechnology	SC-400617

Rab11A HDR Vector	Santa Cruz Biotechnology	SC-400617-HD
BioRad Protein Assay Kit II	BioRad Laboratories	5000002
Ponceau Stain	Boston BioProducts	ST-180-500
Clarity™ Western ECL substrate	BioRad Laboratories	170560
Experimental models: Cell lines		
HeLa Cells with stable GFP-FIP3	Hehnly and Doxsey 2014; Hehnly et al., 2012; Wilson et al., 2005	N/A
HeLa Cells with stable Centrin-GFP	Kuo et al., 2011; Piel et al., 2001	N/A
Rab11KO HeLa Cells with stable GFP-FIP3	Rathbun et al., 2020a	N/A
Rab11 KO HeLa Cells with stable Centrin-GFP	This paper	N/A
Experimental models, organisms and strains		
Zebrafish	Zebrafish International Resource Center	TAB-Wildtype
Zebrafish	Zebrafish International Resource Center	Tg (Sox17:DsRed)
Zebrafish	Gift from Solinca-Krezel lab, generated by Harris Lab	Tg (-5actb2:cent4-GFP)

Zebrafish	Sepuldeva et al., 2018. Gift from Jao Lab UCSD	Tg (*pcnt*^{tup2})
Zebrafish	(Dasgupta and Amack, 2016)	Tg (sox17:GFP-CAAX)^{sny101}
Zebrafish	(Navis et al., 2013)	Tg*BAC*(cftr-GFP)
Zebrafish	This paper	Tg (-5actb2:cent4-GFP), Tg (*pcnt*$^{tup+/-}$)
Recombinant DNA		
Plasmid: PCS2-CRY2	(Rathbun et al., 2020a	Addgene Plasmid #140572
Plasmid: PCS2-CIB1-mCherry-Rab11a	Rathbun et al., 2020a)	Addgene Plasmid #140573
Plasmid: PCS2-CIB1-mCerulean-Rab11a	(Rathbun et al., 2020a)	Addgene Plasmid #140574
Plasmid: mRuby2-MannII-N-10	(Lam et al., 2012)	Addgene Plasmid #55903
Plasmid: PCS2-mCherry-Rab11a	This paper	Addgene in process
Plasmid: PCS2-mCherry-Rab11a (S25N)	This paper	Addgene in process
Plasmid: PCS2-mCherry-Rab11a (Q70L)	This paper	Addgene in process
Plasmid: PCS2-Dendra-Rab11a	This paper	Addgene in process
Plasmid: PCS2-PLK1-mCherry	(Colicino et al., 2019)	Addgene Plasmid #127154
Software and algorithms		

ImageJ/FIJI	NIH and Laboratory for Optical and Computational Instrumentation	https://imagej.net/Fiji
IMARIS, Bitplane	Oxford Instruments	https://imaris.oxinst.com/
PRISM9	GraphPad	https://www.graphpad.com/scientific-software/prism/
LAS-X Software	Leica Microsystems	https://www.leica-microsystems.com/products/microscope-software/p/leica-las-x-ls/
VisiView	Visitron	https://www.visitron.de/products/visiviewr-software.html
AutoQuant X3	Meyer Instruments	https://www.meyerinst.com/mediacybernetics/autoquant/
Zeiss Zen 3.2	Carl Zeiss	https://www.zeiss.com/microscopy/us/products/microscope-software/zen.html

CHAPTER FOUR:

Rab11 dependent mechanisms of centrosome positioning and cilia formation during Kupffer's Vesicle development

This chapter features work from my first author manuscript prepared for publication.

Rab11 dependent mechanisms of centrosome positioning and cilia formation during Kupffer's Vesicle development

Nikhila Krishnan[1, 2], Julie Manikas[1, 3], Christopher Taveras[1, 2], Eric Ingram[1, 2], Nicole A. Hall[1, 3], Lindsay I. Rathbun[1,4], Favour Ononiwu[1, 2], Judy Freshour[1, 2] and Heidi Hehnly[1, 2,*]

[1] Biology Department, Syracuse University, NY, USA

[2] BioInspired Institute, Syracuse University, NY, USA

[3] Current address, Department of Cell Biology, NYU Grossman School of Medicine, NY, USA

[4] Current location: University of Rochester, Rochester, NY

*Lead contact, correspondence: hhehnly@syr.edu, Twitter: @LovelessRadio

4.1 Abstract

An essential process for cilia formation during epithelialization is for the centrosome to move and dock with the cell's forming apical membrane. Our study examined centrosome positioning using *Danio rerio's* left-right organizer (Kupffer's Vesicle, KV) as a model. We found that KV mesenchymal cells while rearranging into epithelial cells organized into a rosette-like structure, the cells moved their centrosomes from random intracellular positions to the forming apical membrane. During this process, these cells' centrosomes were constructing cilia intracellularly while the centrosome was repositioning towards the rosette center. Once the centrosome with associated cilia reaches the rosette center, they remain intracellular until the lumen expands to approximately 300 μm^2. Using optogenetic strategies we identified that the small GTPase, Rab11 and its associated membranes, regulates not only cilia formation, but centrosome movement towards the forming apical membrane, whereas Rab8 was primarily involved in cilia elongation once cilia extend into the KV lumen.

4.2 Introduction

A fundamental question in cell biology is to understand how and when a cilium is made during tissue formation. A primary or motile cilium is a microtubule-based structure that extends from the surface of a cell and can sense extracellular cues to transmit to the cell body. Defects in cilia formation can lead to numerous disease states known as ciliopathies (Hall and Hehnly, 2021). Foundational studies identified two distinct pathways for ciliogenesis *in vivo* using mammalian tissues from chicks and rats (SOROKIN, 1962). The mechanism of ciliogenesis in mammalian lung cells is initiated with the centrosome docking to the plasma membrane that is followed by the growth of the ciliary axoneme and the membrane surrounding it (Sorokin, 1968). The second mechanism identified in mammalian smooth muscle cells and fibroblasts is initiated by the centrosome inside the cell (SOROKIN, 1962). The centrosome recruits the ciliary vesicle and constructs the ciliary axoneme inside the cell. They are then transported to the plasma membrane where the cilia extends into the extracellular space (SOROKIN, 1962). These studies demonstrate that different *in vivo* ciliated tissues may construct their cilia differently potentially due to the nature of how a tissue develops. This presents an important argument that variations in cilia formation mechanisms may occur *in vivo* during specific types of tissue morphogenesis. In our studies we chose to examine how cilia are assembled during Mesenchymal to epithelial transition (MET) in an *in vivo* vertebrate model, *Danio rerio* (zebrafish).

MET is an evolutionarily conserved process that occurs during ciliated tissue formation (Pei et al., 2019), and an excellent example of this is with the vertebrate organ of asymmetry. An organ of asymmetry is required to place visceral and abdominal organs with respect to the two main body axes of the animal (Grimes and

Burdine, 2017). *Z*ebrafish is a genetically tractable model to test how cilia form during organ of asymmetry development. In zebrafish the organ of asymmetry is known as Kupffer's Vesicle (KV). KV development is an ideal model to characterize cilia development during MET due to embryos external development. This allows KV formation to be easily monitored using fluorescent markers to note KV mesenchymal-like precursor cells congregating together and self-organizing into a rosette-like structure where they establish apical-basal polarity at the rosette center (Amack and Yost, 2004; Rathbun et al., 2020a). The rosette center is the site where a fluid-filled lumen forms and KV cells will then extend their primary/motile cilia into (Navis et al., 2013). These cilia then beat in a leftward motion to direct fluid flow essential for the establishment of the embryo's left-right axis (Nonaka et al., 1998). While much is known about KV post-lumen formation, little is known about the spatial and temporal mechanisms that regulate cilia formation during KV cell MET.

One essential structure for cilia formation is the centrosome. The centrosome is commonly known as the main microtubule organizing center of the cell with two barrel shaped microtubule structures called centrioles enclosed in a network of proteins call the pericentriolar matrix (Vertii et al., 2016). The position of the centrosome within the cell is integral to generate specific cues that facilitate cellular processes like 1) where the apical membrane will form and 2) where the cilium will form. In *C. elegans* intestinal cells, the placement of the centrosome during epithelialization is necessary for apical membrane establishment (Feldman and Priess, 2012). The centrosome then docks at the apical membrane and facilitates the growth of a cilium that extends to the extracellular space. One question that arises though, is what molecular and cellular mechanisms dictate when the centrosome should move to the apical membrane? Our recent study found that the

centrosome moves towards the cytokinetic bridge before cytokinetic bridge abscission (Krishnan et al., 2022). This movement was dictated by the small GTPase Rab11 (Krishnan et al., 2022), which has also been implicated in cilia formation in collaboration with another small GTPase Rab8 (Knödler et al., 2010; Lu et al., 2015). Here we first characterize the temporal and spatial dynamics of cilia formation in the developing KV. We then test explore the idea that Rab11 and Rab8 are required for centrosome movement towards the forming apical membrane to regulate cilia formation in the developing KV.

4.3 Results and Discussion

4.3.1. Primary cilia form prior to lumenogenesis during tissue morphogenesis.

We tested when KV cells start to make cilia during KV morphogenesis. To do this Sox17:GFP-CAAX transgenic embryos that mark KV cells were fixed at different stages of KV development, pre-rosette (8-9 hours post fertilization, hpf), rosette (10 hpf), and lumen (12 hpf, Figure 4.1A). The pre-rosette stage is where KV cells are more mesenchymal-like and have yet to organize into a rosette, whereas in the rosette stage KV cells are organized into a rosette-like structure with their newly forming apical membranes pointing towards the center of the rosette (Amack and Yost, 2004; Amack et al., 2007). The lumen stage is where KV cells surround a fluid filled lumen (Figure 4.1A). After fixing embryos at each of these stages, they were immunostained for cilia using an antibody against acetylated tubulin (Figure 1A). Interestingly, we found that a significant population of KV cells had cilia before the KV formed a lumen (Figure 4.1A). To examine this further we calculated the percentage of ciliated cells within the KV where we found that in the pre-rosette (33.25$\pm$3.33%) and rosette (48.06$\pm$5.94%) stages there was a significant population of cells that were already assembling a cilium (Figure 4.1A-B). Once the KV forms a lumen, a significant increase in the number of ciliated KV cells occurs (64.82$\pm$5.27%). These studies suggested a couple of things: 1) KV cells were forming cilia before they had an extracellular space (KV Lumen) to position them into and 2) KV lumen formation correlated with a significant increase in KV cells having cilia.

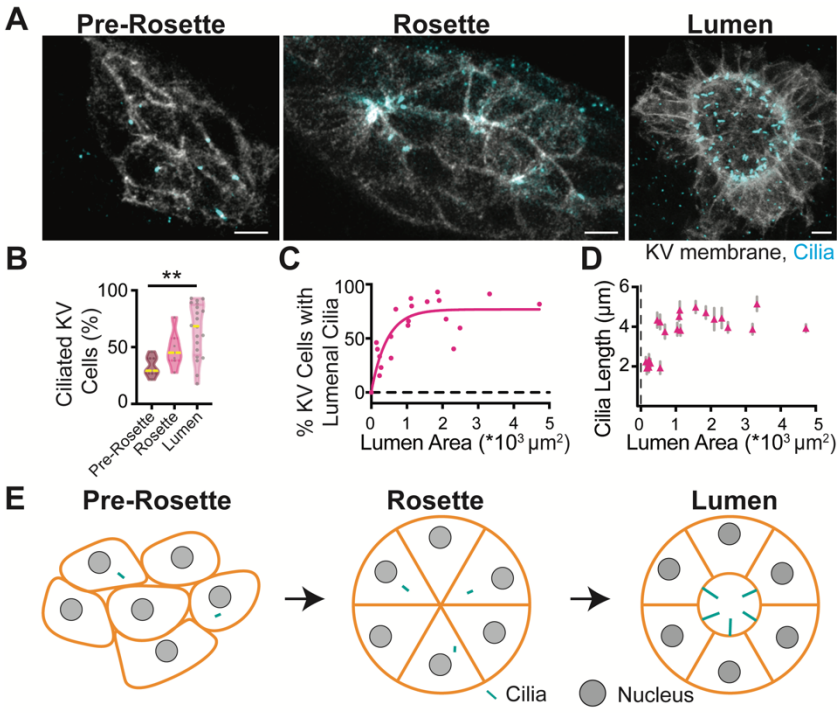

Figure 4.1: Primary cilia form prior to KV lumenogenesis. (A) Confocal micrographs of cilia (acetylated tubulin, cyan) in KV cells (KV membranes, Sox17:GFP-CAAX, gray) during KV developmental stages: pre-rosette, rosette and lumen. (B) Percentage of ciliated KV cells at different KV developmental stages depicted as a violin plot with median (yellow dashed line) and quartiles (gray dotted lines). One way ANOVA across KV developmental stages, n>7 embryos, **p<0.01. (C) Scatter plot depicting relationship between percentage of KV cells with lumenal cilia and two-dimensional lumen area. n=29 embryos. Goodness of fit R2= 0.8577. (D) Scatter plot depicting relationship between cilia length and two-dimensional lumen area. n=37 embryos. (E) Model depicting primary cilia (cyan) form prior to lumenogenesis during KV development. KV membranes (yellow) and nucleus (gray). For graphs: n-values and statistical results detailed in Table S1.

To test whether a relationship exists between lumen opening and expansion and KV cell ciliation, we calculated the percentage of KV cells lumenal cilia (Figure 4.1C) and cilia length (Figure 4.1D) in relation to KV lumen area (0 μm^2 to 5000 μm^2). We find that 50% of the cilia population become lumenal when the lumen area reaches 306.7 μm^2 (Figure 4.1C). Interestingly, this is at around the same lumen area where cilia start to reach its maximum length of 4.5 μm, where half the cilia population reach a length of 2.25 μm at a KV lumen size of 357 μm^2 (Figure 4.1D). The percentage of KV cells with lumenal cilia plateaus at 76.83% when the lumen reaches a size of 2015.3 μm^2 (Figure 4.1C) suggesting that approximately 75-80% of KV cells are ciliated once the lumen is 2015.3 μm^2 or greater (Figure 4.1C). These studies also suggests that cilia extension into the KV lumen is dependent on KV lumen area expansion.

During the Rosette stage (preceding lumen formation) close to 50% of KV cells are ciliated with their average cilia length measuring at 2.25 μm (Figure 4.1B, 4.1D, 4.1E). At this stage, most of the KV cells organize their cilia towards the rosette center where the cilia are perfectly positioned to extend into the lumen once it opens (Figure 4.1B, 4.1E). Once the cilia can extend into the lumen, this is when a significant increase in cilia length occurs where an average length of 4.5 μm is measured (Figure 4.1D). Taken together, these studies suggest that cilia form inside the cell, then position themselves towards the rosette center so that they can extend into the forming KV lumen (Figure 4.1E).

4.3.2 Cilia form inside KV cells before a lumen is made then recruit Arl13b before extending into the lumen.

Our studies in Figure 1 suggest that cilia are formed in KV cells, then positioned at the rosette center to then extend out from the apical membrane into the lumen once the lumen gets to a set area. To test this model, embryos were fixed at the KV pre-rosette stage, rosette stage, and lumen stage. Volumetric projections of surface rendered KV cells were performed at each of these stages. KV cell outlines were noted using GFP-CAAX and cilia were immunostained using acetylated tubulin (Figure 4.2A). Surface rendering using IMARIS software allowed for the spatial positioning of cilia in KV cells across KV developmental stages to be easily assessed (Figure 4.2A). To do this, the boundaries of both the cell (GFP-CAAX) and cilia (acetylated tubulin) were highlighted to create a three-dimensional space filling model of both cell and cilia. We identified that as KV develops from pre-rosette to rosette, to lumen stage, intracellular cilia approach the apical membrane (Figure 4.2A). Once a lumen is formed, the cilia extend into the developing KV lumen (Figure 4.2A). To identify whether cilia positioning was significantly moving towards the forming apical membrane during the rosette stage and during lumen formation we calculated the relative distance of cilia from the cell boundary closest to the KV center (modeled in Figure 4.2B; performed in Figure 4.2C). When values approach 0, cilia are closer to the cell boundary, which is significantly the case as KV transitions from pre-rosette to lumen stages (Figure 4.2C). This finding suggests that KV cell cilia are first constructed intracellularly then positioned at the cell boundary (newly forming apical membrane) during the rosette stage, where they then can extend into expanding lumen.

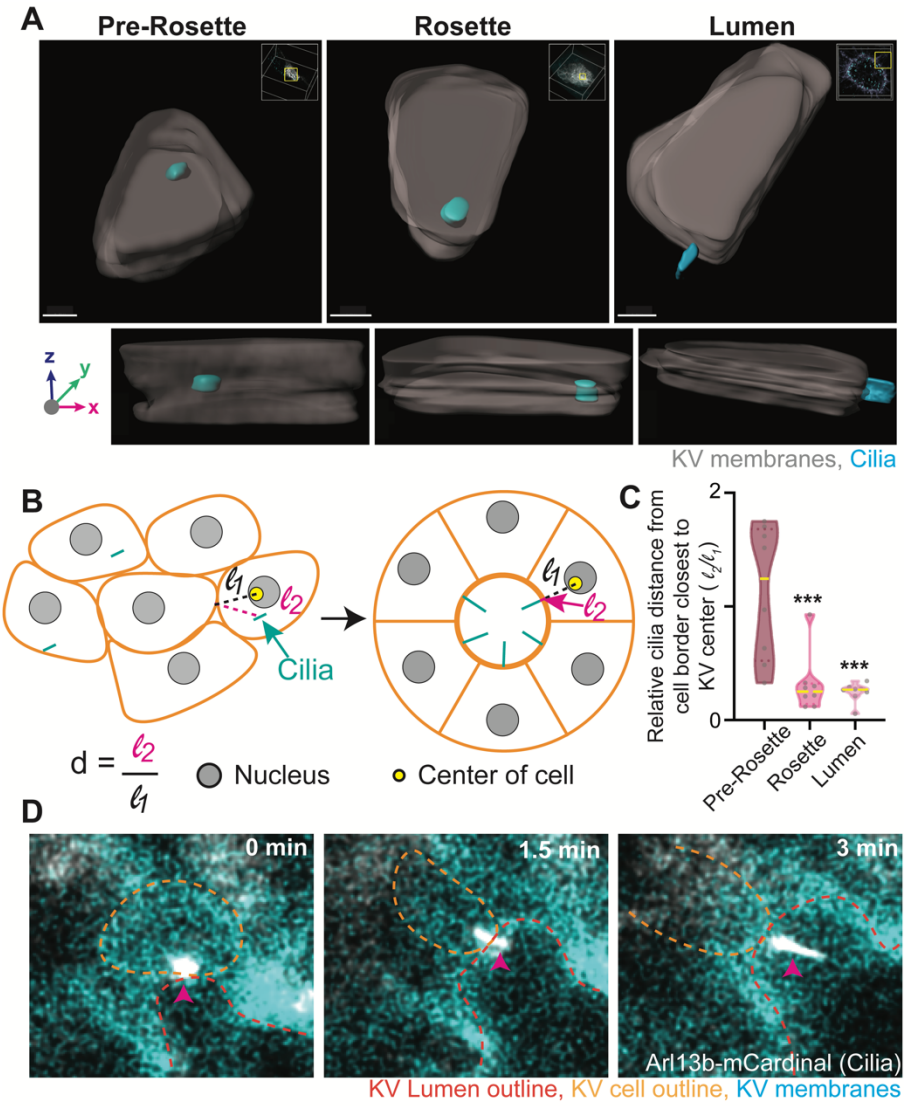

Figure 4.2: Cilia form inside KV cells before a lumen is made then recruit Arl13 before extending into the lumen.
(A) Three-dimensional surface rendering of a representative KV cell during pre-rosette, rosette, and lumen KV developmental stages with cilia (acetyl-tubulin, cyan) and KV plasma membranes (KV membranes, Sox17:GFP-CAAX, gray) rendered. (B) Model depicting quantification of relative distance of the cilium from the cell border closest to KV center. Cilia, cyan. Nucleus, gray. Center of KV cells, yellow. Pink dashed line is distance of cilium from cell membrane. Black dashed line is distance of cell center to cell membrane. (C) Violin plot depicting relative distance of cilia from cell boarder closest to KV center. n=8 cells, from the embryos depicted (A). (D) Time points taken from a lived video micrograph of a KV cell building and extending a cilium (Arl13b-mCardinal) into the lumen of the KV.
For graphs: n-values and statistical results detailed in Table S1.

We next positioned these findings from our fixed developmental stages where cilia were immunolabeled for the structural component, acetylated-tubulin, with live cell microscopy studies where we examined the timing of cilia formation during lumen expansion using the fluorescent cilia membrane marker Arl13b (Figure 4.2D). These studies identified that Arl13b is recruited to the cilium once the cilium is docked at the apical membrane (Figure 4.2D, 0 min), then the cilium starts to extend and elongate into the lumen of the KV once the lumen hits approximately 300 μm2. These studies together suggest that cilia form inside KV cells in random locales before the lumen is made, move to the forming apical membrane at the Rosette center, where they then recruit Arl13b, to then extend into the expanding KV lumen.

4.3.3. Centrosomes and cilia are positioned to the site of lumen formation.

Since we found that cilia position themselves at the apical membrane during KV rosette formation, we wanted to test at what spatial location within the KV cell does a centrosome start to build a cilium. We tested this, using embryos fixed at three different KV developmental stages, pre-rosette, rosette, and lumen (Figure 4.3). Centrosomes and cilia were immunostained for γ-tubulin and acetylated tubulin respectively, and actin was decorated using phalloidin to mark rosette center and cell-cell junctions during the lumen stage (Figure 4.3A). The cilium within each cell was positioned in a way that appeared to be extending from the centrosome (Figure 4.3A, insets in 4.3a'). To test the relationship between centrosome positioning and when it constructs a cilium during KV development, we calculated KV cell centrosome angles and centrosome with cilia angles in relation to the KV center (Figure 4.3B, 4.3C). To do this, KV cell membranes around KV cells were outlined to identify KV centroid. Individual KV cells centroid position was also identified. For

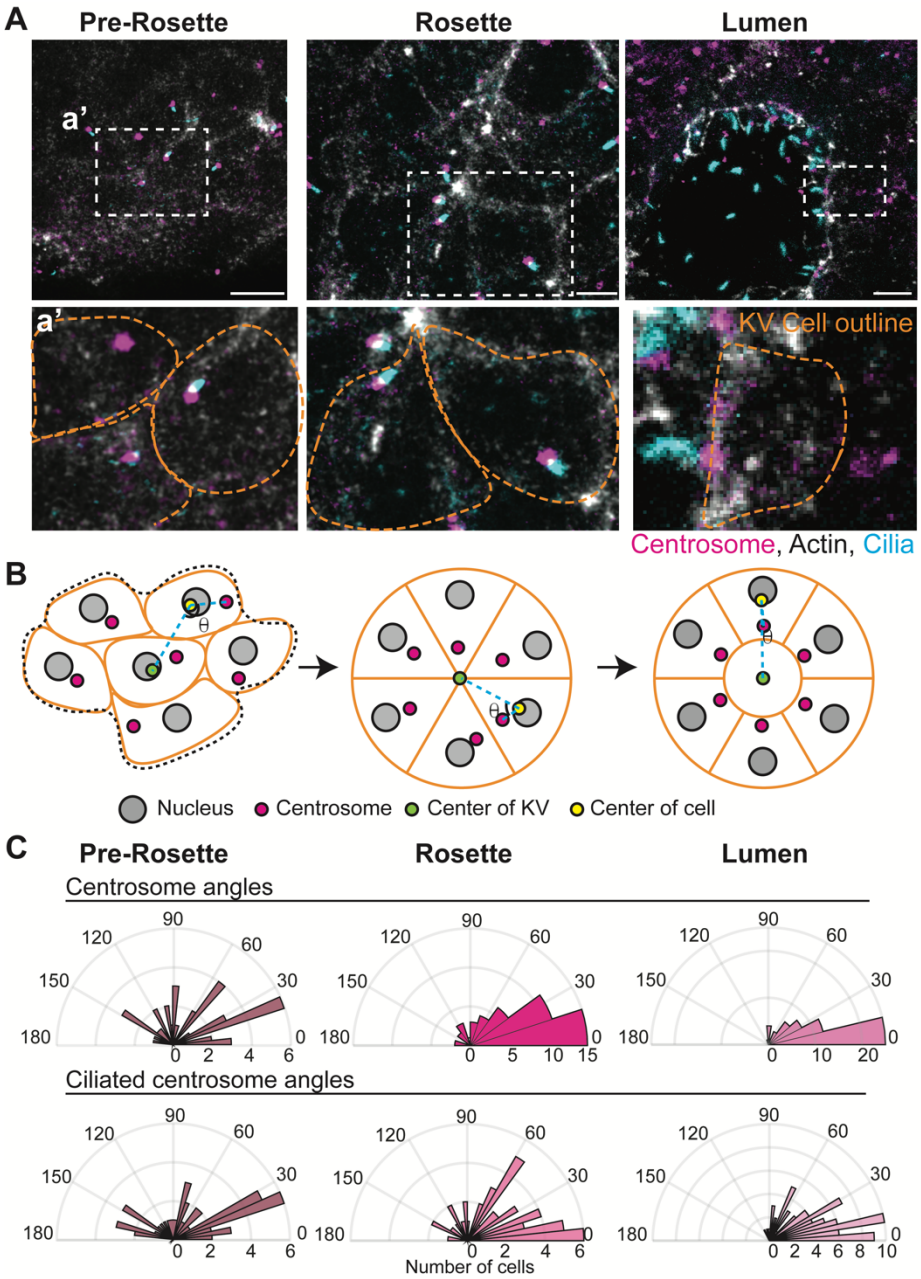

Figure 4.3: Centrosomes and cilia are transported to the site of lumen formation.

(A) Projected confocal micrographs of KV development during pre-rosette, rosette and lumen with cilia (acetylated tubulin, cyan), centrosome (γ-tubulin, magenta), actin (phalloidin, gray) and KV membranes (Sox17:GFP-CAAX, gray) shown. (a') 2X magnified insets from (A) highlighting centrosome and cilia positioning. (B) Model depicting quantification of angle of the centrosome from the center of the KV. Nucleus, gray. Center of KV cells, yellow, Center of KV, green. (C) Polar histogram of angle of centrosome and angle of centrosome containing cilia from the center of the KV at KV developmental stages pre-rosette, rosette and lumen. n>100 cells, n=3 embryos. For graphs: n-values and statistical results detailed in Table S1. See also Figure S1.

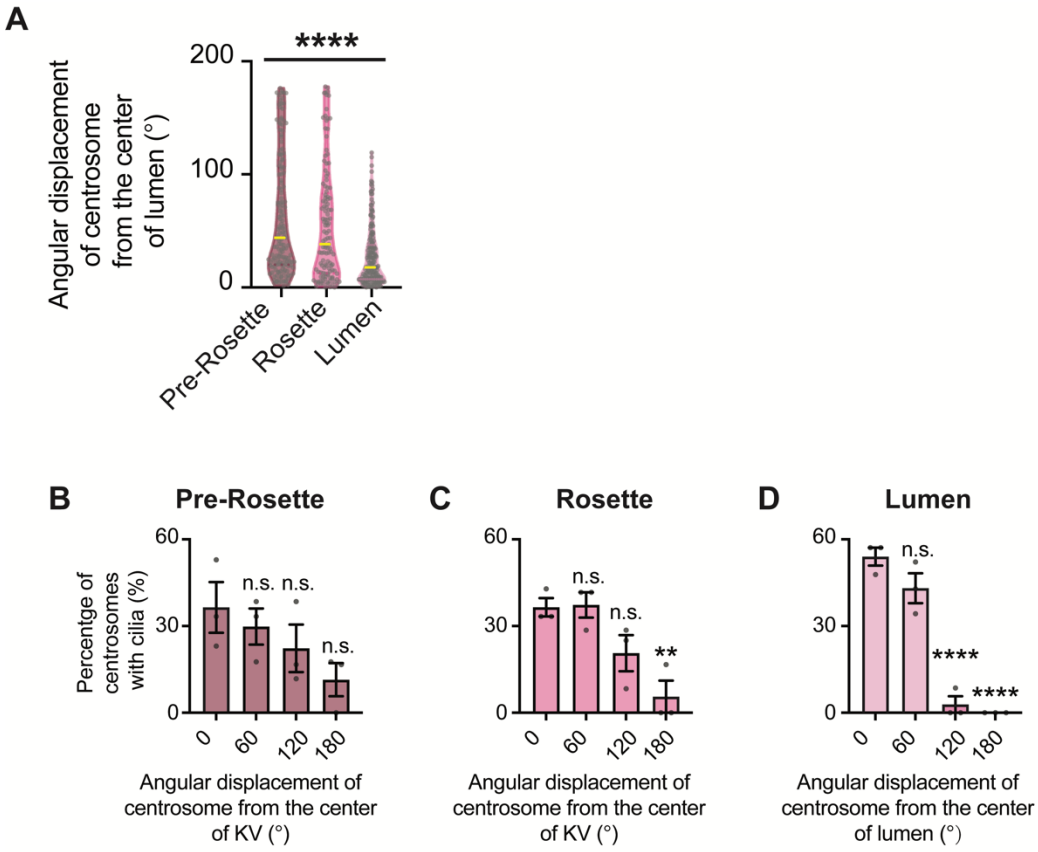

Figure S4.1: Centrosomes and cilia are transported to the site of lumen formation. (Related to Figure 4.3)
(A) Violin plot of angle of centrosomes from center of KV. Gray dotted lines, quartiles. Yellow dashed lines, median. One way ANOVA across all groups (****p<0.0001). n>100 cells, n>3 embryos. (B-D) Histogram of percentage of centrosomes with cilia across 0o, 60o, 120o,180o in pre-rosette (B), rosette (C) and Lumen (D) stages. One way ANOVA with Dunnett's multiple comparison to 0°. n=3 embryos (n.s., not significant, **p<0.01, ****p<0.0001). n>100 cells, n>3 embryos. For graphs: n-values and statistical results detailed in Table S1.

each cell the angle was measured from the centrosome to cell center to KV center (Figure 4.3B). If the centrosome is moving closer to the cell boundary that is towards the KV center, then the angle should approach 0^{o}. Like our findings in Figure 4.2, we identified that the centrosome significantly approaches the cell boundary closest to the KV center during rosette and lumen stages (Figure 4.3C, S4.1A). Using a polar histogram to depict total KV centrosome angles and ciliated centrosome angles, where the cartesian plane is partitioned into 30^{o} sections and the radius of the sector represents cell numbers, we found that the angles of the ciliated centrosomes were distributed from 0^{o} to 180^{o} (Figure 4.3A, 4.3C) before KV rosette formation. This suggests that a population of centrosomes that are randomly positioned during the pre-rosette stage are ciliated and that these ciliated centrosomes reposition themselves towards the cell boundary closest to the KV center (Figure 4.3C, S4.1B-D). Taken together these results indicate that KV destined cells organize into a rosette-like structure, with the cells positioning their centrosomes that are constructing cilia from random intracellular positions to a cell boundary closest to where the apical membrane will be established, and lumen will be formed.

4.3.4. Rab11 endosomes regulate centrosome positioning and cilia formation, independent of Rab8.

Our previous studies identified that the small GTPase, Rab11, is required for centrosome positioning towards the cytokinetic bridge right before cytokinetic bridge cleavage (Krishnan et al., 2022). Interestingly, the cytokinetic bridge and midbody are also thought to mark the position of a newly forming apical membrane (Bernabé-Rubio et al., 2016; Dionne et al., 2015; Rathbun et al., 2020a). In addition, Rab11 in collaboration with another small GTPase, Rab8, were identified as being necessary

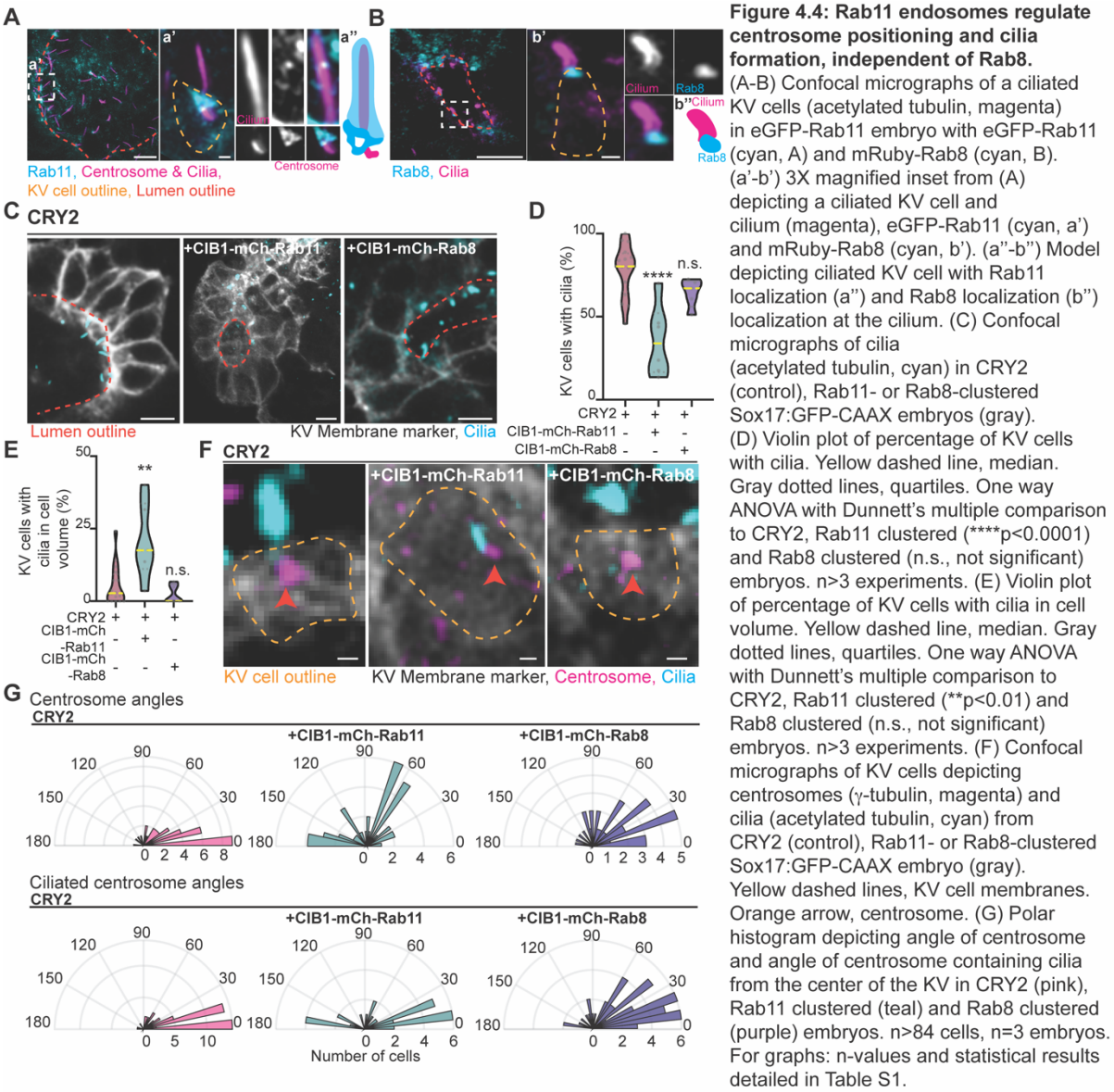

Figure 4.4: Rab11 endosomes regulate centrosome positioning and cilia formation, independent of Rab8. (A-B) Confocal micrographs of a ciliated KV cells (acetylated tubulin, magenta) in eGFP-Rab11 embryo with eGFP-Rab11 (cyan, A) and mRuby-Rab8 (cyan, B). (a'-b') 3X magnified inset from (A) depicting a ciliated KV cell and cilium (magenta), eGFP-Rab11 (cyan, a') and mRuby-Rab8 (cyan, b'). (a''-b'') Model depicting ciliated KV cell with Rab11 localization (a'') and Rab8 localization (b'') localization at the cilium. (C) Confocal micrographs of cilia (acetylated tubulin, cyan) in CRY2 (control), Rab11- or Rab8-clustered Sox17:GFP-CAAX embryos (gray). (D) Violin plot of percentage of KV cells with cilia. Yellow dashed line, median. Gray dotted lines, quartiles. One way ANOVA with Dunnett's multiple comparison to CRY2, Rab11 clustered (****p<0.0001) and Rab8 clustered (n.s., not significant) embryos. n>3 experiments. (E) Violin plot of percentage of KV cells with cilia in cell volume. Yellow dashed line, median. Gray dotted lines, quartiles. One way ANOVA with Dunnett's multiple comparison to CRY2, Rab11 clustered (**p<0.01) and Rab8 clustered (n.s., not significant) embryos. n>3 experiments. (F) Confocal micrographs of KV cells depicting centrosomes (γ-tubulin, magenta) and cilia (acetylated tubulin, cyan) from CRY2 (control), Rab11- or Rab8-clustered Sox17:GFP-CAAX embryo (gray). Yellow dashed lines, KV cell membranes. Orange arrow, centrosome. (G) Polar histogram depicting angle of centrosome and angle of centrosome containing cilia from the center of the KV in CRY2 (pink), Rab11 clustered (teal) and Rab8 clustered (purple) embryos. n>84 cells, n=3 embryos. For graphs: n-values and statistical results detailed in Table S1.

for ciliogenesis (Knödler et al., 2010).Depletion of Rab11 and Rab8 using morpholinos are associated with KV morphology defects such as formation of smaller lumens (Lu et al., 2015; Westlake et al., 2011). To identify Rab11 and Rab8 endosome organization at cilia during KV formation we ectopically expressed mRuby2-Rab8 in a CRISPR generated GFP-tagged Rab11 transgenic zebrafish line (Levic et al., 2021). We found that both Rab11 and Rab8 were localized at the centrosome (Figure 4.4A-B, magnified inset in 4.4a',4.4b'). GFP-Rab11 organizes in a ring-like structure at the distal end of the centriole and at the base of the cilia(Figure 4.4A, magnified in inset 4.4a'), with Rab8 organizing in a tight dot at the base of the cilium (Figure 4.4B, magnified inset in 4.4b'). A population of Rab11 was identified along the cilium itself, but no Rab8 (Figure 4.4A-B, magnified inset in 4.4a'-b'). To specifically test the role of Rab11 or Rab8 in KV cell cilia formation and/or centrosome positioning we acutely inhibited Rab11- or Rab8- associated membranes using an optogenetic oligomerization approach relying on a hetero-interaction between cyptochrome2 (CRY2) and CIB1 upon exposure to blue light specifically during KV developmental stages (as described in (Krishnan et al., 2022; Rathbun et al., 2020a), modeled in Figure S4.2A). Our previous studies, similar to the morpholino studies (Lu et al., 2015; Westlake et al., 2011), found that by optogenetically clustering Rab11-membranes during early KV development caused defects in KV lumen formation (Rathbun et al., 2020a), no noticeable defects in lumen formation were found with Rab8-membrane clustering (Figure 4.4C). When comparing Rab11 and/or Rab8 optogenetically clustered embryos to control (CRY2 injected) embryos, we identified that only 37.43±9.22% of Rab11 clustered KV cells were able to make a cilium compared to Rab8 clustered (63.77±4.9%) and CRY2 controls (77.82±3.32%, Figure 4.4C-D, Rab11 and Rab8 clustering in S4.2B). Of the

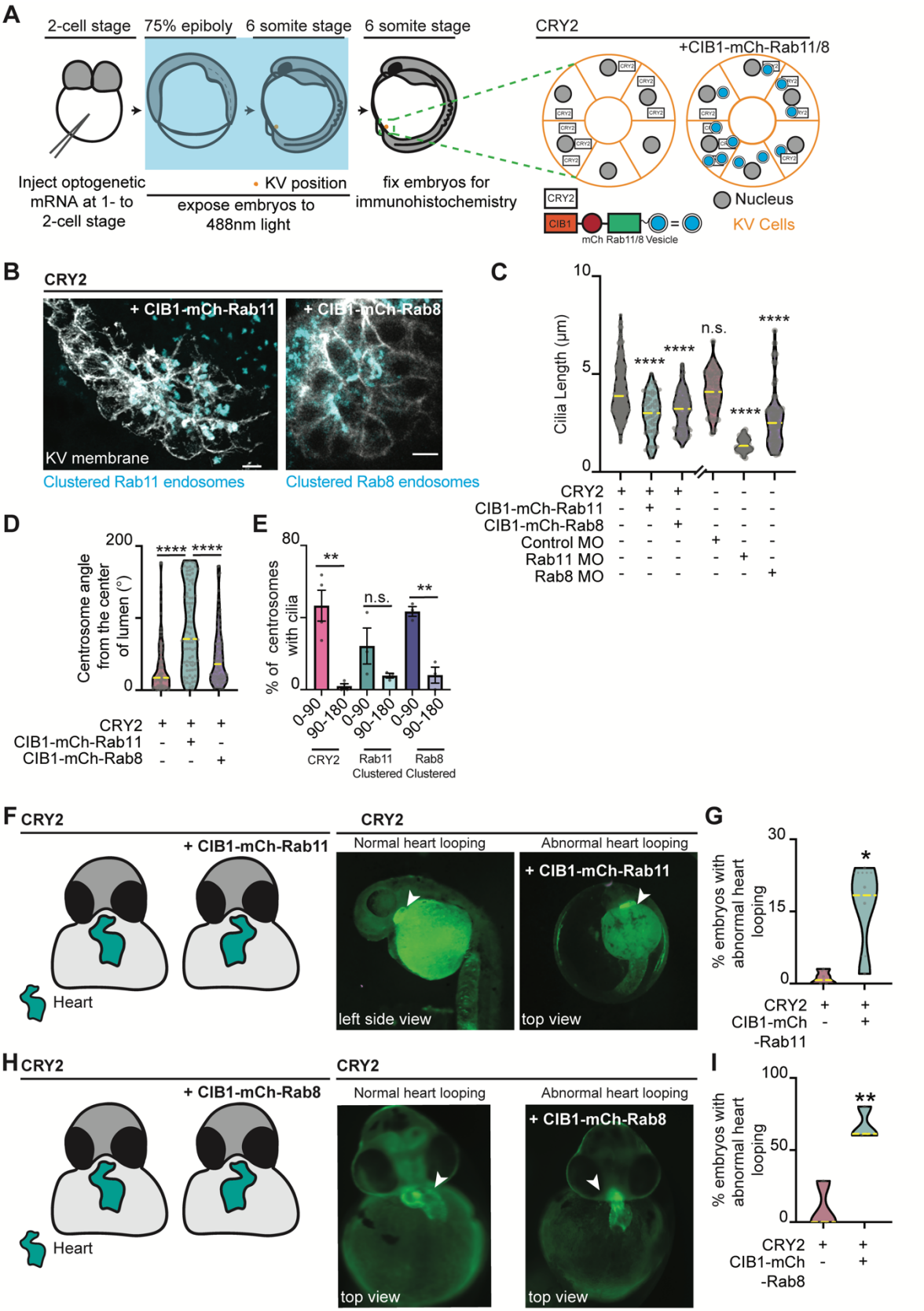

Figure S4.2: Rab11 endosomes regulate centrosome positioning and cilia formation, independent of Rab8.

Figure S4.2: Rab11 endosomes regulate centrosome positioning and cilia formation, independent of Rab8. (Related to Figure 4.4)
(A) Model depicting acute inhibition of Rab11 or Rab8 mediated membrane trafficking using optogenetic clustering. (B) Confocal micrographs of Rab11- or Rab8-clustered embryos with Rab11- or Rab8-clusters (cyan) and Sox17:GFP-CAAX embryos (gray) denoting optogenetic clusters of embryos depicted in Figure 4C. (C) Violin plot depicting cilia length in CRY2, Rab11 clustered, Rab8 clustered, control morpholino (MO), Rab11 MO, Rab8 MO conditions. Yellow dashed line, median. Gray dotted line, quartiles. One way ANOVA with Dunnett's multiple comparison to CRY2, Rab11 clustered (****p<0.0001), Rab8 clustered (****p<0.0001), control MO (n.s., not significant), Rab11 MO (****p<0.0001) and Rab8 MO (****p<0.0001). n>4 embryos. (D) Violin plot of angle of centrosomes from center of KV. Yellow dashed line, median. Gray dotted lines, quartiles. One way ANOVA with Dunnett's multiple comparison to Rab11 clustered embryos, CRY2 (****p<0.0001) and Rab8 clustered (****p<0.0001) embryos. n>4 embryos. (E) Histogram depicting percentage of centrosomes with cilia at acute angles (0o - 90o) and obtuse angles (90o - 180o) in CRY2, Rab11 clustered and Rab8 clustered embryos. Student's t-Test between acute angles (0o - 90o) and obtuse angles (90o - 180o) within CRY2 (pink), Rab11 clustered (teal) and Rab8 clustered (purple) embryos. n>4 embryos. For graphs: n-values and statistical results detailed in Table S1. (F) Epifluorescence micrographs of zebrafish embryos highlighting heart looping (hearts in green) in CRY2 (control), Rab11-clustered conditions. (G) Violin plot of percentage embryos with abnormal heat looping in CRY2 (pink) and Rab11 clustered (teal) embryos. Students t-test, *p<0.05. n>12 embryos, n=4 experiments. Yellow dashed line, median. Gray dotted line, quartiles (H) Epifluorescence micrographs of zebrafish embryos highlighting heart looping (hearts in green) in CRY2 (control), Rab8-clustered conditions. (I) Violin plot of percentage embryos with abnormal heat looping in CRY2 (pink) and Rab8 clustered (teal) embryos Yellow dashed line, median. Gray dotted line, quartiles. Student's t-test, **p<0.01. n>5 embryos, n=3 experiments. For graphs: n-values and statistical results detailed in Table S1.

Rab11 or Rab8-clustered cells that could make cilia, we found that the cilia were significantly decreased in length (2.92±0.14 μm for Rab11 and 3.15±0.08 μm for Rab8) compared to control CRY2 conditions (4.13±0.06 μm, Figure 4.4C, S4.2C). This significant decrease in cilia length with Rab11 or Rab8 clustering is consistent with depleting Rab11 or Rab8 using morpholinos (Figure S4.2C). In the Rab11 clustered KV cells 20.59±5.34% cilia were stuck within the cell volume compared to Rab8 clustered cells (2.32±1.45%) or CYR2 controls (5.44±1.69%, Figure 4.4C, 4.4E). Taken together, these studies suggest that in the Rab11 clustered cells' centrosomes that can construct a cilium are unable to extend it into the lumen potentially due to an inability to relocate the centrosome and forming cilium to the apical membrane.

We next tested the role of Rab11- and Rab8 endosomes in centrosome positioning during KV development. When comparing the polar histograms of Rab11 optogenetically clustered embryos to control (CRY2) and Rab8 optogenetically clustered embryos (conditions of CRY2 plus CIB1-mCh-Rab8) during KV development, Rab11 clustered embryos (conditions of CRY2 plus CIB1-mch-Rab11) were significantly impaired at reorienting their centrosomes toward the cell boundary positioned closest to the KV center where an apical membrane forms (Figure 4.4F-G, S4.2D). Rab11 clustered membranes also demonstrated significant defects in centrosomes with cilia reorienting towards the cell boundary positioned closest to the KV compared to control or Rab8 optogenetically clustered embryos (Figure 4.4F-G, S4.2E). Taken together these studies suggest that Rab11, regulates not only cilia formation, but centrosome movement towards the forming apical membrane, whereas Rab8 specifically modulates cilia elongation once the cilia are already extended into the KV lumen.

Here we provide a framework for cilia construction during KV development and present a relationship between lumen expansion and cilia extension into the lumen in that lumen expansion beyond 300 μm^2 initiates cilia extension into the lumen. One argument for this relationship is that by inhibiting Rab11, either through morpholino depletion (Lu et al., 2015; Westlake et al., 2011) or acute optogenetic clustering of its associated membranes (Rathbun et al., 2020a), an inhibition in lumen formation/expansion occurs that corresponds with a defect in the percentage of KV cells with lumenal cilia (Figure 4.4E). It's also interesting to speculate that the expansion of the lumen beyond 300 μm^2 is providing some sort of biophysical change in cell shape or state that can be allowing the cilium to then extend into the lumen. By preventing lumen expansion beyond 300 μm^2 through inhibition of Rab11 may cause the cilia to not be able to extend into the small lumen (less than 300 μm^2) that has formed. Downstream consequences associated with defects in KV lumen expansion and cilia length, such as defects in heart looping, were identified with clustering Rab11 or Rab8 -membranes specifically during KV developmental stages (Figure S4.2F-I). Taken together, these studies suggest that Rab11 and/or Rab8 endosome mediated trafficking is necessary for forming a functional KV during development.

In summary, we propose a model where KV cells centrosomes start to construct cilia in a Rab11-dependent manner before lumen formation. The centrosome with the newly formed cilia can be positioned in random locales throughout the KV cell, but then needs to reposition itself towards the cell boundary closest to the KV center. At this time this cell boundary is transitioning into an apical membrane (Amack and Yost, 2004; Rathbun et al., 2020a) and there is significant changes in KV cell shapes. KV cells in the pre-rosette stage present with random

mesenchymal-like cell shapes that then transition into more pizza pie-like shapes. This transition is when we find the centrosome repositioning in a Rab11-dependent manner towards the tip of the pizza pie that is positioned at the KV center (modeled in Figure 1E). Once the centrosome and cilium reach this locale, the cilium reaches an average intracellular length of 2.25 μm. Then once the lumen starts to form and hits a total area of 2015.3 μm^2, 50% of the KV cell cilia extends into the lumen and starts elongating to its average length of 4.5 μm^2.

4.4. Resource Availability

Lead contact: For further information or to request resources/reagents, contact Lead Contact, Dr. Heidi Hehnly (hhehnly@syr.edu)

Materials availability: New materials generated for this study are available for distribution.

Data and code availability: All data sets analyzed for this study are displayed.

4.4.1. Experimental model and subject details

Fish Lines: Zebrafish lines were maintained using standard procedures approved by Syracuse University IACUC (Institutional Animal Care Committee) (Protocol #18-006 and #21-004). Embryos were raised at 28.5^{o}C and staged (as in (Kimmel et al., 1995)). Wildtype and/or transgenic zebrafish lines used for live imaging and immunohistochemistry are listed in key resource table.

4.5. Method Details

4.5.1. Antibodies: Antibody catalog information used in mammalian cell culture and zebrafish embryos are detailed in key resource table.

4.5.2. Plasmids and mRNA: Plasmids were generated using Gibson cloning methods (NEBuilder HiFi DNA assembly Cloning Kit) and maxi-prepped before injection and/or transfection. mRNA was made using mMESSAGE mMACHINE^{TM}SP6 transcription kit. See key resource table for a list of plasmid constructs and mRNA used.

4.5.3. Immunofluorescence: For zebrafish embryo immunofluorescent protocols see (Aljiboury et al., 2021). Briefly, fluorescent transgenic and/or mRNA injected embryos were staged at Kupffer's Vesicle (KV) developmental stages as described in ((Amack and Yost, 2004; Rathbun et al., 2020a)) and fixed using 4% paraformaldehyde with 0.1% triton-100. Standard immunofluorescent protocols were carried out (refer to (Aljiboury et al., 2021)). Embryos were then embedded in 2% agarose with the KV positioned towards a #1.5 glass bottom MatTek plate and imaged using the spinning disk confocal microscope or Laser Scanning Confocal Microscope (LSCM). Zebrafish transgenic lines and mRNAs used listed in key resource table. Injections performed as described in (Aljiboury et al., 2021).

4.5.4. Imaging: Zebrafish embryos were imaged using Leica DMi8 (Leica, Bannockburn, IL) equipped with a X-light V2 Confocal unit spinning disk equipped with a Visitron VisiFRAP-DC photokinetics unit, a Leica SP8 (Leica, Bannockburn,

IL) LSCM and/or a Zeiss LSCM 980 (Carl Zeiss, Germany) with Airyscan 2 detector. The Leica DMi8 is equipped with a Lumencore SPECTRA X (Lumencore, Beaverton, OR), Photometrics Prime-95B sCMOS Camera, and 89 North-LDi laser launch. VisiView software was used to acquire images. The optics used with this unit are HC PL APO x40/1.10W CORR CS2 0.65 water immersion objective. The SP8 laser scanning confocal microscope is equipped with HC PL APO 20x/0.75 IMM CORR CS2 objective, HC PL APO 40x/1.10 W CORR CS2 0.65 water objective and HC PL APO x63/1.3 Glyc CORR CS2 glycerol objective. LAS-X software was used to acquire images. The Zeiss LSM 980 is equipped with a T-PMT, GaASP detector, MA-PMT, Airyscan 2 multiplex with 4Y and 8Y. Optics used with this unit are Plan-Neofluar 40X/1.2NA objective. Zeiss Zen 3.2 was used to acquire the images. A Leica M165 FC stereomicroscope equipped with DFC 9000 GT sCMOS camera was used for staging and phenotypic analysis of zebrafish embryos.

4.5.5. Acute inhibition of Rab11 or Rab8 mediated membrane trafficking using optogenetics in zebrafish embryos: Tg (*sox17*:GFP-CAAX), Tg *BAC*(*cftr*-GFP), Tg(*sox17*:GFP), and Tg(*sox17*:DsRed) zebrafish embryos were injected with 100 pg of CRY2 and/or CIB1-mCherry-Rab11 or CIB1-mCherry-Rab8 at the one cell to four cell stage. Embryos were allowed to develop in the dark until uninjected embryos reached the 75% epiboly stage (8 hpf) where we can screen embryos for KV cells and exposed to 488nm light using the NIGHTSEA fluorescence unit until the six-somite stage, 12 hpf (Rathbun et al., 2020a). Embryos were then fixed using 4% paraformaldehyde with 0.1% triton-100 followed by standard immunofluorescent protocols (Aljiboury et al., 2021).

Depletion of Rab11 or Rab8 using morpholinos in zebrafish embryos: Tg (*sox17*:GFP-CAAX), Tg *BAC*(*cftr*-GFP), Tg(*sox17*:GFP), or Tg(*sox17*:DsRed) zebrafish embryos were injected with 2ng/ul of control morpholino, Rab11a morpholino (Tay et al., 2013) or Rab8 morpholino (Lu et al., 2015; Omori et al., 2008) at the one cell to four cell stage. Embryos were fixed at six somite stage (12 hpf) using 4% paraformaldehyde with 0.1% triton-100 followed by standard immunofluorescent protocols (Aljiboury et al., 2021). Morpholinos listed in Key Resource Table.

***4.5.6. Relative distance of cilia from cell boundary closest to KV center*:**
Volumetric images were obtained from zebrafish embryo KV cells with cilia labeled with acetylated-tubulin and the plasma membrane labeled with GFP-CAAX. Using IMARIS software the cilium of each cell and the cell membrane were surface rendered, and the center of the surface was determined. The length of the center of the cell to the cell boundary closest to the KV center (l_1) and the length of the center of the cilium to the same cell boundary (l_2) were measured for each developmental stage in KV formation. The ratio of l_2 by l_1 was calculated and represented as a violin plot using PRISM9.

4.5.7. Angle measurements between centrosome, cell center, and KV center:
Volumetric images were obtained of Zebrafish KV cells that had their plasma membranes decorated with GFP-CAAX. The boundaries around the cells were outlined in the KV using the freehand tool in FIJI/ImageJ to identify the cell centroid position. Depending on the developmental KV stage, the center of the KV or the KV lumen was identified. A line was drawn from this point, to the center of the cell and

then from the center of the cell to the centrosome (immunostained with γ-tubulin). The angle was determined at the center of the cell point and angles were plotted for each developmental stage using PRISM9 software.

4.5.8. Polar Histogram using MATLAB®: To demonstrate centrosome angles during KV developmental stages with or without cilia a polar histogram was assembled using MatLab®, MathWorks. The script is available in the MatLab, MathWorks directory (link attached https://www.mathworks.com/help/matlab/ref/polarhistogram.html). Centrosome angles were determined and graphed as a polar histogram where the cartesian plane is divided into 30^{o} sections with radius of the sector (highlighted by the width of the sector) representing the number of cells with centrosome angles at 0^{o},30 ^{o},60 ^{o},180 ^{o} away from the center of the KV.

4.5.9. Cilia measurements: Zebrafish embryo KV cells were immunostained with acetylated tubulin, volumetric images were obtained to measure cilia length in 3D (IMARIS). The percentage of KV cells with the presence of cilia, cilia in the KV lumen, or cilia in the cell volume was calculated and represented as a percentage over the total number of cells with cilia in the tissue. Cilia lengths, percentage of cilia in lumen or cell volume were represented as a violin plot using PRISM9.

4.5.10. Phenotypic analysis of zebrafish heart looping: Zebrafish embryos injected with optogenetic constructs were allowed to develop until 24-30 hpf. Heart looping was characterized by leftward, rightward and severely defective looping.

4.5.11. Statistical Analysis: Unpaired two-tailed t-tests and one way ANOVA were performed using PRISM9 software. **** denotes a p-value<0.0001, *** p-value<0.001, **p-value<0.01, *p-value<0.05, n.s. not significant. For further information on detailed statistical analysis see supplemental tables.

4.5.12. METHODS TABLE 1: Table S1. Detailed statistical analysis results reported.

Figures	Y-Axis	Category	n (cell)	n (embryo)	n (expt)	Statistical Test	Parameters	Result	p-value
4.1B	% Ciliated KV cells	Pre-Rosette	N/A	n=7	n>3	One Way ANOVA	F (2,31) = 6.917	**	0.0033
		Rosette	N/A	n=7	n>3				
		Lumen	N/A	n=20	n>3				
4.1C	% KV cells with luminal cilia and Lumen Area	N/A	N/A	n=29	n>3	N/A	N/A	N/A	N/A
4.1D	Cilia length and Lumen Area	N/A	N/A	n=29	n>3	N/A	N/A	N/A	N/A
4.2C	Relative distance of cilia from the apical membrane (μm)	Pre-Rosette	n=8	n=1	N/A	One Way ANOVA	F (2,21) = 13.62		
		Rosette	n=8	n=1	N/A			***	0.0006
		Lumen	n=8	n=1	N/A			***	0.0003
S4.1A	Angular displacement of the centrosome from the center of the KV	Pre-Rosette	n=156	n=3	n>3	One Way ANOVA	F (2, 476) = 34.08	****	<0.0001
		Rosette	n=125	n=3	n>3				
		Lumen	n=198	n=3	n>3				
S4.1B	Percentage of centrosome with cilia (%) Pre-Rosette	0°	N/A	n=3	N/A	One Way ANOVA	F (3, 8) = 2.132		
		60°			N/A			n.s.	0.8592
		120°			N/A			n.s.	0.4315
		180°			N/A			n.s.	0.1009
S4.1C	Percentage of centrosome with cilia (%) Rosette	0°	N/A	n=3	N/A	One Way ANOVA	F (3,8) = 9.180		
		60°			N/A			n.s.	0.9989
		120°			N/A			n.s.	0.1258
		180°			N/A			**	0.0059
S4.1D	Percentage of centrosome	0°	N/A	n=3	N/A	One Way ANOVA	F (3,8) = 68.52		
		60			N/A			n.s.	0.1151
		120°			N/A			****	<0.0001

	with cilia (%) Lumen	180°			N/A			****	<0.0001
4.4B	KV Cells with cilia (%)	CRY2	N/A	n=16	n>3	One Way ANOVA	F(2,24)=25.12		
		+CIB1-Rab11	N/A	n=6	n>3			****	<0.0001
		+CIB1-Rab11	N/A	n=5	n>3			n.s.	0.4108
4.4C	KV Cells with cilia in Lumen(%)	CRY2	N/A	n=16	n>3	One Way ANOVA	F(2,24)=27.58		
		+CIB1-Rab11	N/A	n=6	n>3			****	<0.0001
		+CIB1-Rab11	N/A	n=5	n>3			n.s.	0.8799
S4.2C	Cilia Length (μm)	CRY2	433	n=17	n>3	One Way ANOVA	F(5,819)=76.42		
		CRY2 +CIB1-Rab11	61	n=5	n>3			****	<0.0001
		CRY2 +CIB1-Rab8	145	n=4	n>3			****	<0.0001
		Control MO	52	n=3	n=3			n.s.	0.9999
		Rab11 MO	55	n=3	n=3			****	<0.0001
		Rab8 MO	79	n=3	n=3			****	<0.0001
S4.2D	Angular displacement of centrosome from the center of the KV	CRY2	90	n>3	N/A	One Way ANOVA		****	<0.0001
		CRY2 +CIB1-Rab11	84	n=3	N/A				
		CRY2 +CIB1-Rab8	95	n=3	N/A			****	<0.0001
S4.2E	% Of centrosomes with cilia	CRY2 (0-90)	N/A	n=3	N/A	Student's t-Test	t=5.156, df=6		
		CRY2 (90-180)	N/A	n=3	N/A			**	0.0021
		CRY2 +CIB1-Rab11 (0-90)	N/A	n=3	N/A	Student's t-Test	t=1.626, df=4		
		CRY2 +CIB1-Rab11 (90-180)	N/A	n=3	N/A			n.s.	0.1793
		CRY2 +CIB1-	N/A	n=3	N/A	Student's t-Test	t=6.801, df=4		

		Rab8 (0-90)							
		CRY2 +CIB1-Rab8 (90-180)	N/A	n=3	N/A			**	0.0024
S4.2G	% embryos with abnormal heart looping	CRY2	N/A	n>12	n=4	Student's t-Test		*	0.0241
		CRY2 + CIB1-Rab11							
S4.2I	% embryos with abnormal heart looping	CRY2	N/A	n>5	n=3	Student's t-Test		**	0.0075
		CRY2 + CIB1-Rab8							

4.5.13. METHODS TABLE 2: Supplementary key resource table

Reagent or RESOURCE	Source	Identifier
Antibodies		
Acetylated Tubulin	Sigma Aldrich	T6793: RRID:AB_477585
Gamma-tubulin	Sigma Aldrich	T5192; RRID: AB_261690
ZO-1 Monoclonal Antibody (ZO-1, 1A12) Alexa Fluor 488	Life Technologies	339188; RRID: AB_2532187
ZO-1 Monoclonal Antibody (ZO-1, 1A12) Alexa Fluor 647	Life Technologies	339100; RRID: AB_2663167
Anti-GFP (Chicken)	GeneTex	GTX13970: AB_371416
Anti-GFP (Rabbit)	Molecular Probes	A-11122: AB_221569
ZO-1 Monoclonal Antibody (ZO-1, 1A12) Alexa Fluor 488	Life Technologies	339188; RRID: AB_2532187
Alexa Fluor Anti-Rabbit 488	Life Technologies	A21206; RRID: AB_2535792
Alexa Fluor Anti-Rabbit 568	Life Technologies	A10042; RRID: AB_2534017
Alexa Fluor Anti-Rabbit 647	Life Technologies	A31573; RRID: AB_2536183
Alexa Fluor Anti-Mouse 488	Life Technologies	A21202; RRID: AB_141607
Alexa Fluor Anti-Mouse 568	Life Technologies	A10037; RRID: AB_2534013

Alexa Fluor Anti-Mouse 647	Life Technologies	A31571; RRID: AB_162542
Anti-aTubulin antibody Alexa Fluor 555conjugated	EMD millipore	05-829-AF555
Chemicals, Peptides, and Recombinant Proteins		
DAPI	Sigma Aldrich	D9542-10mg
NucBlue™ Fixed Cell stained Ready Probes	Thermo Fischer	R37606
NucBlue™ Live Ready Probes	Thermo Fischer	R37605
Agarose	Thermo Fischer	16520100
BSA	Fisher Scientific	BP1600-100
BIO BASIC Maxi Prep Kit	BIO BASIC	9K-0060023
Dimethylsulphoxide	Fisher Scientific	BP231-100
Paraformaldehyde	Fisher Scientific	O4042-500
Phosphate Buffered Saline	Fisher Scientific	10010023
Life Technologies Prolong Diamond Antifade Moutant with DAPI	Fisher Scientific	P36971

35 mm Dish| No.1.5. coverslip| 20 mm Glass Diameter	MatTek Corporation	P35G-1.5-20-C
Molecular Probes Prolong Gold Antifade Moutant	Fisher Scientific	P36934
Triton X-100	Fisher Scientific	BP151500
Tween 20	ThermoFischer	BP337500
Sodium Chloride	Fisher Scientific	BP358
NEBuilder HiFi DNA assembly Cloning Kit	New England BioLabs	E5520S
mMESSAGE mMACHINE^{TM}SP6	Invitrogen	AM1340
Experimental models, organisms and strains		
Zebrafish	Zebrafish International Resource Center	TAB-Wildtype
Zebrafish	Zebrafish International Resource Center	Tg (Sox17:DsRed)
Zebrafish	Gift from Solinca-Krezel	Tg (-5actb2:cent4-GFP)

	lab, generated by Harris Lab	
Zebrafish	(Dasgupta and Amack, 2016)	Tg (sox17:GFP-CAAX)^{sny101}
Zebrafish	(Navis et al., 2013)	Tg*BAC*(cftr-GFP)
Zebrafish	(Levic et al., 2020)	TgKIeGFP-Rab11a
Recombinant DNA		
Plasmid: PCS2-CRY2	(Rathbun et al., 2020)	Addgene Plasmid #140572
Plasmid: PCS2-CIB1-mCherry-Rab11a	(Rathbun et al., 2020)	Addgene Plasmid #140573
Plasmid: PCS2-CIB1-mCerulean-Rab11a	(Rathbun et al., 2020)	Addgene Plasmid #140574
Plasmid: mRuby2-MannII-N-10	(Lam et al., 2012)	Addgene Plasmid #55903
Plasmid: PCS2-CIB1-mCherry-Rab8a	This paper	Addgene in process
Plasmid: PCS2-mCardinal-Arl13b	This paper	Addgene in process
Morpholinos		
Control MO	vivo standard control morpholinos	Gene Tools
Rab11 MO	(Westlake et al., 2011)	GTATTCGTCGTCTCGTGTCCCCAT

Rab8 MO	(Lu et al., 2015; Omori et al., 2008)	GAAGACATAAATACCTATCGTCGAG
Software and algorithms		
ImageJ/FIJI	NIH and Laboratory for Optical and Computational Instrumentation	https://imagej.net/Fiji
IMARIS, Bitplane	Oxford Instruments	https://imaris.oxinst.com/
PRISM9	GraphPad	https://www.graphpad.com/scientific-software/prism/
LAS-X Software	Leica Microsystems	https://www.leica-microsystems.com/products/microscope-software/p/leica-las-x-ls/
VisiView	Visitron	https://www.visitron.de/products/visiviewr-software.html
AutoQuant X3	Meyer Instruments	https://www.meyerinst.com/mediacybernetics/autoquant/
Zeiss Zen 3.2	Carl Zeiss	https://www.zeiss.com/microscopy/us/products/microscope-software/zen.html

4.6. ACKNOWLEDGEMENTS

We thank the Michel Bagnat lab at Duke University School of Medicine for sharing their eGFP-Rab11 transgenic zebrafish lines. This work was supported by National Institutes of Health grants R01GM127621 (H.H.) and R01GM130874 (H.H.). This work was supported by the U.S Army Medical Research Acquisition Activity through the FY16 Prostate Cancer Research Programs under Award no. W81XWH-20-1-0585 (H.H.). Opinions, interpretations, conclusions, and recommendations are those of the authors and not necessarily endorsed by the Department of Defense.

4.7. AUTHOR CONTRIBUTIONS

H.H., N.K., J.M., C.T., E.I., N.A.H and F.O. designed, performed, and analyzed experiments; H.H. and N.K. wrote manuscript; J.F. and F.O. provided molecular reagents and zebrafish husbandry. All authors provided edits. H.H. oversaw project.

4.8. DECLARATION OF INTERESTS

The authors declare no competing interests.

CHAPTER FIVE:

Summary and future directions

5.1. Summary

The goal of this thesis was to identify the molecular mechanisms that regulate centrosome positioning during tissue formation *in vivo*. To create a tissue in vivo mesenchymal cells, need to divide and polarize to become epithelial cells by a process called mesenchymal epithelial transition (MET, Figure 5.1, (Pei et al., 2019)). A cellular process that may contribute to cell polarization and cell placement during tissue formation is abscission, a process by which the cytokinetic bridge is cleaved (Mangan et al., 2016; Rathbun et al., 2020a; Taneja et al., 2016). My studies in human cells in culture and zebrafish embryo cells in vivo identify that the centrosome moves towards the cytokinetic bridge during abscission. The aim of chapter 3 was to identify the molecular mechanisms that contribute to bridge directed centrosome movement necessary in regulating abscission. Knowing that Rab11 interacted with the centrosome through older centriolar appendage protein and is involved in regulating abscission we tested the role of Rab11 endosomes in bridge directed centrosome movement during abscission. To do this we generated Rab11-null cells in human cervical cancer cells and an acute optogenetic method to inhibit Rab11 endosomes *in vivo* (Chapter 2). We use live cell confocal microscopy to track centrosome movement during abscission in dividing cells and a vectoral subtraction method to quantitatively measure centrosome movement to the cytokinetic bridge in cells to remove the contribution of cell movement during this process. Using these techniques, we identified that Rab11 endosomes regulate centrosome movement during abscission *in vitro* and *in vivo*. In addition, we found that functional Rab11 is necessary for Pericentrin organization at the centrosome during pre-abscission. When Pericentrin is depleted or Rab11 mediate membrane trafficking is inhibited centrosomes are unable to reorient to the cytokinetic bridge

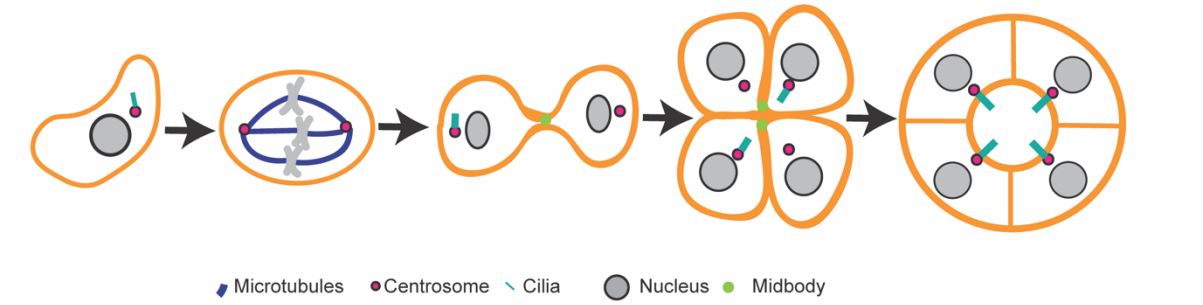

Figure 5.1: Centrosomes construct a cilium during pre-abscission and are transported to the site of lumen formation during tissue development *in vivo*
Shown is a testable model with centrosomes (magenta) constructing cilia (cyan) during pre-abscission and transporting them to the site of lumen formation and apical membrane adjacent to the cytokinetic midbody (green) during tissue development.

during pre-abscission causing abscission defects *in vivo*. These studies determine a molecular mechanism where Rab11 endosomes regulate centrosome organization of Pericentrin necessary to regulate centrosome movement to the cytokinetic bridge required for appropriate abscission completion.

During cellular epithelialization centrosomes need to move to the apical membrane to construct a cilium. The aim of chapter 4 was to identify the temporal and spatial mechanisms of centrosome positioning and cilia formation during MET *in vivo*. To do this we used the KV as a model tissue, ciliated organ of asymmetry as a model. We find that centrosomes in KV mesenchymal cells construct a cilium intracellularly and transport them to the site of lumen formation during KV development. We know KV cells place their cytokinetic bridges at the site of lumen formation to direct Rab11 mediated membrane trafficking to the bridge necessary in regulating abscission and lumen establishment. Taken together with studies from chapter 3 a possible link might exist between Rab11 endosomes, centrosome positioning, cilia formation and abscission during KV tissue formation. Therefore, we tested the role of Rab11 endosomes in centrosome positioning and cilia formation during KV development in vivo. Acute inhibition of Rab11 mediated membrane trafficking during KV development disrupts centrosome positioning and its ability to construct cilia during tissue development *in vivo*. Overall, these studies determined that Rab11 endosomes regulate centrosome function and movement during abscission and possibly facilitate centrosome recruitment to the apical membrane to mediate cilia formation *in vivo*.

5.2. BROAD IMPLICATIONS AND FUTURE STUDIES.

The studies presented here identify the importance of Rab11 endosome regulation of centrosome function and movement to facilitate cilia formation during MET *in vivo*. When cells are unable to polarize and/or when epithelial cells transition to mesenchymal cells by the reverse process of MET called epithelial mesenchymal transition EMT cells disassemble polarity and switch to a more migratory mesenchymal cell phenotype which is a hallmark of aggressive cancers (Figure 1.1 (Pei et al., 2019)) . When centrosome positioning is disrupted in cells in culture, they tend to lose cellular polarization making them susceptible to EMT (Burute et al., 2017). The studies present in chapter 3 have identified a molecular mechanism that regulates bridge directed centrosome movement and abscission completion *in vivo*. Abscission is a cellular process, when disrupted cells become binucleated, contain supernumerary centrosomes and can lead to cell death or progression of diseases like cancer (Godinho and Pellman, 2014; Krishnan et al., 2022; Sagona and Stenmark, 2010; Wilson et al., 2005). A striking phenotype we observed in Pericentrin depleted dividing cells and when Rab11 endosome mediated membrane trafficking was inhibited *in vivo* was that significantly higher percentage of cells had supernumerary centrosomes. The most common phenotype of cancer progression and a marker for the severity of cancer is supernumerary centrosomes (Godinho and Pellman, 2014). Therefore, it is necessary to identify the molecular and cellular mechanisms that contribute to centrosome organization, its function and involvement in abscission during tissue formation *in vivo*. This allows us to understand when and how these mechanisms can be disrupted leading to the accumulation of an abnormal number of centrosomes in cells and escalating the progression of cancer.

While Rab11 endosomes are involved in regulating bridge directed centrosome movement during abscission and cilia formation, the centrosome itself may be able to regulate its positioning during abscission. Depletion of cenexin, a centriolar subdistal appendage protein results in centrosome and spindle orientation defects in human cells in culture (Hung et al., 2016). Additionally, loss of Rab11 does not affect centrosome organization of cenexin during pre-abscission (Krishnan et al., 2022), suggesting that cenexin could be acting upstream of Rab11 in regulating bridge directed centrosome movement during pre-abscission and subsequently appropriate abscission completion. Therefore, future studies are needed to examine the role of centrosome proteins like cenexin that could be involved in organization of Rab11 endosomes at the centrosome during pre-abscission and abscission completion. To test the molecular mechanism that could regulate Rab11 organization at the centrosome, cenexin depleted human cells in culture (HeLa cells, as in (Aljiboury et al., 2022; Colicino et al., 2019)) can be used. Rescue experiments with cenexin truncated at the C-terminal end (necessary for centrosome localization of cenexin and interaction with Rab11) and full length cenexin can then be used to identify whether the interaction of Rab11 with cenexin is necessary for Rab11 organization at the centrosome during the stages of the cell cycle and subsequently bridge directed centrosome movement and possibly abscission completion (Hehnly et al., 2012). If Rab11 endosome organization at the centrosome requires an association with cenexin it raises the possibility that the centrosome through this interaction would be modulating bridge directed Rab11 endosome movement and centrosome movement during pre-abscission.

Even though the conclusions in chapter 4, argue for centrosome movement to the apical membrane during KV development in vivo, when the centrosome is

recruited to the apical membrane is not clearly tested. An explanation could be that the cytokinetic bridge and midbody act as a symmetry breaking event to recruit the centrosome to the site of apical membrane formation to dictate where the cilia will be assembled (Bernabé-Rubio et al., 2016). We are in the process of establishing an experimental paradigm to visualize and characterize the temporal sequence of cilia formation during KV development using electron microscopy (EM). This technique will be used to track when the cilium is made inside the cell during KV development and would strongly indicate whether a centrosome is ciliated before it reaches the apical membrane during KV development. Based on the studies from EM and conclusions from chapter 4 it could suggest two possible mechanisms coordinating centrosome movement and cilia formation to the apical membrane and site of lumen formation during KV development. The first mechanism is that centrosomes move to the apical membrane during pre-abscission, facilitate abscission, and once abscission is complete the centrosome constructs the primary cilium at the apical membrane (similar to the testable model in (Bernabé-Rubio et al., 2016)). The second possibility is that centrosomes construct a cilium and transport to the apical membrane before the cytokinetic bridge is cleaved (Figure 5.1), which is a hypothesis that our data in the KV may fit more tightly to.

Based on the conclusions from chapter 4 that KV cell's centrosome construct cilia inside the cell and are transported to the apical membrane (Figure 4.3). We hypothesize that the cilium is constructed before the cytokinetic bridge is cleaved in pre-abscising KV cells. This mechanism would support the model we propose in Figure 5.1. Other studies that partially support this idea comes from work in neural cells in culture. Here they identify that the ciliary membrane is associated with the

centrosome during mitosis (Paridaen et al., 2013). Preliminary studies in our lab have identified that the centrosome is ciliated in pre-abscising cells in mammalian cells in culture (Figure 5.2, unpublished results from graduate student Favour Ononiwu). Taken together this suggests that pre-abscising KV cell's centrosome may be ciliated. Future studies that target the identification of KV cells in pre-abscission that are ciliated are necessary to validate this hypothesis. Current studies in the lab are pursuing aspects of identifying the temporal and spatial mechanisms that regulate cilia construction during pre-abscission. Myosin-Va (Myo-Va), a myosin motor protein that has been identified to be recruited to the ciliary vesicle inside the cell during ciliogenesis in mammalian cells in culture (Wu et al., 2018). We propose to see if this mechanism is intact during KV cell ciliation, where Myo-Va could be a potential molecular marker for cilia formation intracellularly. Fluorescent markers based on (Wu et al., 2018) will be developed to test the temporal and spatial organization of Myo-Va in relation to Rab11 endosomes during cilia formation in the KV. A possibility is that we observe Myo-Va and Rab11 endosomes colocalized at the cilium. This could suggest that both Rab11 and Myo-Va vesicles potentially work together to regulate ciliogenesis. Subsequent studies that test the requirement of Rab11 endosomes in Myo-Va or Myo-Va vesicles in Rab11 endosome organization during cilia formation will be necessary to support this hypothesis. Taken together, these studies could identify a potential molecular mechanism that identifies the temporal organization of Myo-Va and Rab11 endosome recruitment to the ciliary vesicle during KV development. This potentially connects the involvement of the actin cytoskeleton in centrosome positioning and cilia formation as Myo-Va is an actin based motor protein (Mehta A.D. et al., 1999).

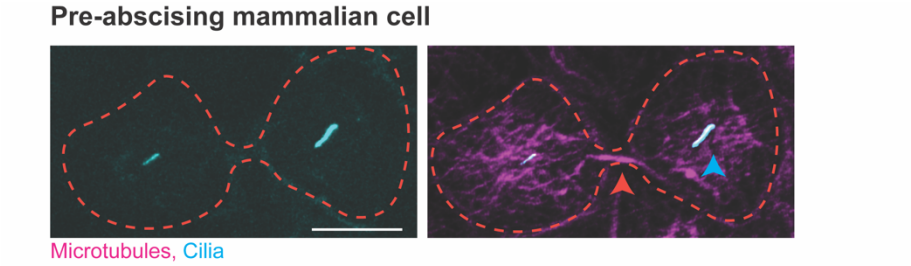

Figure 5.2: Primary cilia start to form during pre-abscission. Confocal micrograph of a pre-abscising mouse inner medullary connecting duct (IMCD) cell in culture with cilia (SSTR3-GFP, cyan) and microtubules (α-tubulin, magenta).

If we observe that KV pre-abscising cell's centrosome is ciliated, a potential mechanism is that the cilium itself is driving centrosome directed bridge movement. Future studies are needed to specifically test the contribution of a cilium in centrosome bridge directed movement. Since there is evidence for centrosome involvement in abscission and that we find cilia at the centrosome (Figure 3.6), laser ablation of the cilia (but not the centrosome) could be employed during pre-abscission. This would identify whether the ciliated centrosome is involved in regulating abscission completion and whether the cilium was required for centrosome positioning towards the cytokinetic bridge. To specifically test the role of the cilium during centrosome movement in pre-abscission, depleting canonical cilia proteins like intraflagellar transport proteins (IFT) can be employed. For example, IFT20 and IFT88 are proteins that have been used to study the contribution of cilia during cellular processes (Follit et al., 2006; Pazour et al., 2000). If the ciliated centrosome is involved in centrosome movement to the cytokinetic bridge and in bridge cleavage, it could potentially suggest a novel cilium driven mechanism to regulate centrosome positioning during cilia formation.

Overall, the significance of centrosome movement during pre-abscission could be involved in a tissue developmental context to dictate the formation of an apical membrane and dictate where the cilium will be formed (Figure 5.1). Identifying the molecular and cellular mechanisms of when and where a cilium is constructed during tissue formation in cells in culture utilize serum starvation methods to stimulate ciliogenesis (Wu et al., 2018). Cells are arrested in the G0 phase of the cell cycle by use of serum free media which facilitates cilia formation. In addition, removal of serum from the media eliminates growth factors necessary for cell cycle progression into M-phase (Avasthi and Marshall, 2012; Goto et al., 2013; Nachury et

al., 2007; Plotnikova et al., 2009; Westlake et al., 2011). Even though these studies have been integral in identifying signaling and cellular mechanisms regulated by cilia in other cellular processes like cell polarization, cell migration and tissue formation. Removal of serum potentially masks the role for a cilium in the context of regulating pre-abscission mechanisms during cell division. Studies in our lab find that cilia can be present in pre-abscising cells in mammalian cells in culture that are grown in a medium supplement with growth serum (Figure 5.2). It is therefore necessary to identify the spatial and temporal mechanisms of cilia formation in the context of a developing tissue in an animal *in vivo*. This is why studies in chapter 4 utilizing KV as a model to study ciliogenesis during tissue formation in zebrafish are integral in identifying the developmental cues regulating centrosome positioning and cilia formation. Taken together, the studies in this thesis highlight the importance of understanding the molecular mechanisms that coordinate centrosome positioning, abscission and cilia formation in the context of a developing tissue *in vivo* which will provide an avenue to understand the developmental cues that are disrupted leading to improper tissue formation that causes disease progression.

REFERENCES

Aljiboury, A., Mujcic, A., Curtis, E., Cammerino, T., Magny, D., Lan, Y., Bates, M., Freshour, J., Ahmed-Braimeh, Y.H., and Hehnly, H. (2022). Pericentriolar matrix (PCM) integrity relies on cenexin and Polo-Like Kinase (PLK)1. Mol. Biol. Cell mbcE22010015.

Aljiboury, A.A., Mujcic, A., Cammerino, T., Rathbun, L.I., and Hehnly, H. (2021). Imaging the early zebrafish embryo centrosomes following injection of small-molecule inhibitors to understand spindle formation. STAR Protoc. *2*, 100293.

Amack, J.D., and Yost, H.J. (2004). The T box transcription factor no tail in ciliated cells controls zebrafish left-right asymmetry. Curr. Biol. *14*, 685–690.

Amack, J.D., Wang, X., and Yost, H.J. (2007). Two T-box genes play independent and cooperative roles to regulate morphogenesis of ciliated Kupffer's vesicle in zebrafish. Dev. Biol. *310*, 196–210.

de Anda, F.C., Pollarolo, G., Da Silva, J.S., Camoletto, P.G., Feiguin, F., and Dotti, C.G. (2005). Centrosome localization determines neuronal polarity. Nature *436*, 704–708.

Anderson, C.T., and Stearns, T. (2009). Centriole Age Underlies Asynchronous Primary Cilium Growth in Mammalian Cells. Curr. Biol. *19*, 1498–1502.

Angus, K.L., and Griffiths, G.M. (2013). Cell polarisation and the immunological synapse. Curr. Opin. Cell Biol. *25*, 85–91.

Aniento, F., Emans, N., Griffiths, G., and Gruenberg, J. (1993). Cytoplasmic dynein-dependent vesicular transport from early to late endosomes. J. Cell Biol. *123*, 1373–1387.

Asano, S.M., Gao, R., Wassie, A.T., Tillberg, P.W., Chen, F., and Boyden, E.S. (2018). Expansion Microscopy: Protocols for Imaging Proteins and RNA in Cells and Tissues. Curr. Protoc. Cell Biol. *80*, 1–41.

Avasthi, P., and Marshall, W.F. (2012). Stages of ciliogenesis and regulation of ciliary length. Differentiation *83*, S30–S42.

Azimzadeh, J., and Bornens, M. (2007). Structure and duplication of the centrosome. J. Cell Sci. *120*, 2139–2142.

Barnes, A.P., and Polleux, F. (2009). Establishment of axon-dendrite polarity in developing neurons. Annu. Rev. Neurosci. *32*, 347–381.

Baum, B., and Georgiou, M. (2011). Dynamics of adherens junctions in epithelial establishment , maintenance , and remodeling. *192*, 907–917.

Bernabé-Rubio, M., Andrés, G., Casares-Arias, J., Fernández-Barrera, J., Rangel, L., Reglero-Real, N., Gershlick, D.C., Fernández, J.J., Millán, J., Correas, I., et al. (2016). Novel role for the midbody in primary ciliogenesis by polarized epithelial cells. J. Cell Biol. *214*, 259–273.

Blasky, A.J., Mangan, A., and Prekeris, R. (2015). Polarized Protein Transport and Lumen Formation during Epithelial Tissue Morphogenesis. Annu. Rev. Cell Dev. Biol. *31*, 575–591.

Bryant, D.M., and Mostov, K.E. (2008). From cells to organs: Building polarized tissue. Nat. Rev. Mol. Cell Biol. *9*, 887–901.

Bryant, D.M., Datta, A., Rodríguez-Fraticelli, A.E., PeräCurrency Signnen, J., Martín-Belmonte, F., and Mostov, K.E. (2010). A molecular network for de novo generation of the apical surface and lumen. Nat. Cell Biol. *12*, 1035–1045.

Burute, M., Prioux, M., Blin, G., Truchet, S., Letort, G., Tseng, Q., Bessy, T., Lowell, S., Young, J., Filhol, O., et al. (2017). Polarity Reversal by Centrosome Repositioning Primes Cell Scattering during Epithelial-to-Mesenchymal Transition. Dev. Cell *40*, 168–184.

Carter, S.B. (1967). Effects of cytochalasins on mammalian cells. Nature *213*, 261–

264.

Chang, P., and Stearns, T. (2000). Delta-tubulin and epsilon-tubulin: two new human centrosomal tubulins reveal new aspects of centrosome structure and function. Nat. Cell Biol. *2*, 30–35.

Chen, C.-T., Hehnly, H., Yu, Q., Farkas, D., Zheng, G., Redick, S.D., Hung, H.-F., Samtani, R., Jurczyk, A., Akbarian, S., et al. (2014). A unique set of centrosome proteins requires pericentrin for spindle-pole localization and spindle orientation. Curr. Biol. *24*, 2327–2334.

Chen, C.T., Hehnly, H., and Doxsey, S.J. (2012). Orchestrating vesicle transport, ESCRTs and kinase surveillance during abscission. Nat. Rev. Mol. Cell Biol. *13*, 483–488.

Colicino, E.G., Garrastegui, A.M., Freshour, J., Santra, P., Post, D.E., Kotula, L., and Hehnly, H. (2018). Gravin regulates centrosome function through PLK1. Mol. Biol. Cell *29*, 532–541.

Colicino, E.G., Stevens, K., Curtis, E., Rathbun, L., Bates, M., Manikas, J., Amack, J., Freshour, J., and Hehnly, H. (2019). Chromosome misalignment is associated with PLK1 activity at cenexin-positive mitotic centrosomes. Mol. Biol. Cell *30*, 1598–1609.

Dasgupta, A., and Amack, J.D. (2016). Cilia in vertebrate left-right patterning. Philos. Trans. R. Soc. London. Ser. B, Biol. Sci. *371*.

Decarreau, J., Wagenbach, M., Lynch, E., Halpern, A.R., Vaughan, J.C., Kollman, J., and Wordeman, L. (2017). The tetrameric kinesin Kif25 suppresses pre-mitotic centrosome separation to establish proper spindle orientation. Nat. Cell Biol. *19*, 384–390.

Delaval, B., Bright, A., Lawson, N.D., and Doxsey, S. (2011). The cilia protein IFT88

is required for spindle orientation in mitosis. Nat. Cell Biol. *13*, 461–468.

Dionne, L.K., Wang, X.J., and Prekeris, R. (2015). Midbody: From cellular junk to regulator of cell polarity and cell fate. Curr. Opin. Cell Biol. *35*, 51–58.

Donati, A., Anselme, I., Schneider-Maunoury, S., and Vesque, C. (2021). Planar polarization of cilia in the zebrafish floor-plate involves Par3-mediated posterior localization of highly motile basal bodies. Development *148*.

Dotti, C.G., Sullivan, C.A., and Banker, G.A. (1988). The establishment of polarity by hippocampal neurons in culture. J. Neurosci. Off. J. Soc. Neurosci. *8*, 1454–1468.

Eggert, U.S., Mitchison, T.J., and Field, C.M. (2006). Animal Cytokinesis: From Parts List to Mechanisms. Annu. Rev. Biochem. *75*, 543–566.

Elia, N., Sougrat, R., Spurlin, T.A., Hurley, J.H., and Lippincott-Schwartz, J. (2011). Dynamics of endosomal sorting complex required for transport (ESCRT) machinery during cytokinesis and its role in abscission. Proc. Natl. Acad. Sci. U. S. A. *108*, 4846–4851.

Etienne-Manneville, S. (2013). Microtubules in cell migration. Annu. Rev. Cell Dev. Biol. *29*, 471–499.

Etienne-Manneville, S., and Hall, A. (2001). Integrin-mediated activation of Cdc42 controls cell polarity in migrating astrocytes through PKCζ. Cell *106*, 489–498.

Feldman, J.L., and Priess, J.R. (2012). A role for the centrosome and PAR-3 in the hand-off of MTOC function during epithelial polarization. Curr. Biol. *22*, 575–582.

Finetti, F., Paccani, S.R., Riparbelli, M.G., Giacomello, E., Perinetti, G., Pazour, G.J., Rosenbaum, J.L., and Baldari, C.T. (2009). Intraflagellar transport is required for polarized recycling of the TCR/CD3 complex to the immune synapse. Nat. Cell Biol. *11*, 1332–1339.

Finetti, F., Patrussi, L., Masi, G., Onnis, A., Galgano, D., Lucherini, O.M., Pazour,

G.J., and Baldari, C.T. (2014). Specific recycling receptors are targeted to the immune synapse by the intraflagellar transport system. J. Cell Sci. *127*, 1924–1937.

Follit, J.A., Tuft, R.A., Fogarty, K.E., and Pazour, G.J. (2006). The intraflagellar transport protein IFT20 is associated with the Golgi complex and is required for cilia assembly. Mol. Biol. Cell *17*, 3781–3792.

Fomicheva, M., Tross, E.M., and Macara, I.G. (2020). Polarity proteins in oncogenesis. Curr. Opin. Cell Biol. *62*, 26–30.

Giansanti, M.G., Belloni, G., and Gatti, M. (2007). Rab11 is required for membrane trafficking and actomyosin ring constriction in meiotic cytokinesis of Drosophila males. Mol. Biol. Cell *18*, 5034–5047.

Gjorevski, N., and Nelson, C.M. (2010). The mechanics of development: Models and methods for tissue morphogenesis. Birth Defects Res. C. Embryo Today *90*, 193–202.

Godinho, S.A., and Pellman, D. (2014). Causes and consequences of centrosome abnormalities in cancer. Philos. Trans. R. Soc. London. Ser. B, Biol. Sci. *369*.

Goldstein, B., and Macara, I.G. (2007). The PAR Proteins: Fundamental Players in Animal Cell Polarization. Dev. Cell *13*, 609–622.

Goss, J.W., and Toomre, D.K. (2008). Both daughter cells traffic and exocytose membrane at the cleavage furrow during mammalian cytokinesis. J. Cell Biol. *181*, 1047–1054.

Goto, H., Inoko, A., and Inagaki, M. (2013). Cell cycle progression by the repression of primary cilia formation in proliferating cells. Cell. Mol. Life Sci. *70*, 3893–3905.

Graser, S., Stierhof, Y.-D., Lavoie, S.B., Gassner, O.S., Lamla, S., Le Clech, M., and Nigg, E.A. (2007). Cep164, a novel centriole appendage protein required for primary cilium formation. J. Cell Biol. *179*, 321–330.

Grimes, D.T., and Burdine, R.D. (2017). Left–Right Patterning: Breaking Symmetry to Asymmetric Morphogenesis. Trends Genet. *33*, 616–628.

Gromley, A., Yeaman, C., Rosa, J., Redick, S., Chen, C.T., Mirabelle, S., Guha, M., Sillibourne, J., and Doxsey, S.J. (2005). Centriolin anchoring of exocyst and SNARE complexes at the midbody is required for secretory-vesicle-mediated abscission. Cell *123*, 75–87.

Guo, W.H., and Wang, Y.L. (2012). A three-component mechanism for fibroblast migration with a contractile cell body that couples a myosin II - Independent propulsive anterior to a myosin II - Dependent resistive tail. Mol. Biol. Cell *23*, 1657–1663.

Hall, N.A., and Hehnly, H. (2021). A centriole's subdistal appendages: Contributions to cell division, ciliogenesis and differentiation. Open Biol. *11*.

Hannaford, M.R., Liu, R., Billington, N., Swider, Z.T., Galletta, B.J., Fagerstrom, C.J., Combs, C., Sellers, J.R., and Rusan, N.M. (2022). Pericentrin is a Kinesin-1 Activator that Drives Centriole Motility. BioRxiv 2022.01.12.476023.

Hao, Y., Du, Q., Chen, X., Zheng, Z., Balsbaugh, J.L., Maitra, S., Shabanowitz, J., Hunt, D.F., and MacAra, I.G. (2010). Par3 controls epithelial spindle orientation by aPKC-mediated phosphorylation of apical pins. Curr. Biol. *20*, 1809–1818.

Hehnly, H., and Doxsey, S. (2014). Rab11 Endosomes Contribute to Mitotic Spindle Organization and Orientation. Dev. Cell *28*, 497–507.

Hehnly, H., Sheff, D., and Stamnes, M. (2006). Shiga toxin facilitates its retrograde transport by modifying microtubule dynamics. Mol. Biol. Cell *17*, 4379–4389.

Hehnly, H., Chen, C.T., Powers, C.M., Liu, H.L., and Doxsey, S. (2012). The centrosome regulates the Rab11- dependent recycling endosome pathway at appendages of the mother centriole. Curr. Biol. *22*, 1944–1950.

Hong, E., Jayachandran, P., and Brewster, R. (2010). The polarity protein Pard3 is required for centrosome positioning during neurulation. Dev. Biol. *341*, 335–345.

Hung, H.F., Hehnly, H., and Doxsey, S. (2016). The mother centriole appendage protein cenexin modulates lumen formation through spindle orientation. Curr. Biol. *26*, 793–801.

Inaba, M., Yuan, H., Salzmann, V., Fuller, M.T., and Yamashita, Y.M. (2010). E-Cadherin is required for centrosome and spindle orientation in Drosophila male germline stem cells. PLoS One *5*, 1–7.

Ishikawa, H., Kubo, A., Tsukita, S., and Tsukita, S. (2005). Odf2-deficient mother centrioles lack distal/subdistal appendages and the ability to generate primary cilia. Nat. Cell Biol. *7*, 517–524.

Ivanov, A.I., Young, C., Den Beste, K., Capaldo, C.T., Humbert, P.O., Brennwald, P., Parkos, C.A., and Nusrat, A. (2010). Tumor suppressor scribble regulates assembly of tight junctions in the intestinal epithelium. Am. J. Pathol. *176*, 134–145.

Jiang, T., McKinley, R.F.A., McGill, M.A., Angers, S., and Harris, T.J.C. (2015). A Par-1-Par-3-Centrosome Cell Polarity Pathway and Its Tuning for Isotropic Cell Adhesion. Curr. Biol. *25*, 2701–2708.

Jimenez, A.J., Schaeffer, A., De Pascalis, C., Letort, G., Vianay, B., Bornens, M., Piel, M., Blanchoin, L., and Théry, M. (2021). Acto-myosin network geometry defines centrosome position. Curr. Biol. *31*, 1206-1220.e5.

Jonsdottir, A.B., Dirks, R.W., Vrolijk, J., Ogmundsdottir, H.M., Tanke, H.J., Eyfjörd, J.E., and Szuhai, K. (2010). Centriole movements in mammalian epithelial cells during cytokinesis. BMC Cell Biol. *11*, 34.

Kim, J.C., Badano, J.L., Sibold, S., Esmail, M.A., Hill, J., Hoskins, B.E., Leitch, C.C., Venner, K., Ansley, S.J., Ross, A.J., et al. (2004). The Bardet-Biedl protein BBS4

targets cargo to the pericentriolar region and is required for microtubule anchoring and cell cycle progression. Nat. Genet. *36*, 462–470.

Kim, J.C., Ou, Y.Y., Badano, J.L., Esmail, M.A., Leitch, C.C., Fiedrich, E., Beales, P.L., Archibald, J.M., Katsanis, N., Rattner, J.B., et al. (2005). MKKS/BBS6, a divergent chaperonin-like protein linked to the obesity disorder Bardet-Biedl syndrome, is a novel centrosomal component required for cytokinesis. J. Cell Sci. *118*, 1007–1020.

Kimmel, C.B., Ballard, W.W., Kimmel, S.R., Ullmann, B., and Schilling, T.F. (1995). Stages of embryonic development of the zebrafish. Dev. Dyn. an Off. Publ. Am. Assoc. Anat. *203*, 253–310.

Knödler, A., Feng, S., Zhang, J., Zhang, X., Das, A., Peränen, J., and Guo, W. (2010). Coordination of Rab8 and Rab11 in primary ciliogenesis. Proc. Natl. Acad. Sci. U. S. A. *107*, 6346–6351.

Krishnan, N., Swoger, M., Rathbun, L.I., Fioramonti, P.J., Freshour, J., Bates, M., Patteson, A.E., and Hehnly, H. (2022). Rab11 endosomes and Pericentrin coordinate centrosome movement during pre-abscission in vivo. Life Sci. Alliance *5*, 1–15.

Kuo, T.-C., Chen, C.-T., Baron, D., Onder, T.T., Loewer, S., Almeida, S., Weismann, C.M., Xu, P., Houghton, J.-M., Gao, F.-B., et al. (2011). Midbody accumulation through evasion of autophagy contributes to cellular reprogramming and tumorigenicity. Nat. Cell Biol. *13*, 1214–1223.

Lam, A.J., St-Pierre, F., Gong, Y., Marshall, J.D., Cranfill, P.J., Baird, M.A., McKeown, M.R., Wiedenmann, J., Davidson, M.W., Schnitzer, M.J., et al. (2012). Improving FRET dynamic range with bright green and red fluorescent proteins. Nat. Methods *9*, 1005–1012.

Lee, J., Magescas, J., Fetter, R.D., Feldman, J.L., and Shen, K. (2021). Inherited apicobasal polarity defines the key features of axon-dendrite polarity in a sensory neuron. Curr. Biol. *31*, 3768-3783.e3.

Lerit, D.A., and Rusan, N.M. (2013). PLP inhibits the activity of interphase centrosomes to ensure their proper segregation in stem cells. J. Cell Biol. *202*, 1013–1022.

Levic, D.S., Yamaguchi, N., Wang, S., Knaut, H., and Bagnat, M. (2021). Knock-in tagging in zebrafish facilitated by insertion into non-coding regions. Development *148*, dev199994.

Little, J.N., and Dwyer, N.D. (2021). Cep55: abscission boss or assistant? Trends Cell Biol. *31*, 789–791.

Liu, H., Yu, X., Li, K., Klejnot, J., Yang, H., Lisiero, D., and Lin, C. (2008). Photoexcited CRY2 interacts with CIB1 to regulate transcription and floral initiation in Arabidopsis. Science *322*, 1535–1539.

Lu, Q., Insinna, C., Ott, C., Stauffer, J., Pintado, P.A., Rahajeng, J., Baxa, U., Walia, V., Cuenca, A., Hwang, Y.S., et al. (2015). Early steps in primary cilium assembly require EHD1/EHD3-dependent ciliary vesicle formation. Nat. Cell Biol. *17*, 228–240.

Luxton, G.W.G., and Gundersen, G.G. (2011). Orientation and function of the nuclear-centrosomal axis during cell migration. Curr. Opin. Cell Biol. *23*, 579–588.

Macara, I., and Seldin, L. (2017). Epithelial spindle orientation diversities and uncertainties: Recent developments and lingering questions. F1000Research *6*, 1–10.

Mangan, A.J., Sietsema, D. V, Li, D., Moore, J.K., Citi, S., and Prekeris, R. (2016). Cingulin and actin mediate midbody-dependent apical lumen formation during polarization of epithelial cells. Nat. Commun. *7*, 12426.

Mayor, R., and Etienne-Manneville, S. (2016). The front and rear of collective cell migration. Nat. Rev. Mol. Cell Biol. *17*, 97–109.

Mehta A.D., Rock R.S., Rief M., Spudich J.A., Mooseker M.S., and Cheney R.E. (1999). Myosin-V is a processive actin-based motor. Nature *400*, 590–593.

Mirvis, M., Stearns, T., and James Nelson, W. (2018). Cilium structure, assembly, and disassembly regulated by the cytoskeleton. Biochem. J. *475*, 2329–2353.

Montagnac, G., Echard, A., and Chavrier, P. (2008). Endocytic traffic in animal cell cytokinesis. Curr. Opin. Cell Biol. *20*, 454–461.

Nachury, M. V, Loktev, A. V, Zhang, Q., Westlake, C.J., Peränen, J., Merdes, A., Slusarski, D.C., Scheller, R.H., Bazan, J.F., Sheffield, V.C., et al. (2007). A core complex of BBS proteins cooperates with the GTPase Rab8 to promote ciliary membrane biogenesis. Cell *129*, 1201–1213.

Nakamuta, S., Funahashi, Y., Namba, T., Arimura, N., Picciotto, M.R., Tokumitsu, H., Soderling, T.R., Sakakibara, A., Miyata, T., Kamiguchi, H., et al. (2011). Local application of neurotrophins specifies axons through inositol 1,4,5-trisphosphate, calcium, and Ca2+/calmodulin-dependent protein kinases. Sci. Signal. *4*, ra76.

Naslavsky, N., and Caplan, S. (2020). Endocytic membrane trafficking in the control of centrosome function. Curr. Opin. Cell Biol. *65*, 150–155.

Navis, A., Marjoram, L., and Bagnat, M. (2013). Cftr controls lumen expansion and function of Kupffer's vesicle in zebrafish. Development *140*, 1703–1712.

Nejsum, L.N., and Nelson, W.J. (2009). Epithelial cell surface polarity: the early steps. Front. Biosci. (Landmark Ed. *14*, 1088–1098.

Nelson, W.J. (2009). Remodeling epithelial cell organization: transitions between front-rear and apical-basal polarity. Cold Spring Harb. Perspect. Biol. *1*, 1–20.

Nguyen, M.K., Kim, C.Y., Kim, J.M., Park, B.O., Lee, S., Park, H., and Heo, W. Do

(2016). Optogenetic oligomerization of Rab GTPases regulates intracellular membrane trafficking. Nat. Chem. Biol. *12*, 431–436.

Nobes, C.D., and Hall, A. (1995). Rho, Rac, and Cdc42 GTPases regulate the assembly of multimolecular focal complexes associated with actin stress fibers, lamellipodia, and filopodia. Cell *81*, 53–62.

Nonaka, S., Tanaka, Y., Okada, Y., Takeda, S., Harada, A., Kanai, Y., Kido, M., and Hirokawa, N. (1998). Randomization of left-right asymmetry due to loss of nodal cilia generating leftward flow of extraembryonic fluid in mice lacking KIF3B motor protein. Cell *95*, 829–837.

Ohno, S. (2001). Intercellular junctions and cellular polarity: the PAR-aPKC complex, a conserved core cassette playing fundamental roles in cell polarity. Curr. Opin. Cell Biol. *13*, 641–648.

Omori, Y., Zhao, C., Saras, A., Mukhopadhyay, S., Kim, W., Furukawa, T., Sengupta, P., Veraksa, A., and Malicki, J. (2008). Elipsa is an early determinant of ciliogenesis that links the IFT particle to membrane-associated small GTPase Rab8. Nat. Cell Biol. *10*, 437–444.

Paridaen, J.T.M.L., Wilsch-Bräuninger, M., and Huttner, W.B. (2013). Asymmetric inheritance of centrosome-associated primary cilium membrane directs ciliogenesis after cell division. Cell *155*, 333–344.

Pazour, G.J., and Witman, G.B. (2003). The vertebrate primary cilium is a sensory organelle. Curr. Opin. Cell Biol. *15*, 105–110.

Pazour, G.J., Dickert, B.L., Vucica, Y., Seeley, E.S., Rosenbaum, J.L., Witman, G.B., and Cole, D.G. (2000). Chlamydomonas IFT88 and its mouse homologue, polycystic kidney disease gene tg737, are required for assembly of cilia and flagella. J. Cell Biol. *151*, 709–718.

Pei, D., Shu, X., Gassama-Diagne, A., and Thiery, J.P. (2019). Mesenchymal–epithelial transition in development and reprogramming. Nat. Cell Biol. *21*, 44–53.

Piel, M., Meyer, P., Khodjakov, A., Rieder, C.L., and Bornens, M. (2000). The respective contributions of the mother and daughter centrioles to centrosome activity and behavior in vertebrate cells. J. Cell Biol. *149*, 317–329.

Piel, M., Nordberg, J., Euteneur, U., and Bornens, M. (2001). Centrosome-dependent exit of cytokinesis in animal cells. Science (80-.). *291*, 1550–1553.

Pihan, G.A., Wallace, J., Zhou, Y., and Doxsey, S.J. (2003). Centrosome abnormalities and chromosome instability occur together in pre-invasive carcinomas. Cancer Res. *63*, 1398–1404.

Plotnikova, O. V, Pugacheva, E.N., and Golemis, E.A. (2009). Primary cilia and the cell cycle. Methods Cell Biol. *94*, 137–160.

Pouthas, F., Girard, P., Lecaudey, V., Ly, T.B.N., Gilmour, D., Boulin, C., Pepperkok, R., and Reynaud, E.G. (2008). In migrating cells, the Golgi complex and the position of the centrosome depend on geometrical constraints of the substratum. J. Cell Sci. *121*, 2406–2414.

Qin, H., Wang, Z., Diener, D., and Rosenbaum, J. (2007). Intraflagellar transport protein 27 is a small G protein involved in cell-cycle control. Curr. Biol. *17*, 193–202.

Qin, Y., Meisen, W.H., Hao, Y., and Macara, I.G. (2010). Tuba, a Cdc42 GEF, is required for polarized spindle orientation during epithelial cyst formation. J. Cell Biol. *189*, 661–669.

Rathbun, L.I., Colicino, E.G., Manikas, J., O'Connell, J., Krishnan, N., Reilly, N.S., Coyne, S., Erdemci-Tandogan, G., Garrastegui, A., Freshour, J., et al. (2020a). Cytokinetic bridge triggers de novo lumen formation in vivo. Nat. Commun. *11*, 1269.

Rathbun, L.I., Aljiboury, A.A., Bai, X., Hall, N.A., Manikas, J., Amack, J.D.,

Bembenek, J.N., and Hehnly, H. (2020b). PLK1- and PLK4-Mediated Asymmetric Mitotic Centrosome Size and Positioning in the Early Zebrafish Embryo. Curr. Biol. *30*, 4519-4527.e3.

Rebollo, E., Sampaio, P., Januschke, J., Llamazares, S., Varmark, H., and González, C. (2007). Functionally Unequal Centrosomes Drive Spindle Orientation in Asymmetrically Dividing Drosophila Neural Stem Cells. Dev. Cell *12*, 467–474.

Reck-Peterson, S.L., Redwine, W.B., Vale, R.D., and Carter, A.P. (2018). The cytoplasmic dynein transport machinery and its many cargoes. Nat. Rev. Mol. Cell Biol. *19*, 382–398.

Reichl, E.M., Ren, Y., Morphew, M.K., Delannoy, M., Effler, J.C., Girard, K.D., Divi, S., Iglesias, P.A., Kuo, S.C., and Robinson, D.N. (2008). Interactions between Myosin and Actin Crosslinkers Control Cytokinesis Contractility Dynamics and Mechanics. Curr. Biol. *18*, 471–480.

Renzova, T., Bohaciakova, D., Esner, M., Pospisilova, V., Barta, T., Hampl, A., and Cajanek, L. (2018). Inactivation of PLK4-STIL Module Prevents Self-Renewal and Triggers p53-Dependent Differentiation in Human Pluripotent Stem Cells. Stem Cell Reports *11*, 959–972.

Ritter, A.T., Asano, Y., Stinchcombe, J.C., Dieckmann, N.M.G., Chen, B.C., Gawden-Bone, C., van Engelenburg, S., Legant, W., Gao, L., Davidson, M.W., et al. (2015). Actin Depletion Initiates Events Leading to Granule Secretion at the Immunological Synapse. Immunity *42*, 864–876.

Roche, J. (2018). The Epithelial-to-Mesenchymal Transition in Cancer. Cancers (Basel). *10*.

Rodriguez-Boulan, E., and Nelson, W.J. (1989). Morphogenesis of the polarized epithelial cell phenotype. Science *245*, 718–725.

Rusan, N.M., and Peifer, M. (2007). A role for a novel centrosome cycle in asymmetric cell division. J. Cell Biol. *177*, 13–20.

Sagona, A.P., and Stenmark, H. (2010). Cytokinesis and cancer. FEBS Lett. *584*, 2652–2661.

Sahabandu, N., Kong, D., Magidson, V., Nanjundappa, R., Sullenberger, C., Mahjoub, M.R., and Loncarek, J. (2019). Expansion microscopy for the analysis of centrioles and cilia. J. Microsc. *276*, 145–159.

Satir, P., and Christensen, S.T. (2007). Overview of structure and function of mammalian cilia. Annu. Rev. Physiol. *69*, 377–400.

Sawin, K.E., LeGuellec, K., Philippe, M., and Mitchison, T.J. (1992). Mitotic spindle organization by a plus-end-directed microtubule motor. Nature *359*, 540–543.

Schelski, M., and Bradke, F. (2017). Neuronal polarization: From spatiotemporal signaling to cytoskeletal dynamics. Mol. Cell. Neurosci. *84*, 11–28.

Schiel, J.A., Simon, G.C., Zaharris, C., Weisz, J., Castle, D., Wu, C.C., and Prekeris, R. (2012). FIP3-endosome-dependent formation of the secondary ingression mediates ESCRT-III recruitment during cytokinesis. Nat. Cell Biol. *14*, 1068–1078.

Schmidt, K.N., Kuhns, S., Neuner, A., Hub, B., Zentgraf, H., and Pereira, G. (2012). Cep164 mediates vesicular docking to the mother centriole during early steps of ciliogenesis. J. Cell Biol. *199*, 1083–1101.

Schmoranzer, J., Fawcett, J.P., Segura, M., Tan, S., Vallee, R.B., Pawson, T., and Gundersen, G.G. (2009). Par3 and Dynein Associate to Regulate Local Microtubule Dynamics and Centrosome Orientation during Migration. Curr. Biol. *19*, 1065–1074.

Schnurr, M.E., Yin, Y., and Scott, G.R. (2014). Temperature during embryonic development has persistent effects on metabolic enzymes in the muscle of zebrafish. J. Exp. Biol. *217*, 1370–1380.

Seetharaman, S., and Etienne-Manneville, S. (2020). Cytoskeletal Crosstalk in Cell Migration. Trends Cell Biol. *30*, 720–735.

Seldin, L., and Macara, I. (2017). Epithelial spindle orientation diversities and uncertainties: recent developments and lingering questions. F1000Research *6*, 984.

SenGupta, S., Parent, C.A., and Bear, J.E. (2021). The principles of directed cell migration. Nat. Rev. Mol. Cell Biol. *22*, 529–547.

Sepulveda, G., Antkowiak, M., Brust-Mascher, I., Mahe, K., Ou, T., Castro, N.M., Christensen, L.N., Cheung, L., Jiang, X., Yoon, D., et al. (2018). Co-translational protein targeting facilitates centrosomal recruitment of PCNT during centrosome maturation in vertebrates. Elife *7*.

Shah, A.S., Ben-Shahar, Y., Moninger, T.O., Kline, J.N., and Welsh, M.J. (2009). Motile cilia of human airway epithelia are chemosensory. Science *325*, 1131–1134.

Shi, S.H., Jan, L.Y., and Jan, Y.N. (2003). Hippocampal neuronal polarity specified by spatially localized mPar3/mPar6 and PI 3-kinase activity. Cell *112*, 63–75.

Sobajima, T., Yoshimura, S.I., Iwano, T., Kunii, M., Watanabe, M., Atik, N., Mushiake, S., Morii, E., Koyama, Y., Miyoshi, E., et al. (2015). Rab11a is required for apical protein localisation in the intestine. Biol. Open *4*, 86–94.

Sorokin, S.P. (1968). Reconstructions of centriole formation and ciliogenesis in mammalian lungs. J. Cell Sci. *3*, 207–230.

SOROKIN, S. (1962). Centrioles and the formation of rudimentary cilia by fibroblasts and smooth muscle cells. J. Cell Biol. *15*, 363–377.

Stinchcombe, J.C., Majorovits, E., Bossi, G., Fuller, S., and Griffiths, G.M. (2006). Centrosome polarization delivers secretory granules to the immunological synapse. Nature *443*, 462–465.

Stinchcombe, J.C., Randzavola, L.O., Angus, K.L., Mantell, J.M., Verkade, P., and

Griffiths, G.M. (2015). Mother Centriole Distal Appendages Mediate Centrosome Docking at the Immunological Synapse and Reveal Mechanistic Parallels with Ciliogenesis. Curr. Biol. *25*, 3239–3244.

Strauss, B., Adams, R.J., and Papalopulu, N. (2006). A default mechanism of spindle orientation based on cell shape is sufficient to generate cell fate diversity in polarised Xenopus blastomeres. Development *133*, 3883–3893.

Taneja, N., Fenix, A.M., Rathbun, L., Millis, B.A., Tyska, M.J., Hehnly, H., and Burnette, D.T. (2016). Focal adhesions control cleavage furrow shape and spindle tilt during mitosis. Sci. Rep. *6*, 1–11.

Tanenbaum, M.E., and Medema, R.H. (2010). Mechanisms of Centrosome Separation and Bipolar Spindle Assembly. Dev. Cell *19*, 797–806.

Tanenbaum, M.E., Macůrek, L., Galjart, N., and Medema, R.H. (2008). Dynein, Lis1 and CLIP-170 counteract Eg5-dependent centrosome separation during bipolar spindle assembly. EMBO J. *27*, 3235–3245.

Tapon, N., and Hall, A. (1997). Rho, Rac and Cdc42 GTPases regulate the organization of the actin cytoskeleton. Curr. Opin. Cell Biol. *9*, 86–92.

Tay, H.G., Schulze, S.K., Compagnon, J., Foley, F.C., Heisenberg, C.P., Yost, H.J., Abdelilah-Seyfried, S., and Amack, J.D. (2013). Lethal giant larvae 2 regulates development of the ciliated organ Kupffer's vesicle. Dev. *140*, 1550–1559.

Tsai, J.W., Bremner, K.H., and Vallee, R.B. (2007). Dual subcellular roles for LIS1 and dynein in radial neuronal migration in live brain tissue. Nat. Neurosci. *10*, 970–979.

Tuncay, H., Brinkmann, B.F., Steinbacher, T., Schürmann, A., Gerke, V., Iden, S., and Ebnet, K. (2015). JAM-A regulates cortical dynein localization through Cdc42 to control planar spindle orientation during mitosis. Nat. Commun. *6*.

Uytingco, C.R., Williams, C.L., Xie, C., Shively, D.T., Green, W.W., Ukhanov, K., Zhang, L., Nishimura, D.Y., Sheffield, V.C., and Martens, J.R. (2019). BBS4 is required for intraflagellar transport coordination and basal body number in mammalian olfactory cilia. J. Cell Sci. *132*.

Vaughan, S., and Dawe, H.R. (2011). Common themes in centriole and centrosome movements. Trends Cell Biol. *21*, 57–66.

Vertii, A., Hehnly, H., and Doxsey, S. (2016). The centrosome, a multitalented renaissance organelle. Cold Spring Harb. Perspect. Biol. *8*.

Wang, Q., and Margolis, B. (2007). Apical junctional complexes and cell polarity. Kidney Int. *72*, 1448–1458.

Wang, M., Nagle, R.B., Knudsen, B.S., Cress, A.E., and Rogers, G.C. (2020). Centrosome loss results in an unstable genome and malignant prostate tumors. Oncogene *39*, 399–413.

Welz, T., Wellbourne-Wood, J., and Kerkhoff, E. (2014). Orchestration of cell surface proteins by Rab11. Trends Cell Biol. *24*, 407–415.

Westlake, C.J., Baye, L.M., Nachury, M. V., Wright, K.J., Ervin, K.E., Phu, L., Chalouni, C., Beck, J.S., Kirkpatrick, D.S., Slusarski, D.C., et al. (2011). Primary cilia membrane assembly is initiated by Rab11 and transport protein particle II (TRAPPII) complex-dependent trafficking of Rabin8 to the centrosome. Proc. Natl. Acad. Sci. U. S. A. *108*, 2759–2764.

Willoughby, P.M., Allen, M., Yu, J., Korytnikov, R., Chen, T., Liu, Y., So, I., Macpherson, N., Mitchell, J.A., Fernandez-Gonzalez, R., et al. (2021). The recycling endosome protein Rab25 coordinates collective cell movements in the zebrafish surface epithelium. Elife *10*.

Wilson, G.M., Fielding, A.B., Simon, G.C., Yu, X., Andrews, P.D., Haines, R.S., Frey,

A.M., Peden, A.A., Gould, G.W., and Prekeris, R. (2005). The FIP3-Rab11 protein complex regulates recycling endosome targeting to the cleavage furrow during late cytokinesis. Mol. Biol. Cell *16*, 849–860.

Wood, C.R., Wang, Z., Diener, D., Zones, J.M., Rosenbaum, J., and Umen, J.G. (2012). IFT proteins accumulate during cell division and localize to the cleavage furrow in Chlamydomonas. PLoS One *7*, e30729.

Wu, C.T., Chen, H.Y., and Tang, T.K. (2018). Myosin-Va is required for preciliary vesicle transportation to the mother centriole during ciliogenesis. Nat. Cell Biol. *20*, 175–185.

Xie, S., Farmer, T., Naslavsky, N., and Caplan, S. (2019). MICAL-L1 coordinates ciliogenesis by recruiting EHD1 to the primary cilium. J. Cell Sci. *132*.

Yogev, S., and Shen, K. (2017). Establishing Neuronal Polarity with Environmental and Intrinsic Mechanisms. Neuron *96*, 638–650.

Yvon, A.C., Walker, J.W., Danowski, B., Fagerstrom, C., Khodjakov, A., and Wadsworth, P. (2002). Centrosome Polarité.Pdf. *13*, 1871–1880.

Zegers, M.M., and Friedl, P. (2014). Rho GTPases in collective cell migration. Small GTPases *5*.

Zhang, J., and Wang, Y.L. (2017). Centrosome defines the rear of cells during mesenchymal migration. Mol. Biol. Cell *28*, 3240–3251.

Zhang, J., Guo, W.H., and Wang, Y.L. (2014). Microtubules stabilize cell polarity by localizing rear signals. Proc. Natl. Acad. Sci. U. S. A. *111*, 16383–16388.

Zolessi, F.R., Poggi, L., Wilkinson, C.J., Chien, C.-B., and Harris, W.A. (2006). Polarization and orientation of retinal ganglion cells in vivo. Neural Dev. *1*, 2.

Nikhila Krishnan nikrishn@syr.edu | +1-347-420-9144

EDUCATION

Syracuse University **New York, USA** **Aug 2018-Present**

- Ph.D. in Biology (in-progress). Current C. GPA: 3.76/4.0
- Cell Biology Coursework: Microscopy Cell and Developmental Biology
- Microscopy Coursework: Microscopy Techniques

Brandeis University **Massachusetts, USA** **Aug 2014-Jan 2016**

- M.S. Molecular and Cell Biology, January 2016. GPA: 3.4/4.0
- Masters Student Researcher in Eve Marder's Lab
- Neurobiology Course work: Neurobiology; Neurobiology of Human Diseases; Human Genetics.

Anna University **Tamil Nadu, India** **Sept 2009-May 2013**

- B. Tech, Biotechnology, May 2013

SKILLS:

Wet Lab Techniques:
Human cell culture, Zebrafish model organism for studying cell biology, Gibson cloning, Immunohistochemistry, Western Blot, Microinjection.

Microscopy:
Laser Scanning Confocal Microscopy, Spinning Disk Confocal Microscopy, Widefield Fluorescence Microscopy, Zeiss LSM 980 with Airy Scan2 Confocal Microscope, Live Cell Fluorescence Microscopy, Fluorescence Recovery After Photobleaching (FRAP), Ablation.

Software:
Fiji, ImageJ, Imaris, GraphPad (PRISM 9), Microsoft office, Adobe Acrobat **(Illustrator)**, MATLAB, Auto Quant X3, LASX, ZEN, VisiView.

RESEARCH EXPERIENCE:

PhD Candidate, Hehnly Lab at Syracuse University **(Aug'18-present)**

Rab11 recycling endosomes coordinate centrosome movement and function during tissue morphogenesis

- Study the role of Rab11 endosomes and the centrosome during cell division and during the formation of a three-dimensional tissue.
- Employed live cell microscopy, fixed cell confocal microscopy, mammalian tissue culture system and CRISPR/Cas9 genome editing system to understand role of Rab11 endosomes and the centrosome during cell division and tissue morphogenesis.
- Utilized Zebrafish model organism for studying cell biology questions.
- Employed immunohistochemistry, molecular biology and molecular cloning (Gibson cloning).

Research Fellow, Bhalla Lab at National Center for Biological Science **(Jul'16-Jul'17)**

Memory and Plasticity in rodent hippocampus

- Employed intracranial virus injections coupled with in vitro patch clamp in mouse hippocampal slices to study the mechanisms underlying sequences that are known to arise in CA1 neurons.
- Characterization of transgenic mouse lines using PCR.

Research Technician, Marder Lab at Brandeis University **(Oct'14-Jan'16)**

Molecular characterization and spatial distribution of receptors in the stomatogastric nervous system (STNS) and the muscles they innervate

- Utilized immunohistochemistry combined with fluorescent and confocal microscopy to map receptors and ion channels in identified STG neurons.
- One of the few students encouraged to learn and employ single cell real time RT-PCR, to understand receptor transcript levels in identified neurons in the STG.
- Characterized ion channels and receptor mRNA transcript levels present in the muscular targets of STG neurons.

Research Internship at **Hospira Healthcare Pvt. Ltd.** **(June'13-Dec'13)**

Cloning and Characterization of Mammalian Promoter Sequences

- Worked on cloning and characterization of promoter sequences that would be important in the expression of the protein of interest in mammalian cell lines.

Undergraduate Thesis, Sri Venkateswara College of Engineering, Chennai **(May'12-May'13)**

Extraction of ESBL enzyme from *E. coli* Isolated from hospital environment soil samples and construction of aptamers

- Focused on working with antibiotic resistance in bacteria.
- Beta lactam antibiotics are rendered inactive by an enzyme secreted by the bacteria called betalactamase.
- Constructed ssDNA sequences, docked them with TEM1 betalactamase and studied the interaction between the enzyme and the DNA sequence using bioinformatics.

PUBLICATIONS

a) Rathbun, L.I., Colicino, E.G., Manikas, J., O'Connell J., **Krishnan N.,** Riley N.S., Coyne S., Erdemci-Tandogan G., Garrastegui A., Freshour J., Santra P., Manning M.L., Amack J.D., Hehnly H. Cytokinetic bridge triggers de novo lumen formation in vivo. *Nat Commun* **11,** 1269 (2020). https://doi.org/10.1038/s41467-020-15002-8.

b) **Krishnan, N**., Swoger, M., Rathbun, L. I., Fioramonti, P. J., Freshour, J., Bates, M., Patteson, A. E., & Hehnly, H. (2022). Rab11 endosomes and Pericentrin coordinate centrosome movement during pre-abscission in vivo. *Life science alliance*, *5*(7), e202201362.

PRE-PRINTS

a) Campaña, M.B., Davis, T.R., Cleverdon, E.R., Bates, M., **Krishnan, N.,** Curtis, E.R., Childs, M.D., Morales-Rodriguez, Y., Sieburg, M.A., Hehnly, H., et al. (2021). Ghrelin O-acyltransferase interacts with extracellular peptides and exhibits unexpected cellular localization for a secretory pathway enzyme. BioRxiv 2021.06.01.446150.

PROFESSIONAL MEMBERSHIPS

International Zebrafish Society **(2021-present)**
American Society for Cell Biology **(2019-present)**
Society for Neuroscience **(2015-2016)**

SELECTED INVITED SEMINARS AND PLATFORM TALKS

Virtual Rapid fire Presentation, 17th International Zebrafish Conference (IZFC) **Jun'22**
Science Slam Centrosome and Spindle pole body meeting (in person), Copenhagen, Denmark **Oct'21**
Poster Presentation Centrosome and Spindle pole body meeting (in person), Copenhagen, Denmark **Oct'21**
In-person Talk Mechanisms of Development and Disease group at Syracuse University **Sept'21**
Virtual Poster 16th International Zebrafish Conference (IZFC) **Poster Finalist **Jun '21***
Presented a *Virtual Talk* with Prof. Hehnly at ASCB Dec'20
Virtual Poster Presentation, American Society for Cell Biology **Dec'20**

Virtual Talk Developmental Biology New York conference, Ithaca, NY **Nov'20**
Virtual Talk Cytoskeleton in tissue morphogenesis. Syracuse, NY **Apr'20**
P**oster Presentation** Stevenson Biomaterial lecture series, Syracuse University, Syracuse, NY **Mar '20**
Poster Presentation American Society for Cell Biology, Washington D.C. **Dec'19**
Talk at Developmental Biology New York (DBNY) conference, Ithaca, NY. * *Outstanding Talk recognition.* **Nov'19**
Talk at Cell Developmental Biology Interest Group 2019. **Nov'19**